MODELING TOOLS AND PROTOTYPE DESIGN OF

LOOP HEAT PIPE FOR ELECTRONICS COOLING

A Dissertation

presented to

the Faculty of the Graduate School

at the University of Missouri-Columbia

In Partial Fulfillment

of the Requirements for the Degree

Doctor of Philosophy

---

by

SHIMIN WANG

Dr. James E. Bryan, Dissertation Supervisor

MAY 2009

The undersigned, appointed by the dean of the Graduate School, have examined the dissertation entitled

MODELING TOOLS AND PROTOTYPE DESIGN OF
LOOP HEAT PIPE FOR ELECTRONICS COOLING

presented by Shimin Wang,

a candidate for the degree of Doctor of Philosophy,

and hereby certify that, in their opinion, it is worthy of acceptance.

Professor James E. Bryan

Professor Yuwen Zhang

Professor Gary L. Solbrekken

Professor Hongbin Ma

Professor Thomas R. Marrero

ACKNOWLEDGEMENTS

First of all, I would like to give my sincere thanks to my adviser, Professor James E. Bryan, for his continuous encouragement, support, and guidance during the past three years. It is he who led me into the amazing world of thermal-fluid engineering and offered me the extraordinary freedom to explore this new world.

I would like to thank Professor Yuwen Zhang, Professor Gary L. Solbrekken, Professor Hongbin Ma, and Professor Thomas Marrero for their time and great efforts in directing my research and dissertation work. Their constructive comments and suggestions are invaluable for me to improve the dissertation.

Professor Robert Tzou, Professor Frank Z. Feng and other faculty members in the Department of Mechanical and Aerospace Engineering gave me tremendous directions and supports. Ms. Melanie Gerlach and other MAE staff members provided me a lot of practical help. I would like to thank all of them as well.

Finally, the support to this research from Dell Inc. is gratefully acknowledged.

TABLE OF CONTENTS

LIST OF ILLUSTRATIONS

Figure Page

LIST OF TABLES

LIST OF SYMBOLS

A	area
A, B	constants in the logarithmic law of the wall for turbulent velocity distribution
A_T, B_T	constants in the logarithmic law of the wall for turbulent temperature distribution
c_p	specific heat at constant pressure
$\hat{c}_p$	specific heat ratio $\hat{c}_p \equiv \frac{c_{p_l}}{c_{p_v}}$
$C_0 - C_5$	coefficients
D	diameter
D_h	hydraulic diameter
E, F, H	coefficients in Friedel correlation, Eq. (2.17)
f	friction factor
Fr	Froude number
g	gravitational acceleration
G	mass flux
h	specific enthalpy
h_{air}	heat transfer coefficient on air flow side
h_{lv}	latent heat
h_{npc}	heat transfer coefficient, no phase change case
h_{pc}	heat transfer coefficient, phase change case
H	height
ΔH	elevation difference
j_g *	dimensionless vapor velocity

k	thermal conductivity
$\hat{k}$	thermal conductivity ratio $\hat{k} \equiv \frac{k_l}{k_v}$
K	permeability
L	Length
$\dot{m}$	mass flow rate
M	mass
n_{gr}	number of vapor grooves
N	figure of merit
Nu	Nusselt number
p	pressure
Pr	Prandtl number
q	heat rate per unit thickness
q_0	heat flux at wall
q''	heat flux
Q	heat rate
r	radial coordinate
r_0	pipe radius
r_1	radius of liquid-vapor interface
r_c	meniscus radius
R_l^+	$R_l^+ = \frac{r_0 \tau_0^{\frac{1}{2}} \rho_l^{\frac{1}{2}}}{\mu_l}$
R_v^+	$R_v^+ = \frac{r_0 \tau_1^{\frac{1}{2}} \rho_v^{\frac{1}{2}}}{\mu_v}$

Re	Reynolds number
s	specific entropy; $s = \frac{(1-\sqrt{\alpha})\sqrt{\hat{\rho}}}{\hat{\mu}} + \sqrt{\alpha}$
$\dot{S}_{gen}$	entropy generation rate
t	$t = \frac{\left(1-\sqrt{\alpha}\right)\hat{c}_p\sqrt{\hat{\rho}}}{\hat{k}} + \sqrt{\alpha}$
T	temperature
T_∞	free stream temperature
u	axial velocity
u^*	friction velocity
u^+	diensionless velocity
U	mean velocity
v	specific volume; radial velocity
V	volume
We	Weber number
x	vapor quality
x, y	cartesian coordinates
x^*	dimensionless plate length, Eq. (3.10)
x^+	dimensionless plate length, Eq. (3.14)
$\hat{x}$	$\hat{x} \equiv \frac{x}{1-x} = \frac{\dot{m}_v}{\dot{m}_l}$
y^+	wall (dimensionless) coordinate
z	coordinate

Greek Letters

α	void fraction
β	liquid fraction; $\beta = \frac{r}{r_0}$
$\delta\dot{Q}$	differential heat transfer rate
$\delta\dot{S}_{gen}$	differential entropy generation rate
Δp	pressure drop
ε	porosity; emissivity
ε_l	momentum eddy diffusivity of liquid flow
ε_M	momentum eddy diffusivity
ε_v	momentum eddy diffusivity of gas/vapor flow
ϕ_{l0}^2	multiplier of frictional pressure gradient
μ	viscosity
$\hat{\mu}$	viscosity ratio $\hat{\mu} \equiv \frac{\mu_l}{\mu_v}$
ν	kinematic viscosity
ρ	density
$\hat{\rho}$	density ratio $\hat{\rho} \equiv \frac{\rho_l}{\rho_v}$
σ	surface tension
σ_{SB}	Stephan-Boltzmann constant
τ	shear stress
τ_0	shear stress at pipe wall
τ_1	shear stress at liquid-vapor interface

ξ	latent-sensible heat ratio $\xi \equiv \dfrac{h_{lv} dx/dz}{c_{pv} dT_{sat}/dz}$

Subscripts

a	acceleration
app	apparent
amb	ambient
avg	average
cc	compensation chamber
cond	condenser; condensation
cr	critical
C	cold case
eff	effective
evap	evaporator
f	friction
gr	vapor grooves
grav	gravitational
h	homogenous
H	hot case
i	inner
in	input
j	*j = l, v*
l	liquid
*l*0	liquid flow with two-phase mass flow rate
lm	logarithmic mean

LL	liquid line
loop	loop
m	mean
max	maximum
o	outer
opt	optimum
pk	peak
s	surface
sat	saturation
total	total
v	vapor
*v*0	vapor flow with two-phase mass flow rate
VL	vapor line
w	wall
wick	wick layer

ABSTRACT

In this dissertation, a set of modeling tools for loop heat pipe (LHP) design is developed, and original analytical models for annular two-phase flow are proposed.

LHPs are promising two-phase thermal transport devices for electronics cooling. The developed modeling tools include a system level model, criteria of selecting working fluids, and individual component models for modularized design of LHP condenser and evaporator. Based on these tools, new figures of merit for measuring capillary limit and heat leak effects are defined, the condensation pressure drop is shown to be always dominating the loop pressure drop in air-cooled LHPs, and a published LHP prototype for laptop computer cooling is simulated. The modeling results agree well with the available experimental data and reveal that the air flow is the bottleneck of this prototype.

The analytical models for annular two-phase flow presented in this work is fundamentally different from the previous two-phase flow models in that both the velocity and temperature distributions for the liquid and gas/vapor phases are represented based on the governing equations for laminar flows and based on the universal profiles for turbulent flows. As a result, analytical relations of void fraction, frictional pressure gradient, acceleration pressure gradient, and heat transfer coefficient for all possible flow regimes are derived on a self-contained and self-consistent basis, with the classical single-phase relations as their extreme limits. Detailed comparison with the modeling results shows that the prevailing empirical correlations in engineering practice generally fail to provide reliable and accurate predictions for annular two-phase flows.

Chapter 1

Literature Review and Research Overview

1.1 Literature Review

In the electronics industry, the continuous increase in component performance and system miniaturization makes the thermal management a major challenge. Issues related to the thermal management of electronics include (Bergman et al. 2008): continuous power increase (application and technology driven); ultra high heat flux; low allowable temperature difference; localized high heat flux (hot spots); temperature uniformity requirements (LED, space applications); demand for low weight, small scale (military and other); integration and small scale; multi-scale problem ranging from nanometers at the transistor level to tens of meters at the data center level; stacking (results in higher power density and thermal resistances); demand for low cost thermal solutions; demand for high reliability for very aggressive application conditions such as mobile systems and military applications; increasing energy cost; and environmental impact of high energy consumption.

As conduction or air convection cooling systems are not efficient to transfer high heat fluxes generated by the electronics, alternative cooling techniques have to be used (Webb and Kim 2005). Among the available techniques, two-phase capillary thermal control devices such as heat pipes, micro heat pipes, capillary pumped loops, and loop heat pipes (LHP) are especially promising. In these devices, heat is removed by phase change and the working fluid is circulated by thermodynamic forces.

LHPs are robust, self-starting, and passive two-phase thermal transport devices, which can transport large thermal power loads over long distances through flexible and small diameter tubes. The characteristics of LHPs make them attractive thermal control devices for both ground and space applications. The LHP was first developed and tested in 1970s in the former Soviet Union (Maydanik 2005). The development of LHPs was a response to the challenge of the specific demand of aerospace technology, which requires high operational reliability and robustness. Although LHPs were originally invented for space applications, they have a considerable potential for ground applications, especially for electronics cooling applications.

The LHPs offer many advantages over heat pipes, in terms of operation against gravity, maximum heat transport capability, smooth-walled flexible transport lines, and fast diode action. Moreover, the separated flow of liquid and vapor phases allows modularized designs for high performance LHP development.

The basic distinction between a LHP and a capillary pumped loop lies in the fluidic and thermal links of the compensation chamber to the evaporator. This distinction has a large impact on the design and operation of the capillary loop. The physical proximity of the reservoir to the evaporator simplifies the LHP start-up and makes the LHP operation vapor-tolerant: both contribute to the robustness of the LHP operation under various conditions. The preconditions required for a capillary pumped loop is a major disadvantage that makes the LHP a good competitive technology.

However, the LHP is a complex system, into which thermal and hydrodynamic mechanisms between the various LHP components are strongly coupled. As an example, temperature and pressure dynamic instabilities, such as under- and overshoot, are

sometimes experimentally reported after changes in operational conditions (e.g. variations in heat load and sink temperature). Under certain conditions, the LHP can even never really reach a true steady-state, but instead displays an oscillating behavior. Such dynamic behaviors can induce various types of failure, like evaporator dry-out, degradation of performance, temperature oscillations, which are not suitable for the thermal control of electronics.

Currently, LHP miniaturization is in the forefront of extensive research and development to provide cooling solutions to the high heat load/heat flux problem of advanced electronic packaging. The constrained space of such applications requires designing specific LHPs. Various models have been developed for the LHP characterization. The steady state models are useful to size new-designed LHPs and to predict LHP performance for various fixed external conditions. All these studies contribute to the improvement of the understanding of LHP operation and help to point out how various parameters may affect their behavior.

Because of the complexity of the related two-phase heat transfer phenomena, there have been few studies on transient modeling of LHP (e.g. Hoang and Ku 2003; Launay et al. 2007a). These modeling efforts have mainly been focused on the steady-state energy balances. Many of the previous studies have either used oversimplified assumptions, or analyzed only one component of LHP. For some studies, the main algorithm of the model and the comparisons of numerical and experimental results were not revealed. Because of the commercial importance, only a limited amount of data and information has been published in the open literature, among which Kaya and Hoang

(1999), Ku (1999), Muraoka et al. (2001), and Furukawa (2006) are some examples of steady state modeling studies. All of these studies focused on space applications.

For most space applications and experimental studies in laboratories, the working fluid is cooled through well controlled heat sink with a temperature lower than the ambient temperature, thus the condenser tube is not very long and the condensation pressure drop may be not very important. However, in electronics cooling applications, the condenser is normally cooled by forced convection of air flow. For such problems, rather long condenser tube is needed, and the two-phase pressure drop can be very important. In LHPs, the thermodynamic properties, like temperature and pressure, are closely related, and the momentum transport and energy transport are usually coupled. Therefore, employing two-phase pressure drop in LHP models is a necessary and important aspect of modeling study of LHP application in electronics cooling. In previous studies, although Hoang and Kaya (1999) presented a mathematical model of LHP with two-phase pressure drop and applied the model to analyze a prototype LHP designed for ICESAT spacecraft, there has been no published modeling study investigating the two-phase pressure drop in LHPs designed for ground applications.

It is undoubtedly accepted that working fluid plays an important role in controlling LHP performance and screening working fluids is a basic step in LHP design. Previous LHP studies have investigated various working fluids, including ammonia, water, acetone, methanol, ethanol, pentane, propylene, R-134a (Launay et al. 2007b). However, there are no widely accepted criteria for selecting working fluid for LHP applications. This may be partially due to the diversity of the broad application areas of LHPs, which makes it difficult to propose a universal merit of figure, but also due to the

lack of systematic studies on the effects of working fluid on the LHP performance. Owing to the complexity and coupling of fluid flow and heat transfer in the LHP operations, it is difficult to evaluate or predict the overall performance of a candidate working fluid, in contrast to identifying the trend of a single thermophysical property that favors heat transfer or fluid flow. For instance, high latent heat, surface tension and liquid density as well as low liquid viscosity are all desirable properties for heat pipe operation and for LHP operation as well, but it is highly questionable that the liquid-based figure of merit (Chi 1976; Dunn and Reay 1994), defined as the product of liquid density, liquid surface tension, and latent heat divided by the liquid viscosity, provides a sufficient criterion for evaluating the overall performance of a working fluid in LHP operation. As an example, the liquid-based figure of merit of water is greater than ammonia by a factor of 4 at 60^{o}C, but we have no confidence to say that a water filled LHP will perform better than ammonia filled LHPs, which have been widely used in space applications.

In addition to the working fluid properties, the overall characteristics of LHPs depend on the performance of the individual components: condenser, evaporator, compensation chamber, wick structure, etc. Since the various components have specific functions relatively independent upon each other, it is possible to construct modeling tools for designing individual components first and integrate components into LHPs afterwards. In other words, the internal structure of LHPs allows modularized design, which provides an additional advantage for LHP development.

1.2 Research Objective and Achievements

In electronics cooling applications, multi-scale mathematical models are often needed but the available models are generously too complex or cumbersome. As a result, lack of simple yet accurate design tools becomes one of the key barriers in the area of information technology with respect to thermal management and transport issues (Bergman, et al. 2008).

On the other hand, accurate design tools must be built upon correct knowledge of the fundamental physics related to the engineering problems. For example, a successful model for condenser or evaporator relies on accurate theoretical relations or experiment-based correlations of void fraction, frictional pressure gradient, acceleration pressure gradient, and heat transfer coefficient. However, at present, successful theoretical models or widely applicable empirical correlations for two-phase flows have not been established yet.

This study has two fundamental objectives. The first objective is to develop a set of modeling tools assisting LHP prototype design, and the second one is to theoretically investigate the fundamental physics of two-phase flow.

A typical LHP design process is shown in Fig. 1.1. It is a comprehensive process, and often involves iterations based on trial-and-error. In chapters 2 and 3, modeling tools for system level analysis, working fluid selection, and individual component design are prsented. With the help of this these tools, the operation of a LHP prototype can be simulated and many potential issues can be addressed before the prototype is actually manufactured. As an example, the LHP prototype designed and tested by Singh et al. (2007) is modeled in chapter 4. The modeling results agree well with the laboratory measurements, and reveal that the air flow is the bottleneck of the prototype and thus

needs to be improved if a higher heat load is required to remove. This simple example is given only for the purpose of demonstrating the usefulness of the modeling tools, and certainly the tools can be applied to various LHP design practice.

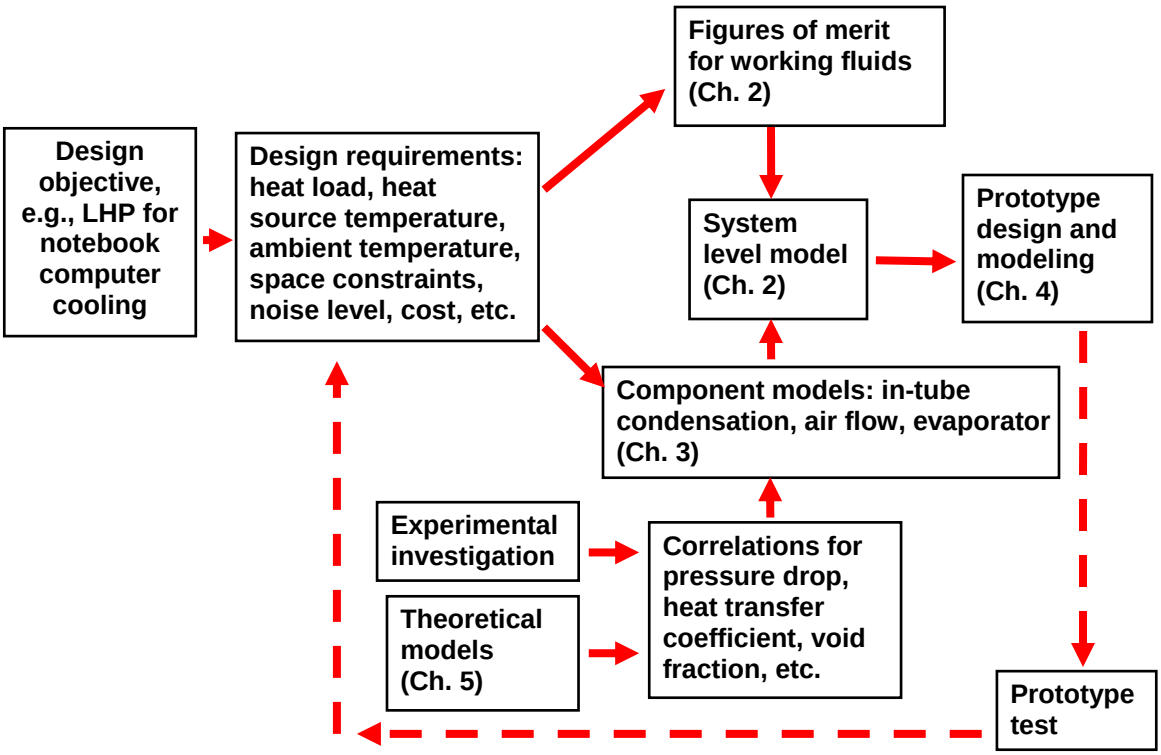

.

Figure 1.1 LHP prototype design process and how this research can help.

In chapter 5, analytical models for annular gas/vapor-liquid flow in a horizontal tube are proposed. Annular flow is chosen to study because it is the predominant flow pattern in various engineering devices, such as evaporators, condensers, natural gas pipelines, and steam heating systems (Wallis 1969; Hewitt & Hall-Taylor 1970), and because it seems impossible to develop a theoretical model that is universally applicable

to all flow regimes. The treatment in chapter 5 is fundamentally different from the previous two-phase flow modeling methods in that both the velocity and temperature distributions for the liquid and gas/vapor phases are represented based on the governing equations for the laminar flows and based on the universal profiles for the turbulent flows, which is in clear contrast against the separated flow model, which assumes uniform velocity for each phase, and the homogeneous flow model, which treats the two-phase flow by a single phase flow that averages the actual two phase flow. On a self-contained and self-consistent basis, the models proposed in this work provide the analytical relations of void fraction, frictional pressure gradient, acceleration pressure gradient, and heat transfer coefficient for all the possible annular flow domains (laminar gas/vapor and liquid, turbulent gas/vapor and laminar liquid, and turbulent gas/laminar and liquid) with or without phase change. It has been shown that all these relations can reduce to the corresponding classical single-phase limits when the two-phase annular flow approaches to single-phase gas/vapor or liquid flows. Moreover, modeling results are compared in detail with the prevailing empirical correlations in engineering practice of void fraction, frictional pressure drop, acceleration pressure drop, and heat transfer (Nusselt number). It has been shown that the empirical correlations examined generally fail to provide reliable and accurate predictions for annular two-phase flows for all the possible annular flow domains. The basic reason for the failure of the empirical correlations is that they are all established based on very limited experimental data and lack physically sound theoretical foundation.

It should be emphasized that the analytical models proposed in chapter 5 are derived in a very general framework, so they can be applied to any annular flow systems, definitely not limited to LHPs or heat pipes.

Chapter 2

System Level Model for LHP and Working Fluid Selection Criteria

2.1 LHP Operating Principles

The operation of a loop heat pipe (LHP) is based on phase change heat transfer and capillary pumping. A typical LHP consists of an evaporator, a compensation chamber, a condenser, and vapor and liquid lines, as shown schematically in Figure 2.1 (Launay et al. 2007b). The evaporator is the component that is in contact with heat source (the object to be cooled) and separated from the compensation chamber by a wick. The wick provides capillary head to circulate the working fluid in the loop. The heat input to the evaporator vaporizes the liquid in the wick structure, and the generated vapor is collected by the vapor grooves (vapor removal channels) in the evaporator and directed to the vapor line. In the condenser, the vapor is condensed, and the liquid leaving the condenser flows through the liquid line to the compensation chamber. The main functions of the compensation chamber are to accommodate excess liquid in the loop and to supply liquid to the capillary wick, compensating the liquid consumption in the wick.

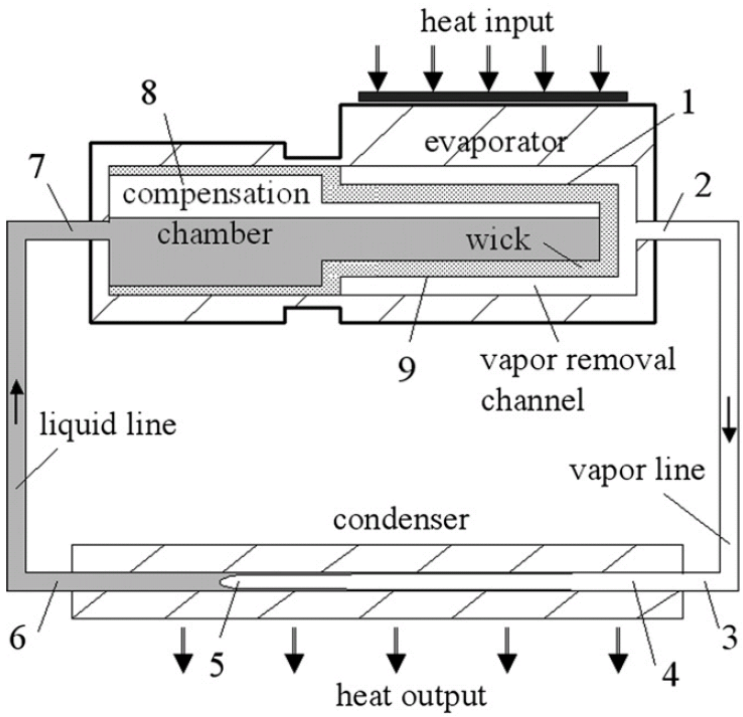

Figure 2.1 Schematic of a LHP (Launay et al. 2007b)

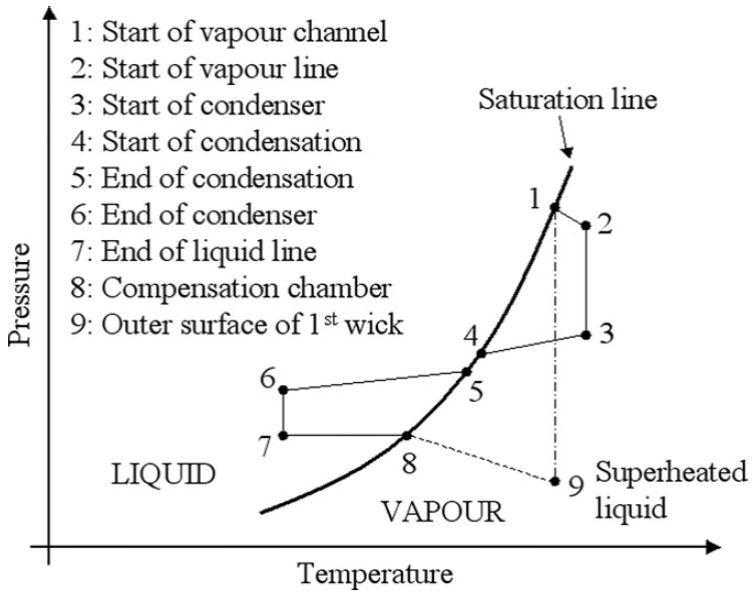

Figure 2.2 Pressure versus temperature diagram of a LHP (Launay et al. 2007b)

The thermal and hydraulic processes in the LHP operation are shown on a pressure-temperature diagram in Figure 2.2 (Launay et al. 2007b). The numbers in the diagram correspond to the physical locations shown in Figure 2.1. The vapor generated at the evaporator wick outlet (point 1) is at a saturation state. It becomes superheated at the exit of the vapor grooves (point 2) due to heating and pressure losses. Assuming that the vapor line is essentially adiabatic, the vapor temperature drop can be neglected. Since the pressure continues to drop along the way, the vapor becomes more and more superheated relatively to the local saturation pressure until it reaches the entrance of the condenser (point 3). The vapor releases its sensible heat and begins to condense inside the condenser (point 4), and the condensation takes place along the saturation line where both the pressure and the temperature decrease. At point 5, the vapor condensation is complete, and the liquid starts to be subcooled inside the condenser until it exits at point 6. The subcooled liquid flows in the liquid line, while its temperature may increase or decrease, depending on whether the liquid loses or gains heat from the ambient. As the liquid reaches the compensation chamber inlet (point 7), the working fluid is heated up to point 8. As long as the working fluid exists in the compensation chamber as liquid-vapor mixture (i.e., the compensation chamber is partially filled with liquid), the thermodynamic state in the compensation chamber (point 8) is saturated. The transition from point 8 to 9 corresponds to the liquid flow through the wick into the evaporation zone. During the transition, the liquid may be superheated, but boiling does not take place because it remains in such a state for a very short time. Point 9 determines the state of the working fluid in the vicinity of the evaporating menisci, and the pressure drop $p_1 – p_9$

corresponds to the value of total pressure losses along the whole loop. It should be noted that, in Figure 2.2, the cycle is enlarged to improve its legibility.

2.2 Mathematical Model

Energy balance for the evaporator under steady operation can be written as

$$Q_{in} = Q_{loop} + Q_{HL}, \tag{2.1}$$

where Q_{in} is the input heat load, Q_{loop} the heat removed by the circulating working fluid, and Q_{HL} is the heat transferred backward to the compensation chamber through the conduction of the wick, called heat leak (or back conduction, parasitic heat). Heat leak is a big issue in LHP operation, since severe heat leak will cause the operation temperature of compensation chamber and evaporator to increase. It will be shown that heat leak is closely related to working fluid properties.

The mass flow rate in the loop is defined by

$$\dot{m} = \frac{Q_{loop}}{h_{lv}}, \tag{2.2}$$

where h_{lv} is the latent heat of the working fluid. The total pressure drop through the loop is the sum of the pressure drops in individual components of the LHP along the flow path

$$\Delta p_{total} = \Delta p_{gr} + \Delta p_{VL} + \Delta p_{cond} + \Delta p_{LL} + \Delta p_{wick} + \Delta p_{grav}. \tag{2.3}$$

In (2.3), the right-hand-side terms are pressure drops, respectively, in vapor grooves, vapor line, condenser, liquid line, wick layer, and that due to gravity. In this study, the total pressure drop minus the wick pressure drop will be called loop pressure drop.

For turbulent vapor flow in vapor grooves and vapor line and laminar flow in liquid line, the pressure drops can be evaluated by (e.g. Schlichting 1968)

$$\Delta p_{gr} = \frac{0.241\mu_v^{0.25}(\dot{m}/n_{gr})^{1.75}(L_{evap}/2)}{\rho_v D_{gr}^4}, \tag{2.4}$$

$$\Delta p_{VL} = \frac{0.241\mu_v^{0.25}\dot{m}^{1.75}L_{VL}}{\rho_v D_{VL}^4}, \tag{2.5}$$

$$\Delta p_{LL} = \frac{128\mu_l \dot{m} L_{LL}}{\pi\rho_l D_{LL}^4}. \tag{2.6}$$

In case there is an elevation difference ΔH between the evaporator and condenser, a hydrostatic pressure results

$$\Delta p_{grav} = \rho_l g \Delta H. \tag{2.7}$$

For condensation in horizontal tubes, the local two-phase pressure gradient consists of frictional and acceleration components (e.g. Marto, 1998)

$$-\frac{dp}{dz} = \left(-\frac{dp}{dz}\right)_f + \left(-\frac{dp}{dz}\right)_a. \tag{2.8}$$

Based on the momentum balance of the two-phase flow, the acceleration pressure gradient is evaluated by

$$\left(-\frac{dp}{dz}\right)_a = G^2 \frac{d}{dz}\left[\frac{(1-x)^2}{\rho_l(1-\alpha)} + \frac{x^2}{\rho_v \alpha}\right], \tag{2.9}$$

where G is mass flux, x is vapor quality, and α is void fraction. According to Zivi (1964), the void fraction is correlated to quality by

$$\alpha = \frac{1}{1+[(1-x)/x](\rho_v/\rho_l)^{2/3}}. \tag{2.10}$$

For liquid-vapor viscosity ratio $\mu_l/\mu_v < 1000$, Hewitt (1983) recommended the Friedel (1979) correlation to evaluate two-phase flow pressure gradient

$$\left(-\frac{dp}{dz}\right)_f = \phi_{l0}^2 \left(-\frac{dp}{dz}\right)_{l0}, \tag{2.11}$$

$$\left(-\frac{dp}{dz}\right)_{l0} = \frac{2 f_{l0} G^2}{\rho_l D_{cond}}, \tag{2.12}$$

where the friction factor f depends on the respective Reynolds number

$$\mathrm{Re}_{l0} = \frac{\rho_l U_l D_{cond}}{\mu_l} = \frac{G D_{cond}}{\mu_l}, \tag{2.13}$$

$$\mathrm{Re}_{v0} = \frac{\rho_v U_v D_{cond}}{\mu_v} = \frac{G D_{cond}}{\mu_v}, \tag{2.14}$$

and

$$f = \frac{16}{\mathrm{Re}} \qquad \text{for } \mathrm{Re} < 2000, \tag{2.15}$$

$$f = 0.079\,\mathrm{Re}^{-0.25} \qquad \text{for } \mathrm{Re} > 2000. \tag{2.16}$$

The frictional multiplier in Equation (2.11) is given by

$$\phi_{l0}^2 = E + \frac{3.23FH}{\mathrm{Fr}^{0.045}\mathrm{We}^{0.035}}, \tag{2.17}$$

where

$$E = (1-x)^2 + x^2 \frac{\rho_l f_{v0}}{\rho_v f_{l0}}, \tag{2.18}$$

$$F = x^{0.78}(1-x)^{0.224}, \tag{2.19}$$

$$H = \left(\frac{\rho_l}{\rho_v}\right)^{0.91} \left(\frac{\mu_v}{\mu_l}\right)^{0.19} \left(1-\frac{\mu_v}{\mu_l}\right)^{0.7}, \tag{2.20}$$

$$\mathrm{Fr} = \frac{G^2}{g D_{cond} \rho_h^2}, \tag{2.21}$$

$$\mathrm{We} = \frac{G^2 D_{cond}}{\rho_h \sigma}, \tag{2.22}$$

$$\rho_h = \frac{\rho_l \rho_v}{x\rho_l + (1-x)\rho_v}. \tag{2.23}$$

The total pressure drop across the condenser is obtained by integrating Equation (2.8) over the condenser length L_{cond}

$$\Delta p_{cond} = \int_0^{L_{cond}} \left(-\frac{dp}{dz}\right) dz \,. \tag{2.24}$$

Since both the frictional pressure gradient and acceleration pressure gradient depend on vapor quality, the dependence of the quality x on axial position z must be known for integrating Equation (2.24). Assuming that the condenser is cooled by forced convection of air with an average heat transfer coefficient h_{pc} over the condenser length, we can write energy balance for the condenser as

$$Q_{cond} = Q_{loop} = \dot{m} h_{fg} = h_{pc} A_s (T_{sat} - T_{amb}), \tag{2.25}$$

where A_s is the total area of the effective fin surface of the condenser heat sink, T_{sat} is average saturation temperature in condenser, and T_{amb} is ambient air temperature. Differentiate Equation (2.25), we have

$$dQ_{cond} = -h_{fg} d\dot{m}_g = h_{pc}(T_v - T_{amb}) \frac{A_s}{L_{cond}} dz = \frac{\dot{m} h_{fg}}{L_{cond}} dz, \tag{2.26}$$

Therefore,

$$dx = \frac{d\dot{m}_g}{\dot{m}} = -\frac{dz}{L_{cond}}. \tag{2.27}$$

It should be emphasized that such a linear x-z relation is only a rough approximation to the real x-z relation, which can be very complicated due to two-phase flow and heat transfer. Substituting (2.27) into (2.9) and (2.10), and after some mathematical manipulations, the pressure gradient is expressed by

$$-\frac{dp}{dz}=\left(-\frac{dp}{dz}\right)_f-\frac{G^2}{L_{cond}}\left[\frac{2x}{\rho_g}+\frac{1-2x}{\rho_g^{1/3}\rho_l^{2/3}}-\frac{2(1-x)}{\rho_l}+\frac{1-2x}{\rho_g^{2/3}\rho_l^{1/3}}\right], \quad (2.28)$$

and it can be numerically integrated by substituting into (2.24).

With the pressure drops from the evaporator through vapor line, condenser and liquid line to the compensation chamber being obtained, the temperature difference across the wicks between the evaporator and the compensation chamber can be calculated by

$$\Delta T_{wick}=\left(\frac{dT}{dp}\right)_{sat}\Delta p_{loop}=\left(\frac{dT}{dp}\right)_{sat}(\Delta p_{gr}+\Delta p_{VL}+\Delta p_{cond}+\Delta p_{LL}+\Delta p_{grav}), \quad (2.29)$$

since both sides of the wicks are under saturation state. It should be noted that (2.29) is only valid for the case of compensation chamber partially filled with liquid; if the compensation chamber is fully filled with liquid, the LHP operation mode is different (Chernysheva et al. 2007), which is not modeled here.

The saturation temperature-pressure gradient in (2.29) can be calculated by Clausius-Clapeyron equation

$$\left(\frac{dT}{dp}\right)_{sat}=\frac{T}{h_{fg}}\left(\frac{1}{\rho_v}-\frac{1}{\rho_l}\right)=\frac{T}{h_{lv}\rho_l}\left(\frac{\rho_l}{\rho_v}-1\right), \quad (2.30)$$

The heat leak from the evaporator to the compensation chamber by the conduction of the wick layer is calculated by

$$Q_{HL}=\frac{2\pi k_{eff}L_{wick}}{\ln(D_{w,o}/D_{w,i})}\Delta T_{wick}, \quad (2.31)$$

where the effective thermal conductivity of the wick of sintered particles may be calculated by (Faghri 1995)

$$k_{eff} = k_{wick}\left\{\frac{2+(k_l/k_{wick})-2\varepsilon[1-(k_l/k_{wick})]}{2+(k_l/k_{wick})+\varepsilon[1-(k_l/k_{wick})]}\right\}, \tag{2.32}$$

and for cubic packed particles, the porosity is (Faghri 1995)

$$\varepsilon \approx 0.48\,. \tag{2.33}$$

According to Darcy's law, the pressure drop across the wick is

$$\Delta p_{wick} = \frac{\mu_l \dot{m} L_{wick}}{K_{wick} A_{wick} \rho_l}\,. \tag{2.34}$$

For unconsolidated packed sintered spherical particles with a diameter *D* (Faghri 1995), the permeability

$$K_{wick} = \frac{D^2 \varepsilon^3}{150(1-\varepsilon)^2}\,. \tag{2.35}$$

Since the capillary head is the driving force for the LHP, the total pressure drop must be less than the capillary head

$$\Delta p_{total} \le \frac{2\sigma}{r_c}\,. \tag{2.36}$$

Thus a maximum meniscus radius is defined by

$$r_{c,\max} = \frac{2\sigma}{\Delta p_{total}}, \tag{2.37}$$

while the effective meniscus radius formed by sintered particles correlates with the particle diameter by (Faghri 1995)

$$r_{eff} = 0.21D\,. \tag{2.38}$$

The compensation chamber is a critical component of the LHP. The volume of the compensation chamber must be carefully designed so as to accommodate at least the liquid swing volume and density changes between the hot case and the cold case of the

loop operation. Sizing of the compensation chamber and the loop fluid inventory are usually considered concurrently (Ku 1999). Under the cold case, the fluid inventory must satisfy

$$M = \rho_{l,C}(V_{loop} + \beta V_{cc}) + \rho_{v,C}(1-\beta)V_{cc}\,, \tag{2.39}$$

where M is the desired fluid mass in the LHP, V_{loop} is the loop total volume excluding the compensation chamber volume V_{cc}

$$V_{loop} = V_{LL} + V_{wick} + V_{gr} + V_{VL} + V_{cond}\,, \tag{2.40}$$

and β is the fraction of compensation chamber volume occupied by liquid in cold case. The same fluid inventory must also satisfy the following relation under the hot case

$$M = \rho_{l,H}[V_{LL} + V_{wick} + (1-\alpha)V_{cc}] + \rho_{v,H}(V_{gr} + V_{VL} + V_{cond} + \alpha V_{cc})\,, \tag{2.41}$$

where α is the void fraction of compensation chamber volume in hot case.

The average density of the working fluid in the LHP is essentially constant

$$\rho_{avg} = \frac{M}{V_{loop} + V_{cc}}\,, \tag{2.42}$$

since the LHP is a closed system with negligible pipe deformation. This average density must be lower than the liquid density at the maximum non-operating temperature in order to prevent bursting due to hydrostatic pressure.

2.3 Modeling Results and Discussion

In terms of the above developed model, steady state operations of three LHPs are simulated: LHP-A charged with ammonia, LHP-H charged with HFE-7000, and LHP-W charged with water. Ammonia is the most widely used LHP working fluid, particularly in spacecraft thermal control, but its toxic nature and relatively high saturation pressure at

room temperature prevent it from an ideal working fluid for electronics cooling. Modeling results of LHP-A provide useful reference for the other two heat pipes and also help in comparing the obtained results in this study with previous studies. Water is the dominant working fluid used in current conventional heat pipes for electronics cooling, for example, notebook computer cooling, and also an attractive LHP working fluid for next generation electronics cooling. HFE-7000 is a promising working fluid designed for electronics cooling, however, its application as LHP working fluid has never been investigated by experimental or modeling approaches.

Table 2.1 LHP geometry

Component	Length (mm)	Inner diameter (mm)	Outer diameter (mm)
Vapor line	200	2	
Liquid line	200	2	
Condenser tube	400	2	
Wick in evaporator	9	6	8.2
Each of the 16 vapor grooves in evaporator	10	0.8	
Evaporator cylinder	10	9	

Table 2.2 Prescribed operational conditions

Heat load	100 W
LHP operating temperature (T_{cc})	60^{o}C
Ambient temperature	20^{o}C
Cold case temperature	280 K
Fraction of compensation chamber volume occupied by liquid in cold case	0.1
Hot case temperature	60^{o}C
Void fraction of compensation chamber volume in hot case	0.1
Heat transfer coefficient of condenser heat sink	50 W/m^2 K
Heat sink surface area	0.05 m^2
Wick porosity (sintered spherical particles)	0.48

Table 2.3 Thermophysical properties of working fluids at saturation

Fluid	Ammonia	HFE-7000	Water
Temperature	330 K	332 K	60^{o}C
Saturation pressure (10^5 Pa)	24.196	2.186	0.199190
Latent heat (kJ/kg)	1014	122.4	2358.4
Liquid density (kg/m^3)	550.9	1314.3	983.28
Vapor density (kg/m^3)	18.89	17.5	0.13020
Liquid-vapor density ratio	29	75	7564
Liquid viscosity (10^{-6} Pa s)	101.9	316.7	463.0
Vapor viscosity (10^{-6} Pa s)	12.74	11.94[a]	10.50
Liquid thermal conductivity (W/m K)	0.408	0.0681	0.653
Vapor thermal conductivity (W/m K)	0.0368	0.01134[a]	0.0216
Liquid specific heat (kJ/kg K)	5.170	1.313	4.185
Vapor specific heat (kJ/kg K)	4.088	0.767[a]	1.924
Liquid surface tension (10^{-3} N/m)	13.7	9.91	66.07

[a]Vapor properities estimated from R-123 vapor at 60^{o}C, which has a density of 17.33 kg/m^3.

The geometry and the prescribed operating conditions are exactly the same for the three LHPs, as shown in Tables 2.1 and 2.2, and the thermophysical properties of the working fluids are listed in Table 2.3. The predicted operational characteristics of the three LHPs are listed in Table 2.4. For the same loop heat load, the mass flow rate in LHP-H is an order higher than that in LHP-A and LHP-W. This is simply a result of the fact that HFE-7000 has a latent heat an order lower than ammonia and water. Since all pressure drops of single phase flows in the loop are positively correlated to mass flow rate, LHP-H has higher pressure drops in vapor grooves, vapor line, liquid line, and wick layer than the other two LHPs. However, the two-phase pressure drop across the condenser, which is 24 kPa for LHP-W, 3 kPa for LHP-H, and 0.3 kPa for LHP-A, is not positively correlated to mass flow rate.

It is clear from the results shown in Table 2.4 that for all the three LHPs the pressure drop of two-phase flow in the condenser is the dominant component in the loop pressure drop. This is also true for other pipe sizes, as shown in Figure 2.3, given the pipe lengths keep unchanged. The dominating condenser pressure drop cannot be explained by the greater length of the condenser tube, since the condenser tube is only twice the lengths of vapor line and liquid line, but a direct consequence of higher pressure drop of two-phase flow.

Table 2.4 Predicted LHP operational characteristics

LHP	LHP-A	LHP-H	LHP-W
Mass flow rate, 10^{-5} kg/s	9.86	81.7	4.24
Reynolds number for vapor line	4928	43561	2571
Reynolds number for liquid line	616	1642	58
Pressure drop across vapor grooves, Pa	0.007	0.3	0.2
Pressure drop across vapor line, Pa	0.93	40	29.3
Pressure drop through condenser tube, Pa	290	3168	24285
Pressure drop across liquid line, Pa	9.3	100	10.2
Pressure drop across wick layer, Pa	1.6	3978	491
Temperature difference between evaporator and compensation chamber, ^{o}C	0.005	0.5	26.4
Effective thermal conductivity of copper wick, W/m K	168	168	169
Effective thermal conductivity of titanium wick, W/m K	9.1	8.9	9.3
Heat leak to compensation chamber through copper wick, W	0.15	15	805
Heat leak to compensation chamber through titanium wick, W	0.008	0.8	44
Wick capillary radius, μm	91	6.0	5.4
Sintered particle diameter, μm	430	28	26
Wick permeability, 10^{-12} m^2	510	2.2	1.8
Compensation chamber volume, cm^3	2.9	2.8	2.5
Working fluid mass, g	1.9	4.5	3.0
Average density of working fluid, kg/m^3	343.0	803	576.6

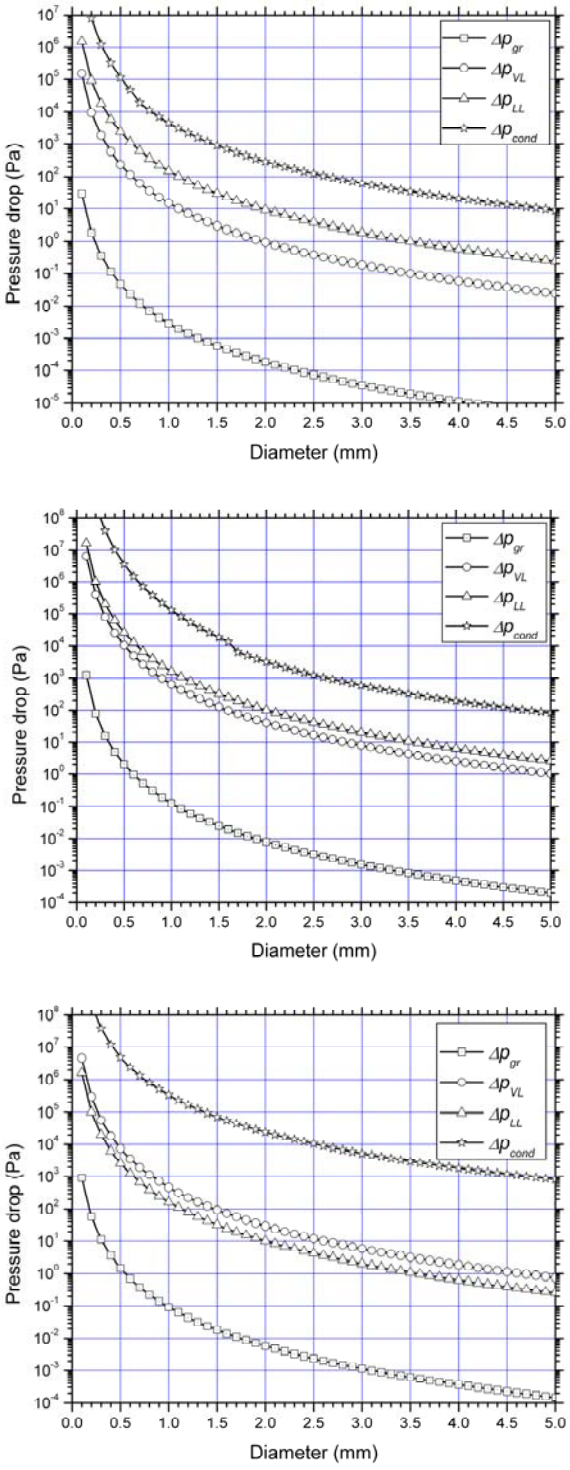

Figure 2.3 Pressure drop versus tube diameter for LHP-A (top), LHP-H (middle), and LHP-W (bottom)

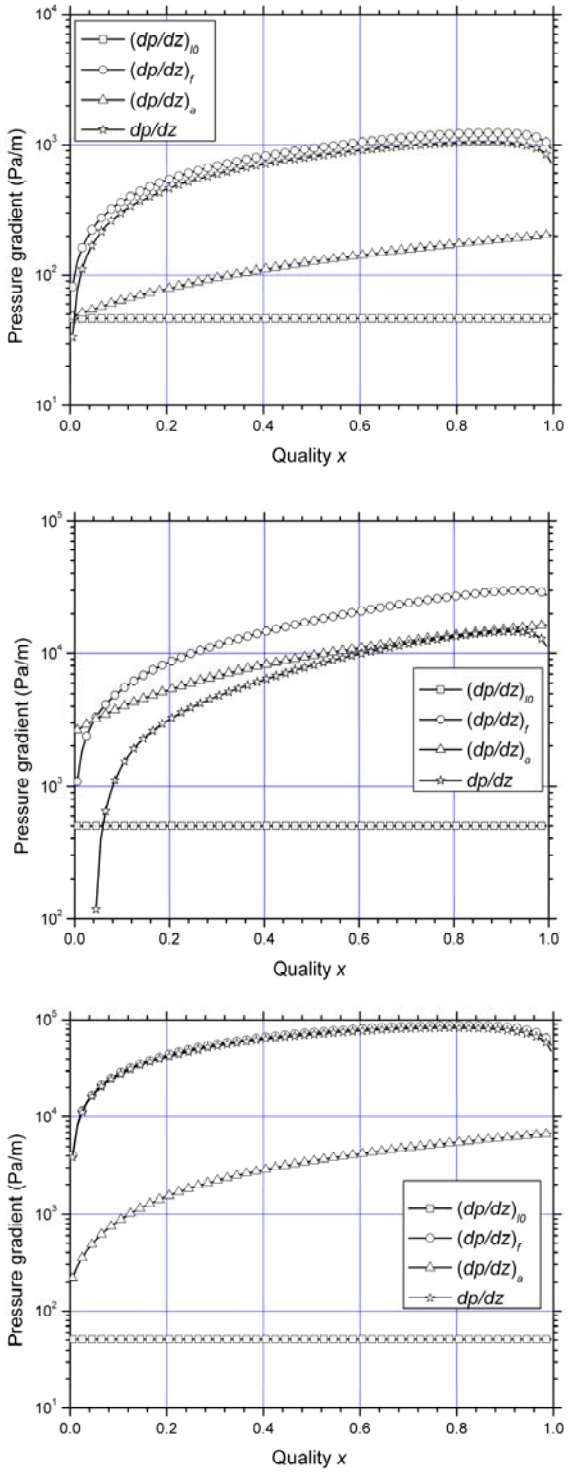

Figure 2.4 Pressure gradient versus vapor quality during condensation for LHP-A (top), LHP-H (middle), and LHP-W (bottom)

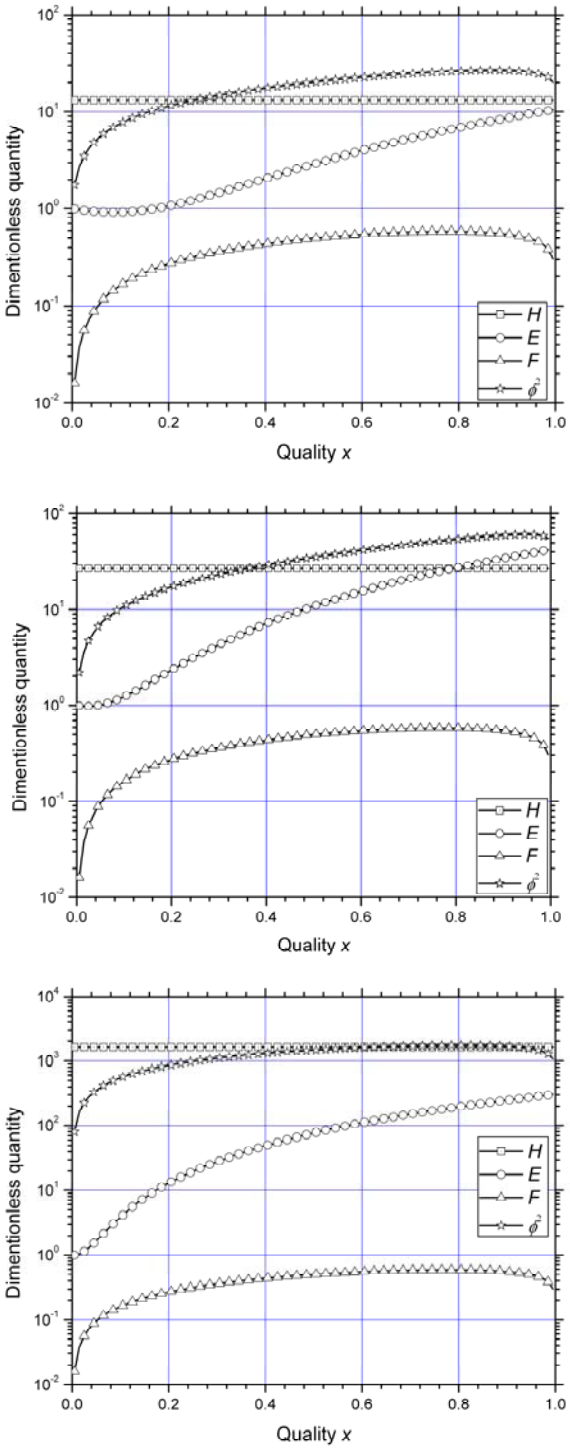

Figure 2.5 Frictional multiplier and its components versus vapor quality during condensation for LHP-A (top), LHP-H (middle), and LHP-W (bottom)

In Figure 2.4, the two-phase pressure gradient in the condenser is shown as a function of quality. It is obvious that the two-phase pressure gradient is dominated by the frictional component shown in (2.8): the acceleration term is significantly smaller than the frictional term. An interesting observation from Figure 2.4 is that the liquid frictional pressure gradient $\left(-dp/dz\right)_{l0}$ is very close for LHP-A and LHP-W, but the two-phase frictional pressure gradient $\left(-dp/dz\right)_f$ of LHP-W is much higher that of LHP-A. In other words, the water two-phase flow has a much higher frictional multiplier ϕ_{l0}^2 than the ammonia two-phase flow. This is confirmed by the modeling results shown in Figure 2.5.

In Figure 2.5, the frictional multiplier ϕ_{l0}^2 is shown along with three other dimensionless quantities appearing in (2.17): *E*, *F* and *H*. Although the *E* term for LHP-W is significantly greater than that for LHP-A, it is only the less important addend in (2.17), because the frictional multiplier ϕ_{l0}^2 is significantly greater than the *E* term for all the three LHPs. Actually, Figure 2.5 clearly shows that the frictional multiplier ϕ_{l0}^2 has a magnitude very close to the constant *H* value. The higher frictional multiplier ϕ_{l0}^2 for water flow is basically a consequence of a higher *H* value of water, which is in turn a consequence of a higher liquid-vapor density ratio, according to (2.20). So the higher value of liquid density to vapor density of water, which is two orders higher than that of ammonia and HFE-7000 (Table 2.3), is the major reason for higher pressure drop of water two-phase flow, as compared with ammonia and HFE-7000 two-phase flows.

The higher two-phase pressure drop in condenser results in a higher total pressure drop in the LHP-W loop, which requires higher capillary head thus smaller particles in wick structure, as shown in Table 2.4. Furthermore, the high pressure drop in the LHP-W

loop also contributes to the larger temperature difference between the evaporator and the compensation chamber, as evident in (2.29),

$$\Delta T_{wick} = \left(\frac{dT}{dp}\right)_{sat} \Delta p_{loop} = \left(\frac{dT}{dp}\right)_{sat} (\Delta p_{gr} + \Delta p_{VL} + \Delta p_{cond} + \Delta p_{LL} + \Delta p_{grav}). \quad (2.29)$$

This temperature difference is the driving force for heat leak. However, the pressure drop in the LHP loop is not the sole factor controlling the temperature difference between the evaporator and the compensation chamber and thus controlling the heat leak. Another factor is the temperature-pressure gradient $(dT/dp)_{sat}$ in (2.29). Using Clausius-Clapeyron equation (2.30),

$$\left(\frac{dT}{dp}\right)_{sat} = \frac{T}{h_{lv}}\left(\frac{1}{\rho_v} - \frac{1}{\rho_l}\right) = \frac{T}{h_{lv}\rho_l}\left(\frac{\rho_l}{\rho_v} - 1\right), \quad (2.30)$$

we can easily find that the temperature-pressure gradient is also positively correlated to the liquid–vapor density ratio. In (2.29), the multiplication of two-phase pressure drop dominated loop pressure drop and the saturation temperature-pressure gradient, both positively correlated to the liquid–vapor density ratio, reflects the controlling role of the liquid–vapor density ratio on the evaporator-compensation chamber temperature difference and on the heat leak. Although heat leak may be reduced by adopting wick material with low thermal conductivity, e.g., titanium, or increasing the wick layer thickness, the temperature difference between the evaporator and the compensation chamber, which is predicted to be 26.4^{o}C for LHP-W, 0.5^{o}C for LHP-H, and 0.005^{o}C for LHP-A, cannot be reduced as long as the loop pressure drop keeps unchanged. For electronics cooling applications, the total temperature gap between the evaporator and the ambient air is strictly limited, and a greater temperature difference between evaporator

and compensation chamber will undoubtedly narrow the temperature range assigned for condenser and transport lines thus hurt the overall performance of the LHP.

2.4 Figures of Merit for LHP Working Fluids

Similar to heat pipe design, the first step of LHP design is usually to screen working fluids. For this purpose, it can be very useful initially to select a working fluid and/or to compare one fluid with another regardless of the LHP geometry.

In conventional heat pipes, the capillary limit is the main constraint for heat pipe operation, and the greatest pressure loss is typically associated with the liquid flow in the wick structure. Equating the Laplace-Young equation for capillary pressure to the wick pressure drop predicted by Darcy's law, Chi (1976) was able to separate the fluid properties from the geometric and produce a liquid-based figure of merit (Ochterbeck 2003)

$$N_l = \frac{\sigma \rho_l h_{lv}}{\mu_l}, \tag{2.43}$$

which is also called merit number in the literature (e.g., Dunn and Reay 1994; Singh et al. 2007). Working fluid candidates with high figures of merit are considered to have better performance characteristics.

In case where the pressure drop due to flow through the wick structure is not the dominant pressure drop, Dunbar and Cadell (1998) developed a figure of merit for capillary pumped loop and LHP under the assumption that the pressure drop in the vapor flow is the dominate pressure drop loss term. Their analysis, equating the frictional pressure drop due to turbulent flow in the vapor channel to the Laplace-Young equation

for capillary pressure and separating the fluid terms from geometric terms, yielded the vapor-based figure of merit (Ochterbeck 2003)

$$N_v = \frac{\sigma \rho_v h_{fg}^{1.75}}{\mu_v^{0.25}}. \tag{2.44}$$

This figure of merit may be applicable to capillary pumped loops and LHPs designed for space applications, as long as vapor flow pressure drop dominates the total pressure drop. However, for air-cooled condensation LHP applications, as in electronics cooling applications, the condensation pressure drop is usually the dominant pressure drop, and a new figure of merit is needed.

In terms of the LHP model developed in this study, we can define figures of merit for LHP working fluids in a united way. Equations (2.3) and (2.37) can be rewritten as

$$\Delta p_{total} = \Delta p_{gr} + \Delta p_{VL} + \Delta p_{cond} + \Delta p_{LL} + \Delta p_{wick} + \Delta p_{grav} = \frac{2\sigma}{r_{c,\max}}. \tag{2.45}$$

When pressure drop in the liquid line dominates the total pressure drop, combining Equations (2.45), (2.2), and (2.6) gives

$$Q_{loop} \approx \left(\frac{\sigma \rho_l h_{lv}}{\mu_l} \right) \frac{\pi D_{LL}^4}{64 r_{c,\max} L_{LL}} = N_l \frac{\pi D_{LL}^4}{64 r_{c,\max} L_{LL}}. \tag{2.46}$$

Similarly, when pressure drop across the wick layer dominates the total pressure drop, combining Equations (2.45), (2.2), and (2.34) gives

$$Q_{loop} \approx \left(\frac{\sigma \rho_l h_{lv}}{\mu_l} \right) \frac{2 K_{wick} A_{wick}}{r_{c,\max} L_{wick}} = N_l \frac{2 K_{wick} A_{wick}}{r_{c,\max} L_{wick}}. \tag{2.47}$$

Equations (2.46) and (2.47) show that the liquid-based figure of merit is applicable to LHPs operating under conditions when liquid pressure drops dominate, either in liquid line or across wick layer.

When pressure drop in the vapor line dominates the total pressure drop, combining Equations (2.45), (2.2), and (2.5) gives

$$Q_{loop}^{\ 1.75} \approx \left(\frac{\sigma \rho_v h_{lv}^{\ 1.75}}{\mu_l^{\ 0.25}} \right) \frac{8.3 D_{LL}^{\ 4}}{r_{c,\max} L_{VL}} = N_v \frac{8.3 D_{LL}^{\ 4}}{r_{c,\max} L_{VL}}, \tag{2.48}$$

i.e., the vapor-based figure of merit is an appropriate measure for working fluid performance under given conditions.

In case when the condensation pressure drop dominates the total pressure drop, as for most of the electronics cooling applications, Equations (2.2), (2.11)-(2.13), and (2.24) give

$$\Delta p_{cond} \approx \phi_{l0}^2 \frac{128 \mu_l Q_{loop} L_{cond}}{\pi \rho_l h_{fg} D_{cond}^{\ 4}}, \tag{2.49}$$

where the contribution of acceleration pressure drop is neglected based on the results shown in Figure 2.4. Substituting Equation (2.49) into Equations (2.45) yield

$$Q_{loop} \approx \frac{1}{\phi_{l0}^2} \left(\frac{\sigma \rho_l h_{lv}}{\mu_l} \right) \frac{\pi D_{cond}^{\ 4}}{64 r_{c,\max} L_{cond}}. \tag{2.50}$$

The numerical results shown in Figure 2.5 suggest that the value of frictional multiplier is controlled by the value of *H* in Equation (2.17), which is in turn controlled by the liquid-vapor density ratio, according to Equation (2.20). As a result, combining Equations (2.17), (2.20), and (2.49) gives a figure of merit for LHP operation when condensation pressure drop dominates

$$N_{cond} = \frac{\sigma \rho_v h_{lv}}{\mu_l}. \tag{2.51}$$

In the above discussion, the main concern is the capillary limit, as shown in Equation (2.45). It is undoubtedly true that capillary limit is an important constraint for

LHP operation, as it is for the conventional heat pipes, but it is not the sole important constraint. Heat leak in LHP is an issue that is as important as capillary limit, and it must be considered in working fluid screening. Equations (2.29)-(2.31) suggest that for the condensation pressure drop dominant case

$$Q_{HL} \sim \Delta T_{wick} \sim \frac{\Delta p_{cond}}{h_{lv}\rho_v}. \tag{2.52}$$

Substituting Equation (2.49) into Equation (2.52) gives

$$\frac{Q_{loop}}{Q_{HL}} \sim \frac{\rho_v^{\,2} h_{lv}^{\,2}}{\mu_l}. \tag{2.53}$$

Accordingly a figure of merit measuring LHP working fluid performance with respect to heat leak can be defined as

$$N_{HL} = \frac{\rho_v^{\,2} h_{lv}^{\,2}}{\mu_l}. \tag{2.54}$$

In fact, a combined figure of merit that considers both the capillary limit and heat leak effects may be defined by combining Equations (2.51) and (2.53)

$$N_{cond-HL} = \frac{\sigma \rho_v^{\,2} h_{lv}^{\,2}}{\mu_l}. \tag{2.55}$$

This combined figure of merit provides a convenient tool for screening LHP working fluids for electronics cooling applications, where the condensation pressure drop generally dominates the total pressure drop.

Table 2.5 compares the values for the above defined various figures of merit, in terms of the working fluid properties listed in Table 2.3. It is clear that the figures of merit defined in this study provide correct measurement for the performance of LHP

working fluids, as is evident from a comparison with the modeling results shown in Table 2.4.

Table 2.5 Figures of merit for LHP working fluids

Fluid	Ammonia	HFE-7000	Water
Temperature	330 K	332 K	60°C
Saturation pressure (10^5 Pa)	24.196	2.186	0.199190
$N_l = \frac{\sigma \rho_l h_{lv}}{\mu_l}$	0.751E+11	0.503E+10	0.331E+12
$N_v = \frac{\sigma \rho_v h_{lv}^{1.75}}{\mu_v^{0.25}}$	0.140E+12	0.236E+10	0.214E+11
$N_{cond} = \frac{\sigma \rho_v h_{lv}}{\mu_l}$	0.258E+10	0.670E+08	0.438E+08
$N_{HL} = \frac{\rho_v^2 h_{lv}^2}{\mu_l}$	0.360E+19	0.145E+17	0.204E+15
$N_{cond-HL} = \frac{\sigma \rho_v^2 h_{lv}^2}{\mu_l}$	0.493E+17	0.144E+15	0.135E+14

2.5 Summary

A mathematical model for LHP simulation and design is developed in this study. Pressure drops in individual components are modeled based on appropriate single phase flow theory or two-phase flow correlation. The analysis of all LHP-A, LHP-H and LHP-W shows that the two-phase flow pressure drop in condenser dominates the loop pressure drop. The tremendous difference in operational characteristics of the LHP-A and LHP-W is mainly caused by the tremendous difference of vapor density. The much lower density of water vapor, as compared with ammonia vapor, results in a much higher liquid-vapor density ratio for water, which causes much higher two-phase pressure drop, and also leads to much higher saturation temperature-pressure gradient, as shown in Clausius-

Clapeyron equation. The multiplication of the higher pressure drop and the higher temperature-pressure gradient is responsible for the large temperature difference and extremely high heat leak predicted for the water based LHP, while the predicted good performance of the ammonia based LHP may explain the popularity of using ammonia as the working fluid for LHPs. Although HFE-7000 has a latent heat only 1/200 of the water, requiring a mass flow rate 200 times higher than that in water filled LHP, the predicted overall performance of LHP-H is much better tha LHP-W, as a result of the lower liquid-vapor density ratio of HFE-7000, as compared with water. In conclusion, the modeling results show that low liquid-vapor density ratio is a desirable property for LHP working fluid that controls the overall performance of LHPs.

In order to quantitatively measure the performance of LHP working fluids, figures of merit corresponding different operation conditions are discussed. New figures of merit for LHP operating with condensation pressure drop dominant situations are defined, with both the capillary limit and heat leak effects being considered.

Since the uncertainty and limitation of the adopted two-phase flow correlation is not available due to the complicated nature of two-phase flow, the modeling predictions presented in this study may only make sense in a qualitative way, and carefully designed experimental validation is needed to test the model in a quantitative manner.

Chapter 3

Mathematical Models for LHP Components

3.1 In-tube Condensation Model

The process of in-tube condensation is widely prevalent in refrigeration and air conditioning industries, and in LHP condensers as well. In this section, a simple model of in-tube condensation will be presented based on the first and second laws of thermodynamics. Using this model as a frame work, experiment-based heat transfer and pressure drop correlations can be readily integrated and the overall performance of the working fluid condensation inside LHP condensers can be quantitatively evaluated.

Taking the two-phase flow in a differential segment *dz* of a circular tube as a system, the energy balance can be written as

$$\delta\dot{Q} = -h_{pc}\pi D(T - T_w)dz = \dot{m}dh\,, \tag{3.1}$$

where h_{pc} is heat transfer coefficient including phase change effect, and the enthalpy change is a result of both latent and sensible heat transfer, i.e.,

$$dh = h_{lv}dx + [(1-x)c_{p,l} + xc_{p,v}]dT\,. \tag{3.2}$$

The change of saturation temperature depends on pressure change according to the Clausius-Clapeyron equation

$$dT = \frac{Tv_{lv}}{h_{lv}}dp\,, \tag{3.3}$$

where $v_{lv} = v_v - v_l$. For condensation or evaporation occurring in horizontal tubes, there is no gravitational pressure gradient and thus only frictional pressure gradient and acceleration pressure gradient contribute to the pressure change

$$dp = \left[\left(\frac{dp}{dz} \right)_f + \left(\frac{dp}{dz} \right)_a \right] dz . \tag{3.4}$$

From the momentum balance, the acceleration pressure gradient can be related to the void fraction by

$$\left(\frac{dp}{dz} \right)_a = -G^2 \frac{d}{dz} \left[\frac{x^2}{\rho_v \alpha} + \frac{(1-x)^2}{\rho_l (1-\alpha)} \right]. \tag{3.5}$$

where G is mass flux. In order to close the above equations, correlations for heat transfer coefficient h_{pc}, frictional pressure gradient $(dp/dz)_f$, and void fraction α as functions of vapor quality and refrigerant properties are needed. With these correlations being specified, the processes of condensation can be modeled by numerically integrating the energy balance equation from x = 1 to $x = 0$ and solving for T, p, and z as functions of x.

The irreversibilities during the condensation processes are completely expressed by entropy generation rate, which can be calculated by using the second law of thermodynamics

$$\delta \dot{S}_{gen} = \dot{m} ds - \frac{\delta \dot{Q}}{T_w} = \dot{m} \frac{dh - v dp}{T} - \frac{\delta \dot{Q}}{T_w} = \delta \dot{Q} \left(\frac{1}{T} - \frac{1}{T_w} \right) - \frac{\dot{m} v dp}{T}, \tag{3.6}$$

where $v = v_l + (1-x) v_v$. Therefore,

$$\delta \dot{S}_{gen} = \frac{\alpha \pi D (T - T_w)^2}{T T_w} dz + \frac{\dot{m} v}{T} (-dp), \tag{3.7}$$

where the two terms on the right-hand-side account for irreversibilities from heat transfer across finite temperature difference and from pressure drop in two-phase flow, respectively. The departure of such obtained entropy generation rate with that of a constant pressure condenser provides a measure of the irreversibilities caused by the pressure drop.

The entropy generation rate of a constant pressure condenser can be expressed by

$$\begin{aligned}\dot{S}_{gen} &= \dot{m}(s_l - s_v) - \frac{\dot{m}(h_l - h_v)}{T_w} \\ &= -\dot{m}h_{lv}(\frac{1}{T} - \frac{1}{T_w}) \\ &= \frac{\dot{m}h_{lv}(T - T_w)}{TT_w},\end{aligned} \tag{3.8}$$

which is independent of the in-tube heat transfer coefficient and the structure of the condenser. Therefore, as long as the entropy generation through pressure drop (flow with friction) is negligible compared with the entropy generation through heat transfer, entropy generation is independent of heat transfer performance and condenser structure, and thus it will not be a meaningful merit to measure the performance of a condenser. This conclusion is verified by the numerical results presented in the next section.

In this study, experiment-based correlations for heat transfer, frictional pressure drop and void fraction, as summarized in Table 3.1, are adopted for smooth, helical and herringbone tubes. Since correlations for tubes smaller than 2 mm and working fluids other than common refrigerants are not available from the public literature, here we use the correlations listed in Table 3.1 to test the model. For electronics cooling application, correlations for smaller tubes and working fluids like water and HFE-7000 are of most interest, but unfortunately not available yet. How to develop condensation correlations through theoretic or numerical approach is an area that is very worthy to explore.

In table 3.1, the correlations for smooth tubes are very popular and widely adopted in the refrigeration and air conditioning industries, while the correlations by Miyara et al. (2000) are the only correlations in the open literature for herringbone tubes. Although there are several correlations available for helical tubes, the Yu and Koyama

(1998) correlation is chosen for it is easy to compare with the Miyara et al. (2000) correlation, because the two correlations are formulated in a similar way and both associated with void fraction evaluated based on the Smith (1969) correlation. By such a choice, the modeling results may reflect the essential difference of the tubes and minimize the discrepancy between different correlation families.

Table 3.1 Correlations used in condensation modeling

	Heat transfer coefficient correlation	Frictional pressure drop correlation	Void fraction correlation
Smooth tube	Cavallini and Zecchin (1971; 1974)	Friedel (1979)	Zivi (1964)
Helical tube	Yu and Koyama (1998)	Yu and Koyama (1998)	Smith (1969)
Herringbone tube	Miyara et al. (2000)	Miyara et al. (2000)	Smith (1969)

The modeled helical and herringbone tubes are assumed to be analogous to the tubes used by Miyara et al. (2000): the augmentation ratio of inner surface area is 1.83 for helical tubes and 2.19 for herringbone tubes. Condensation processes of two refrigerants R-22 and R-410A entering at 40^{o}C in tubes with effective inner diameter of D = 2 - 14 mm are modeled within mass flux range of 10 - 1000 kg/s-m^2. It must be emphasized here that the helical and herringbone correlations have never been tested with such a wide range of tube size and mass flux. Thus, the model-based predictions presented below must be utilized with caution beyond the applicable range of the correlations. The

correlations of heat transfer and pressure drop for helical tubes were established and verified through experiments with tubes larger than 5 mm, and those for herringbone tubes were only established and tested with 8 mm tubes.

In order to be easily compared with analytical results of entropy generation of an ideal constant pressure condenser, the tube inner surface temperature is taken to be constant T_w = 35°C in this project, while the more realistic case with tube temperature varying corresponding to local inside and outside thermal resistances will be considered in future research.

Figures 3.1-3.5 show the predicted variation of saturation temperature, heat transfer coefficient, frictional pressure gradient, acceleration pressure gradient, and required tube length measured from condenser inlet as functions of the refrigerant wetness 1-*x*. The results are presented for two refrigerants R-22 and R-410A condensing in 8 mm inner diameter smooth, helical and herringbone tubes, at mass fluxes of 10, 50, 100, 300, 500, and 800 kg/s-m^2. From these figures, two main observations can be made. The first one is that R-410A condensation results in smaller pressure drop and saturation temperature drop, as compared with R-22 condensation at the same conditions. This is consistent with the result of Cavallini (2006) that R-22 has a greater penalty factor. The second observation, as is evident in Figure 3.5, is that the helical tube and herringbone tube perform better (smaller total tube length is required for complete condensation from x = 1 to x = 0) than the smooth tube for both the R-22 and R-410A at all the mass fluxes investigated. Additionally, the herringbone tube is better than the helical tube in general, with an exception of R-410A condensation at mass fluxes greater than 500 kg/s-m^2.

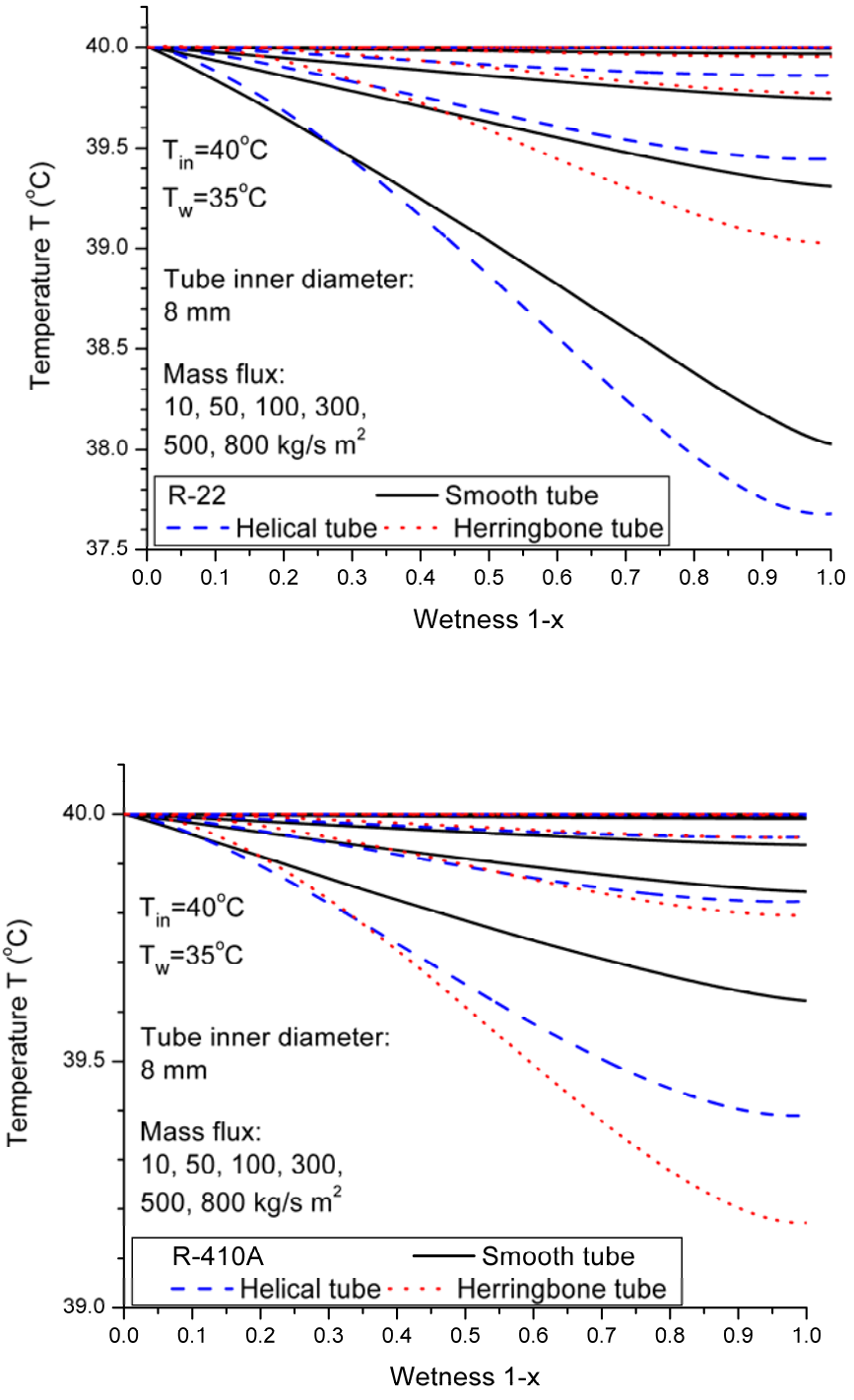

Figure 3.1 Saturation temperature vs. wetness

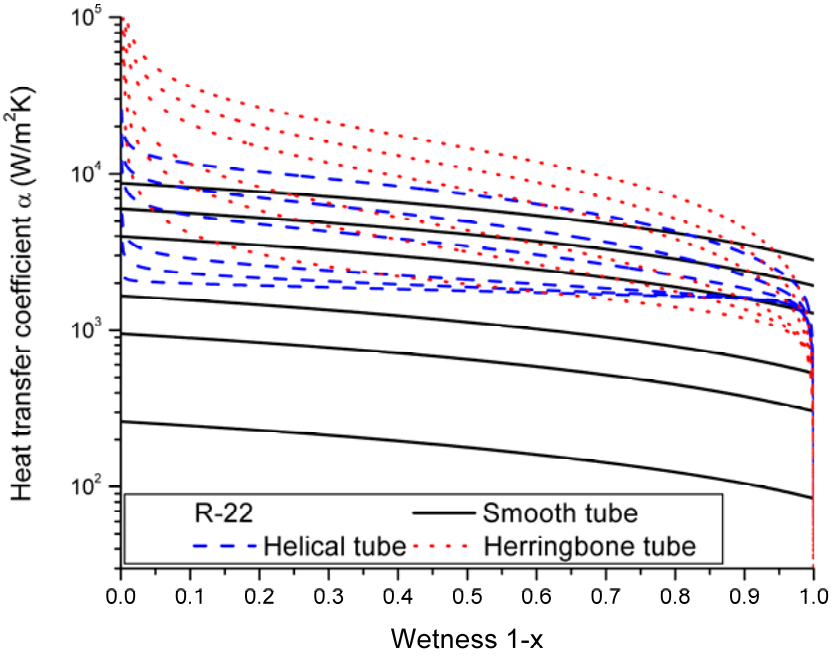

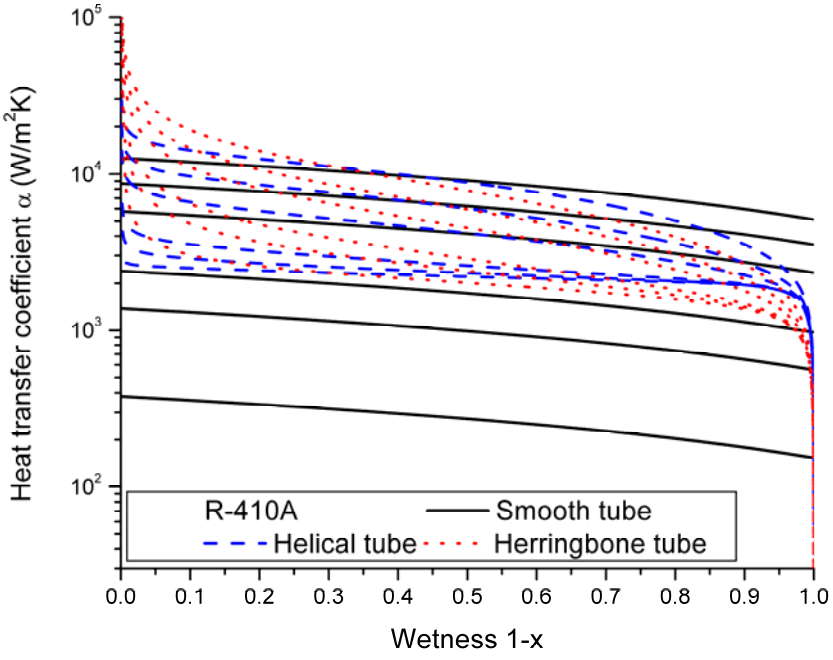

Figure 3.2 Heat transfer coefficient vs. wetness with the same operating conditions shown in Figure 3.1

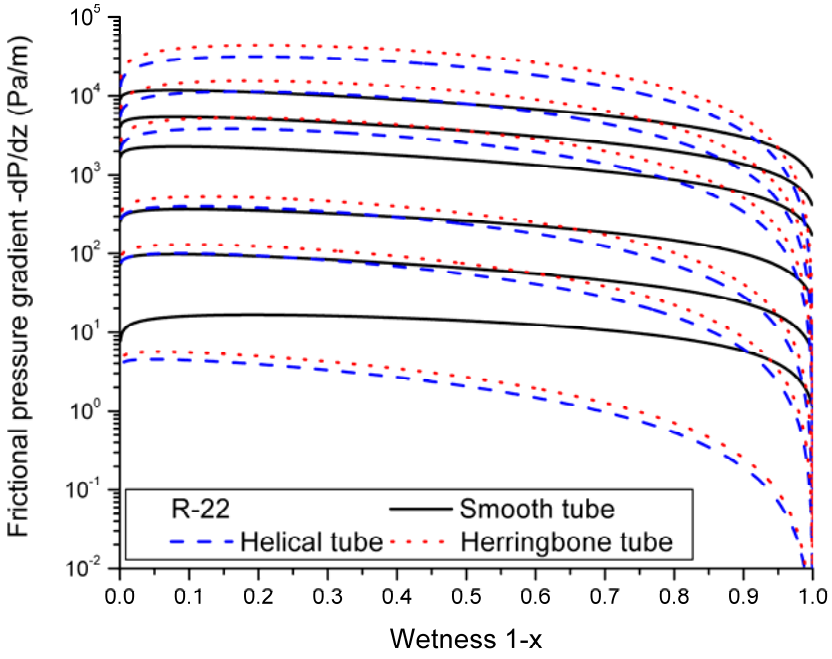

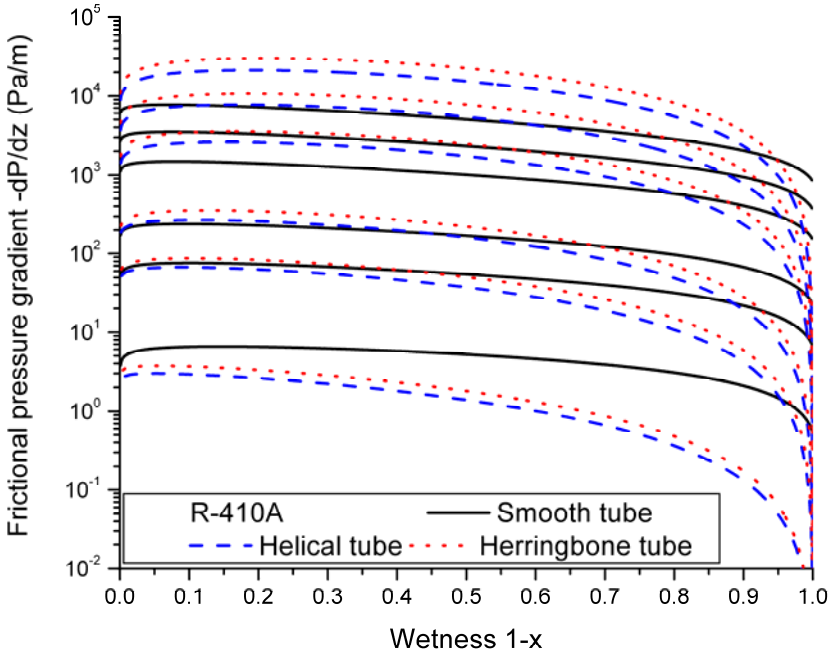

Figure 3.3 Frictional pressure gradient vs. wetness with the same operating conditions shown in Figure 3.1

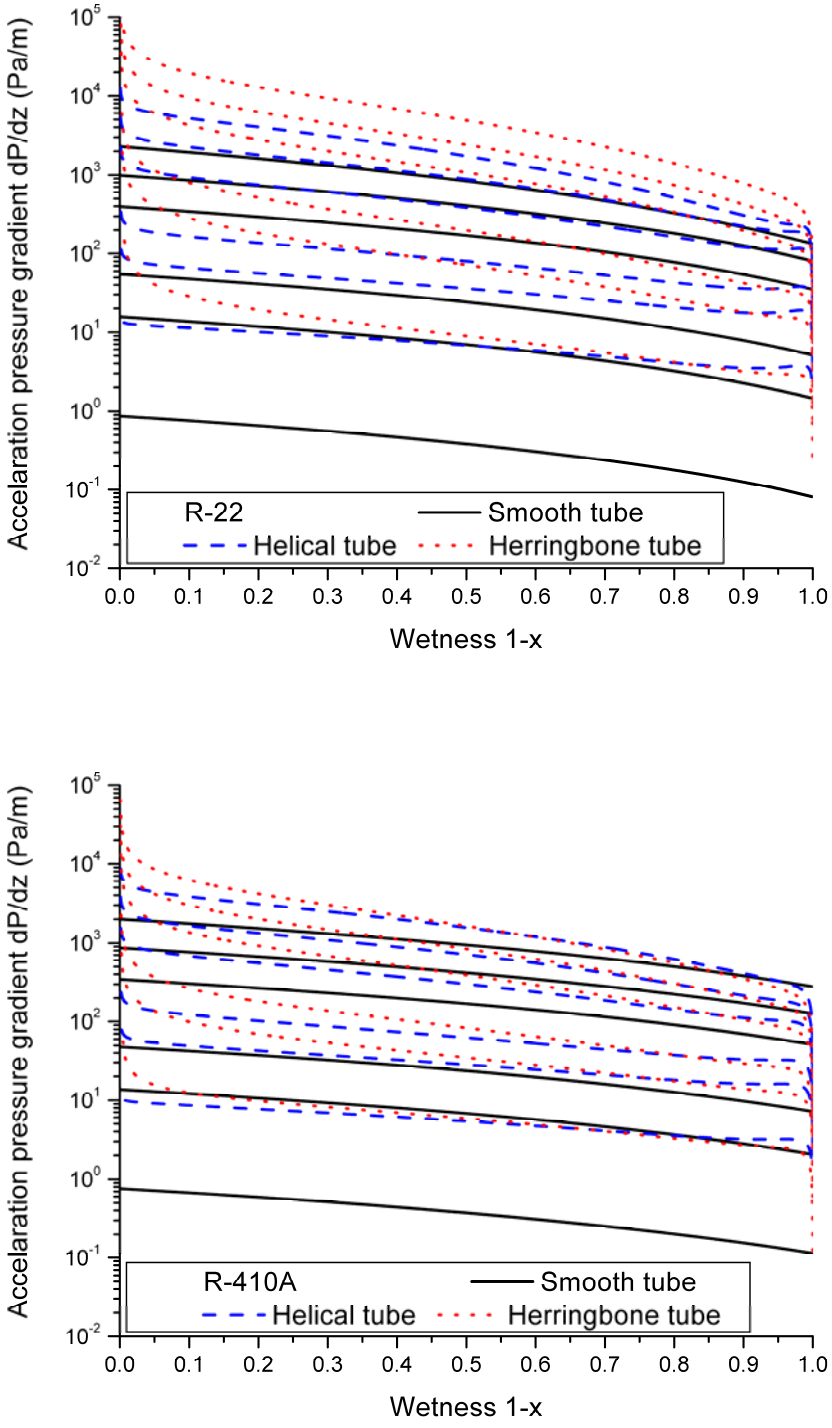

Figure 3.4 Acceleration pressure gradient vs. wetness with the same operating conditions shown in Figure 3.1

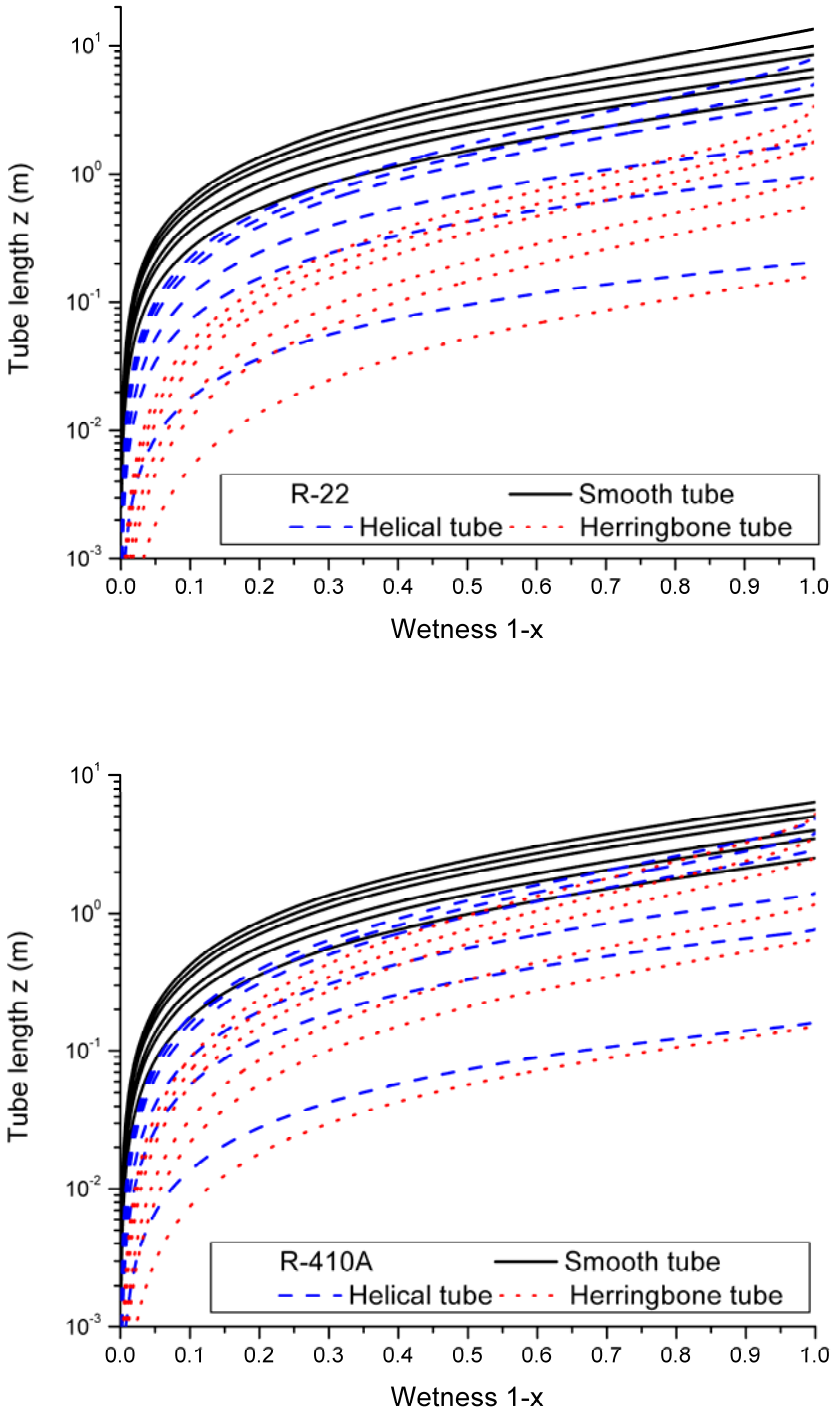

Figure 3.5 Tube length measured from condenser inlet vs. wetness with the same operating conditions shown in Figure 3.1

Figures 3.6-3.8 show modeling results for R-22 and R-410A condensation in smooth, helical and herringbone tubes with effective inner diameters of 2, 5, 8, 11, and 14 mm. Figure 3.6 shows total tube length, outlet temperature, and outlet pressure for complete condensation from $x = 1$ to $x = 0$ as functions of mass flux. For the whole mass flux range investigated, a smaller diameter tube always performs better than a larger tube of the same type (smooth, helical or herringbone). The predicted total tube length, pressure drop and temperature drop decrease with the tube inner diameter. This result is valid for both R-22 condensation and R-410A condensation. For R-22 condensation in tubes with the same cross sectional area (same effective inner diameter), a herringbone tube is generally better than a helical tube, and the helical tube is in turn better than a smooth tube, except for the helical tubes at mass fluxes higher than 800 kg/s-m^2, when pressure drop in the helical tubes is so high that the refrigerant temperature almost drops to the tube wall temperature. For R-410A condensation, helical tubes are always better than the smooth tubes of the same size, whereas herringbone tubes are better than helical and smooth tubes if the tubes are smaller than 5 mm or mass flux is lower than 400 kg/s-m^2. For larger tubes (D > 8 mm) at high mass fluxes, a herringbone tube can be worse than a helical tube or a smooth tube, due to the great pressure drop. It must be emphasized that the observations made above have not been quantified for helical and herringbone tubes knowing that the correlations are developed from a very limited range of application and do not fundamentally account for the tube enhanced geometry.

In order to compare the overall performance of the tubes with different surface structures and inner diameters based on the same heat transfer load, let us imagine

that there are a series of condensers consisting of parallel tubes. Each condenser is constructed by tubes of same type and size, but all the condensers have 1 m^2 total cross sectional area of refrigerant flow, i.e., a condenser constructed by small tubes has more tubes. For example, the 2 mm tube condenser has 16 times more tubes compared to the 8 mm tube condenser. Figure 3.7 shows a comparison between these condensers. The total refrigerant volume and inventory in each condenser as well as the total tube inner surface area (calculated from the effective inner diameter) are shown for condensation duties from 10 kg/s to 1000 kg/s. It is clear from Figure 3.7 that a condenser consisting of small diameter tubes can significantly save space (related to refrigerant volume), refrigerant consumption, and tube material (related to total tube surface area). The relative roles of the smooth, helical and herringbone tubes in performance of space, refrigerant, and tube material consumption are exactly the same as their performance in tube length shown in Figure 3.6. Therefore, the required total tube length for complete condensation serves as a convenient parameter to measure the overall performance of various tubes.

Finally, entropy generation rates associated with these imaginary condensers are shown in Figure 3.8. At low mass flux, when the entropy generation resulting from pressure drop is much less than the entropy generation due to heat transfer, the total entropy generation is almost identical to that of an isobaric condenser, no matter what types of tubes are used. Therefore, entropy generation cannot be used as a criterion to evaluate condenser performance at low mass fluxes. However, when mass flux is so high that entropy generation due to pressure drop is comparable to entropy generation from heat transfer, the rates shown in Figure 3.8 provide useful

information for condenser performance evaluation. Although significant pressure drop reduces entropy generation of heat transfer, the total entropy generation of a condenser accompanied with greater pressure drop is always greater than the total entropy generation of a smaller pressure drop condenser, with an isobaric condenser as a limit case of producing the least entropy generation.

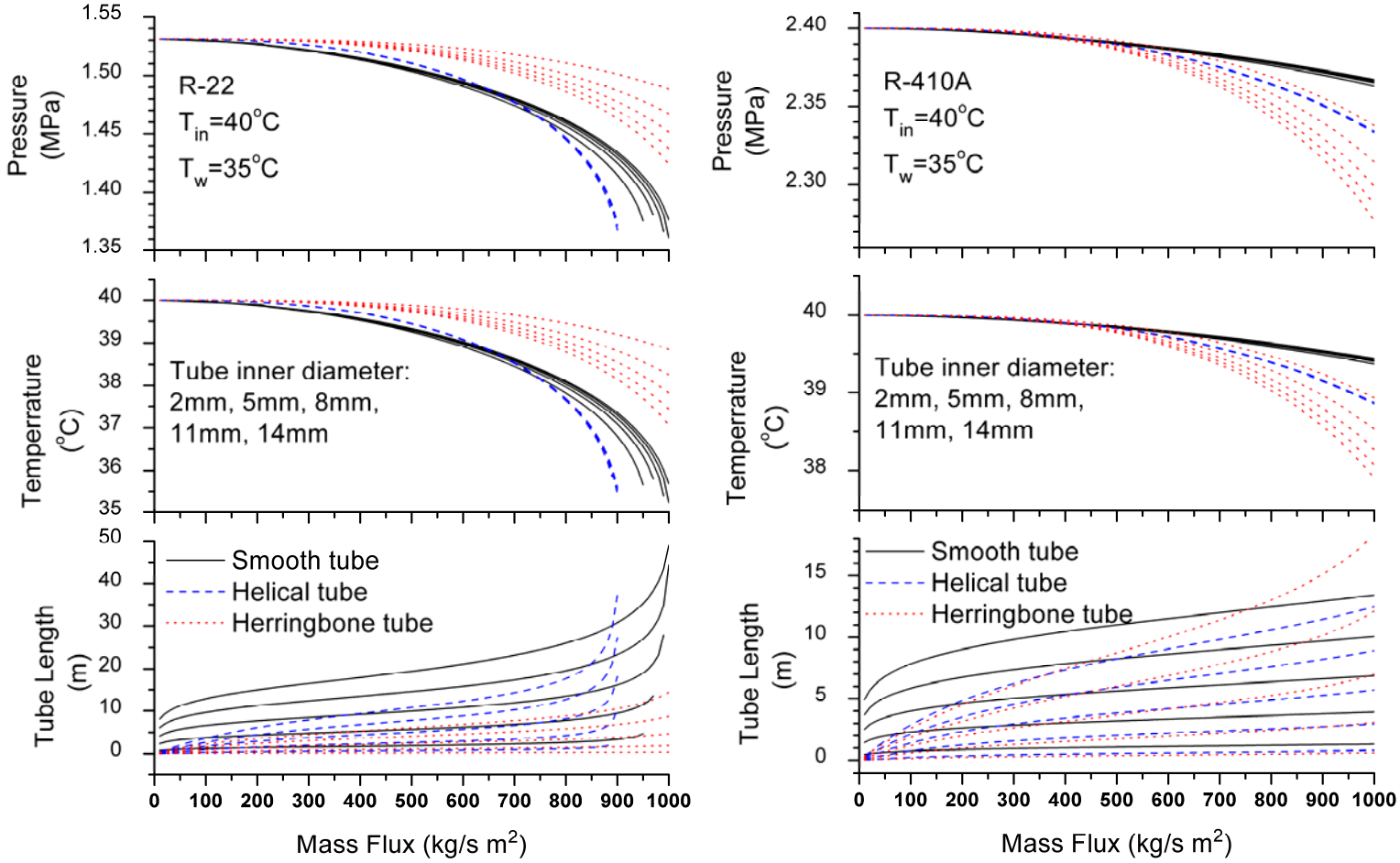

Figure 3.6 Total tube length, outlet temperature and outlet pressure as functions of mass flux

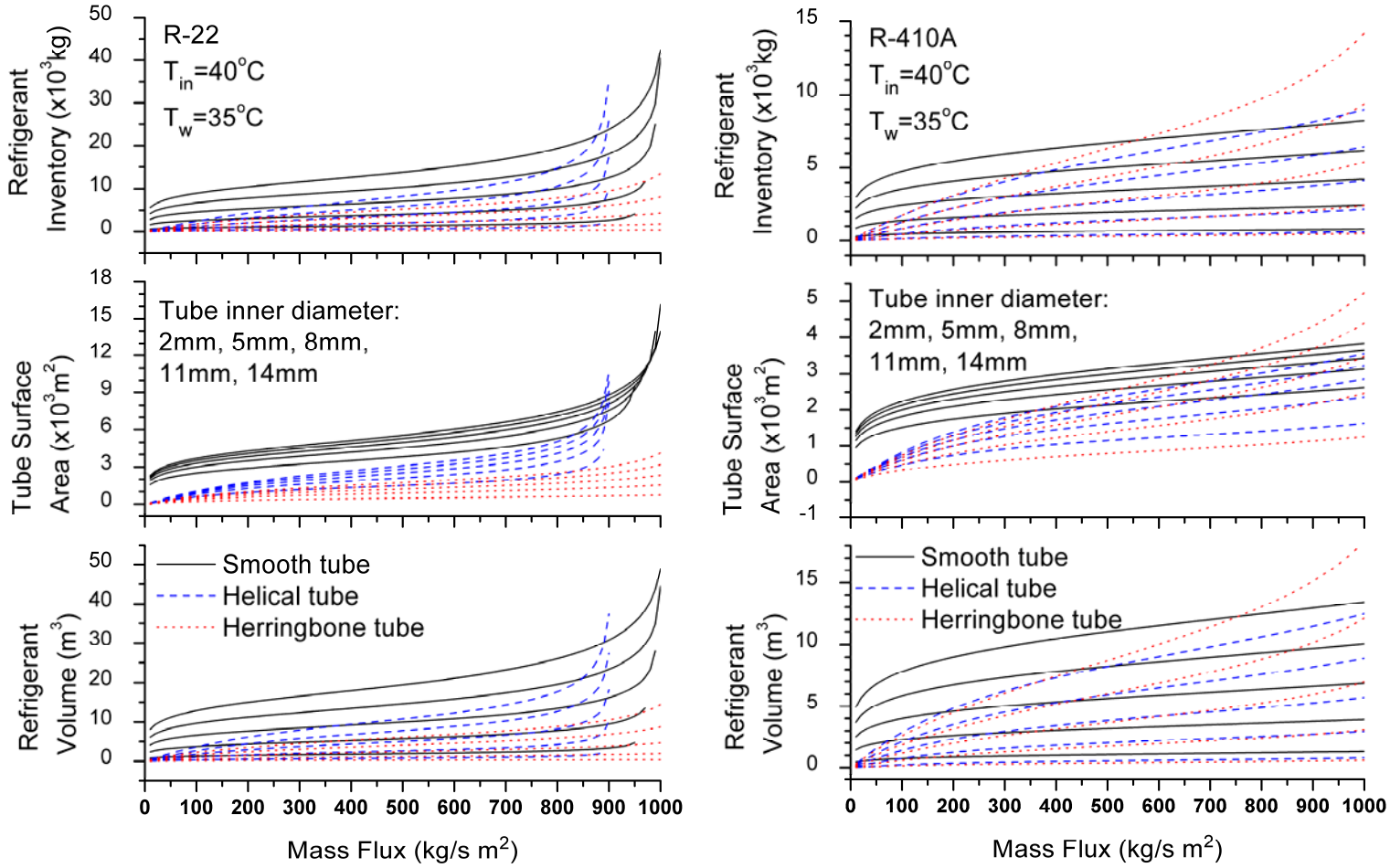

Figure 3.7 Refrigerant volume, tube surface and refrigerant inventory as functions of mass flux

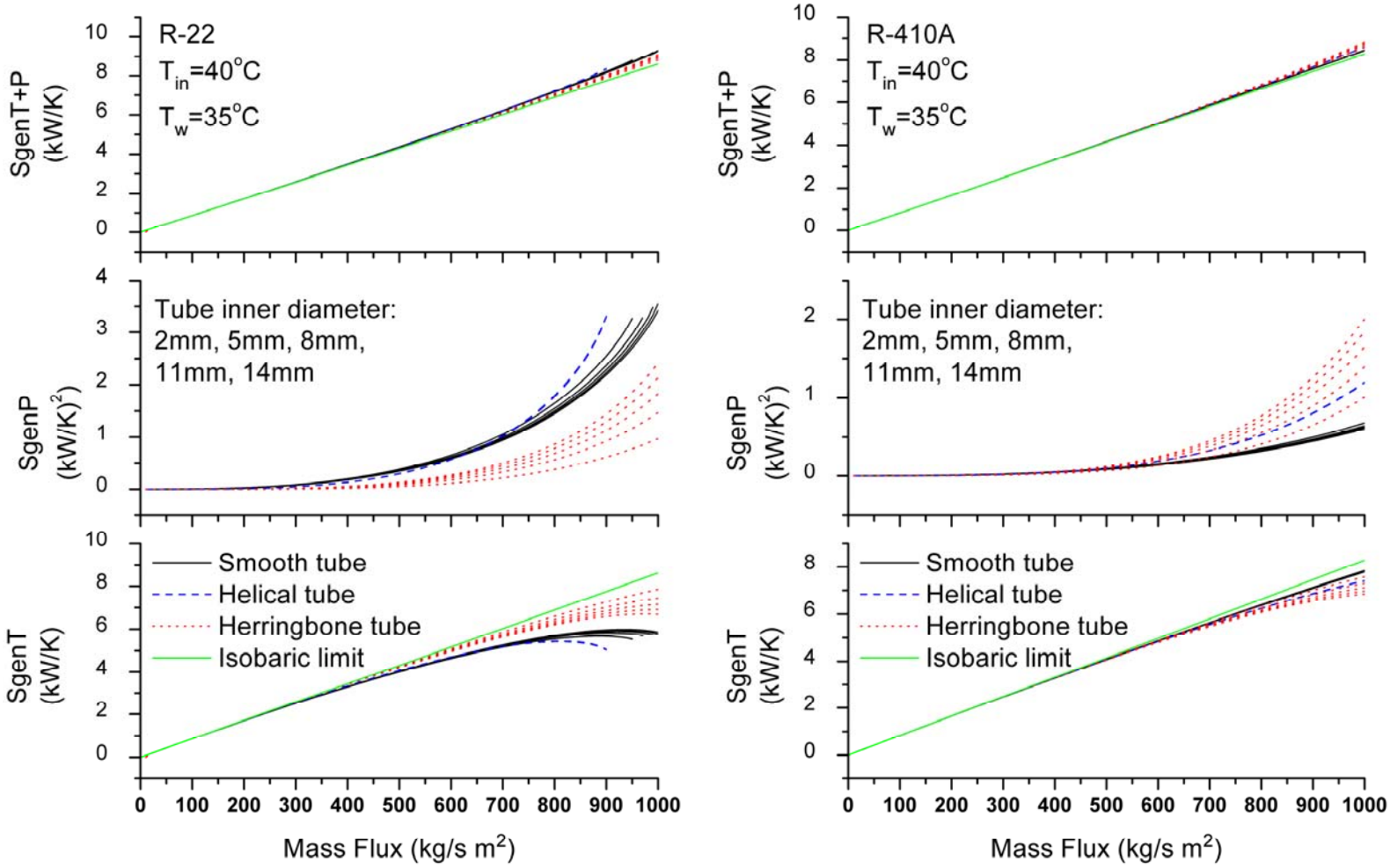

Figure 3.8 Entropy generation rate due to heat transfer, pressure drop and the both as functions of mass flux

3.2 **Air Flow Model**

For a fin-tube condenser, as the one in Singh et al.'s (2007) prototype and shown in Figure 3.9, it is possible to model the air flow across the heat sink in first order approximation as incompressible flow between parallel plates.

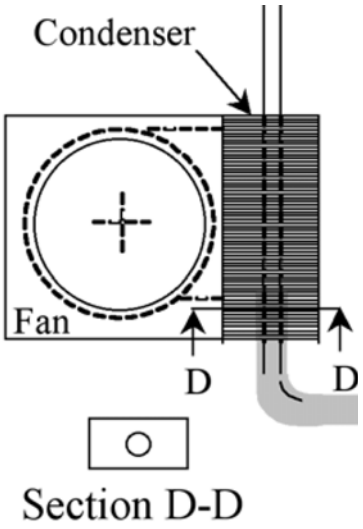

Figure 3.9 Schematic of a LHP condenser (Singh et al. 2007)

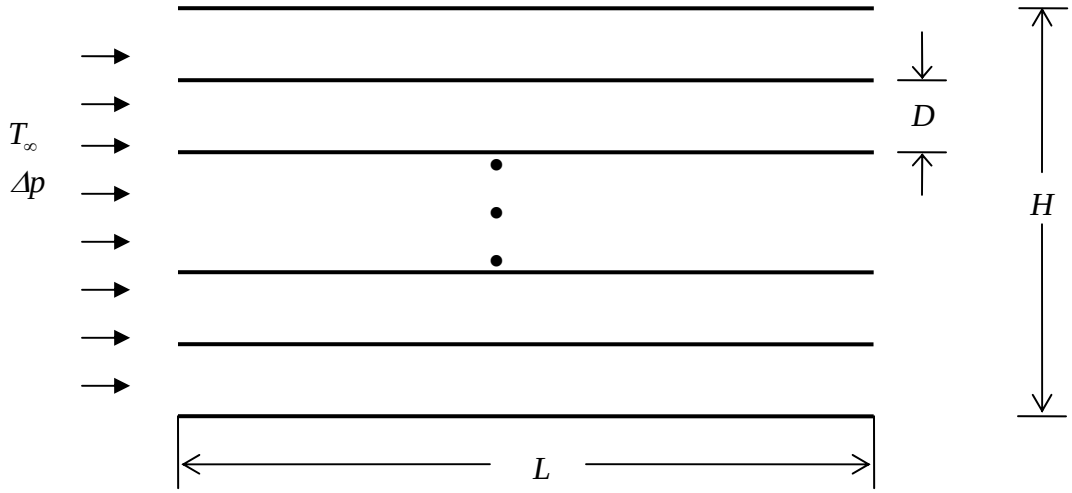

Figure 3.10 Stack of parallel plates cooled by forced convection

For developing laminar flow between parallel plates, as shown in Fig 3.10, there exits analytical solution. The overall Nusselt number for a channel that has a length L comparable with the entrance length is described well by Stephan's empirical formula (Shah and London 1978)

$$\frac{\bar{q}'' D_h}{\Delta T_{lm} k} = 7.55 + \frac{0.024(x^*)^{-1.14}}{1 + 0.0358(x^*)^{-0.64}\,\mathrm{Pr}^{0.17}}, \tag{3.9}$$

where hydraulic diameter $D_h = 2D$, $\bar{q}''$ is the L-averaged heat flux, and

$$x^* = \frac{Lk}{UD_h^{\,2}\rho c_p}, \tag{3.10}$$

$$\Delta T_{lm} = \frac{(T_w - T_\infty) - (T_w - T_{out})}{\ln[(T_w - T_\infty)/(T_w - T_{out})]}, \tag{3.11}$$

where U is the cross-section averaged longitudinal velocity and T_{out} is the bulk temperature of the stream at the channel outlet. Equation (3.9) is valid for 0.1 < Pr < 1000. The pressure drop across the channel can be estimated with the formula (Shah and London 1978)

$$f_{app}\,\mathrm{Re} = \frac{3.44}{(x^+)^{1/2}} + \frac{24 + 0.674/(4x^+) - 3.44/(x^+)^{1/2}}{1 + 0.000029(x^+)^{-2}}, \tag{3.12}$$

in which

$$\mathrm{Re} = \frac{UD_h}{\nu}, \tag{3.13}$$

$$x^+ = \frac{L/D_h}{\mathrm{Re}}, \tag{3.14}$$

$$f_{app} = \frac{D_h}{2L}\frac{\Delta p}{\rho U^2}. \tag{3.15}$$

For Singh et al.'s (2007) condenser, a heat sink with H = 50 mm, consisting of plate fins of L = 20 mm and width B = 10 mm, and operating with air flow rate 0.1 m^3/min, the total heat removal (heat load) as a function of fin spacing predicted by Equations (3.9) and (3.12) is shown in Figure 3.11. The optimum fin spacing in Figure 3.11 is 0.8 mm corresponding to a maximum heat load of 74 W. Singh et al. (2007) did not provide any information for the optimum design of their condenser heat sink, but the fin spacing of their condenser is actually 0.8 mm: an excellent agreement with the optimum spacing shown in Figure 3.11. Furthermore, Singh et al.'s (2007) condenser is designed to dissipate 50 W heat load, which is also in good agreement with the maximum heat load predicted by Equations (3.9) and (3.12).

Based on a dimensionless analysis of Equations (3.9) and (3.12), Bejan and Sciubba (1992) obtained the following relations for optimum fin spacing and maximum heat load

$$D_{opt} = 3.033\left(\frac{\nu k L^2}{c_p \Delta P}\right)^{1/4}, \tag{3.16}$$

$$Q_{\max} = 0.479\left(\frac{\rho \Delta p}{\mathrm{Pr}}\right)^{1/2} HBc_p(T_w - T_\infty). \tag{3.17}$$

which allow quick calculations for optimum fin-tube condenser design.

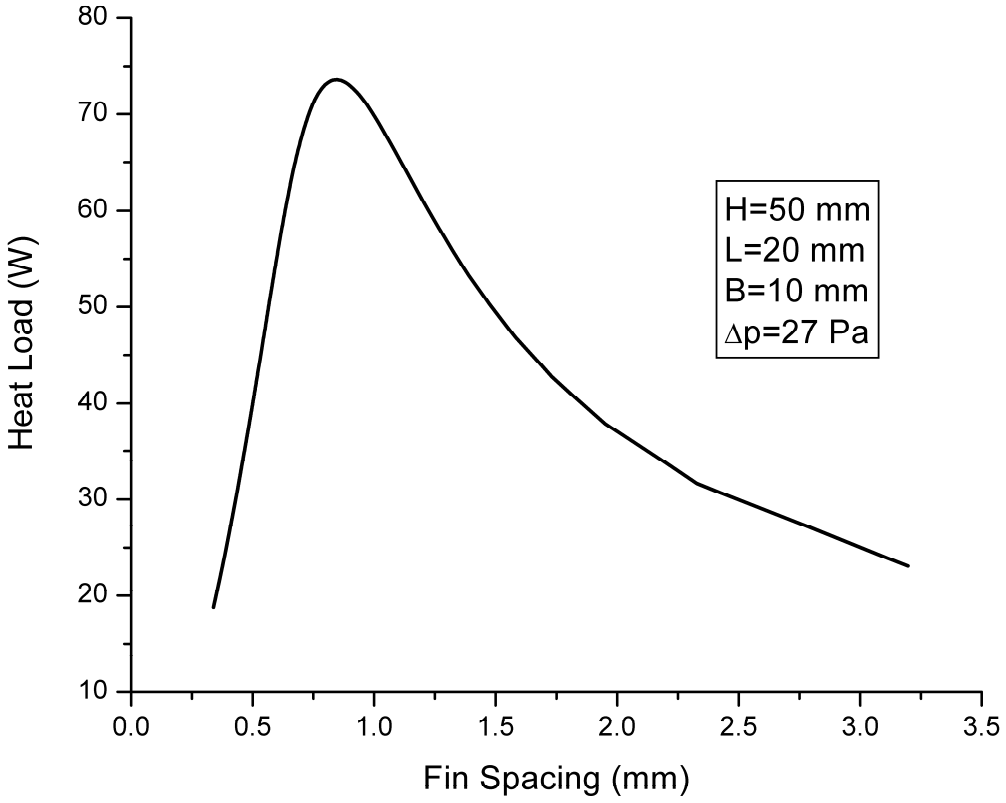

Figure 3.11 Predicted heat load as a function of fin spacing

3.3 Evaporator Model

Evaporator is a critical component of a LHP. There are basically two geometric configurations for LHP evaporators: cylindrical evaporator, which is widely used in space applications, and flat plate evaporator, which is more appropriate to electronics cooling applications.

There have been extensive modeling studies on heat transfer in wick structure. In general, the previous studies can be put into two categories. The first category is macro scale model, analyzing heat and fluid flow through a porous medium based on Darcy's

law. Cao and Faghri (1994a, b) provided analytical solutions and numerical solutions of flow and heat transfer for liquid saturated porous structure. Demidov and Yatsenko (1994) numerically investigated the heat and mass transfer processes with a free boundary corresponding to the surface of the inter-phase transition inside the capillary structure. Many recent numerical modeling studies (e.g., Figus et al. 1999; Kaya and Goldak, 2006; Ren and Wu 2007; Ren et al. 2007a, b) focused on calculating the liquid-vapor interface location. In all these macro scale models, film evaporation at a pore level has not been considered, so the local heat transfer coefficient cannot be obtained.

The modeling studies in the second category calculate heat and mass transfer in the pore level of the porous structure based on thin film evaporation theory and integrate local heat transfer to obtain overall heat transfer rate, as did by Khrustalev and Faghri (1995).

Zhao and Liao (2000) experimentally investigated the characteristics of capillary-driven flow and phase-change heat transfer in a porous structure heated with a finned heating plate. Their experimental apparatus is shown in Figure 3.12.

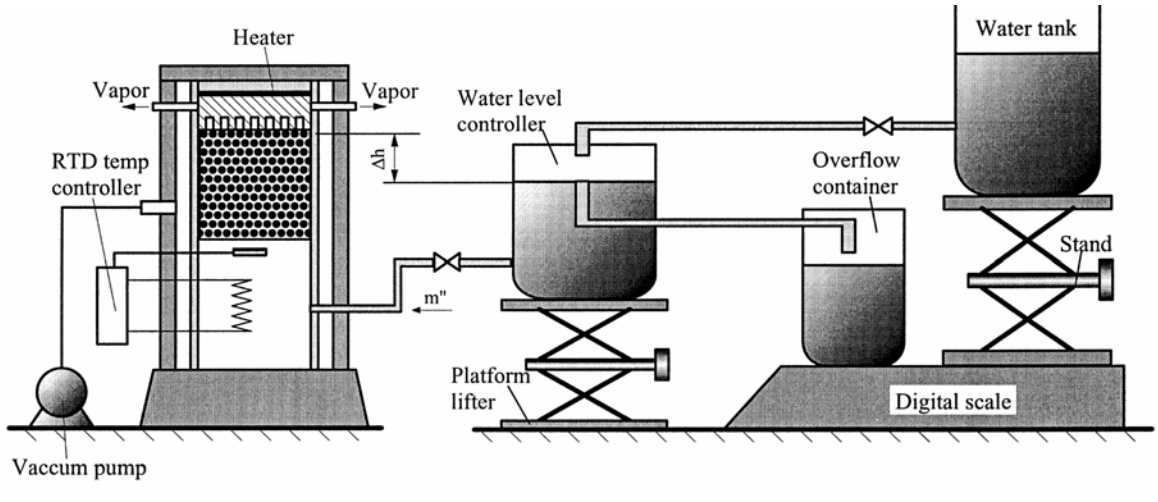

Figure 3.12 Schematic of experimental apparatus for studying phase-change heat transfer in porous structure (Zhao and Liao 2000)

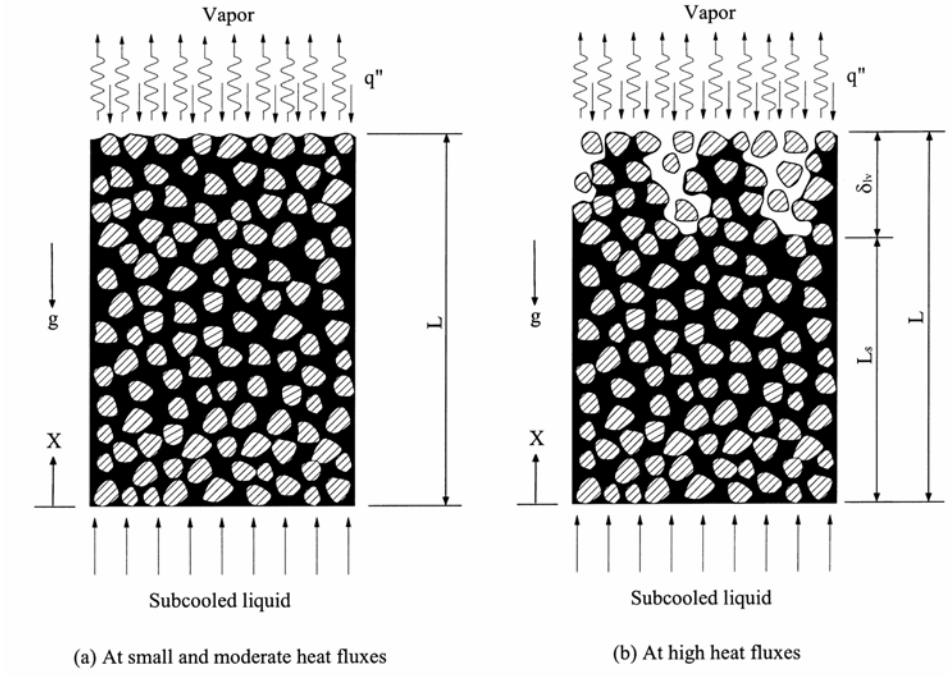

Figure 3.13 Phase-change behaviors at different heat loads (Zhao and Liao 2000)

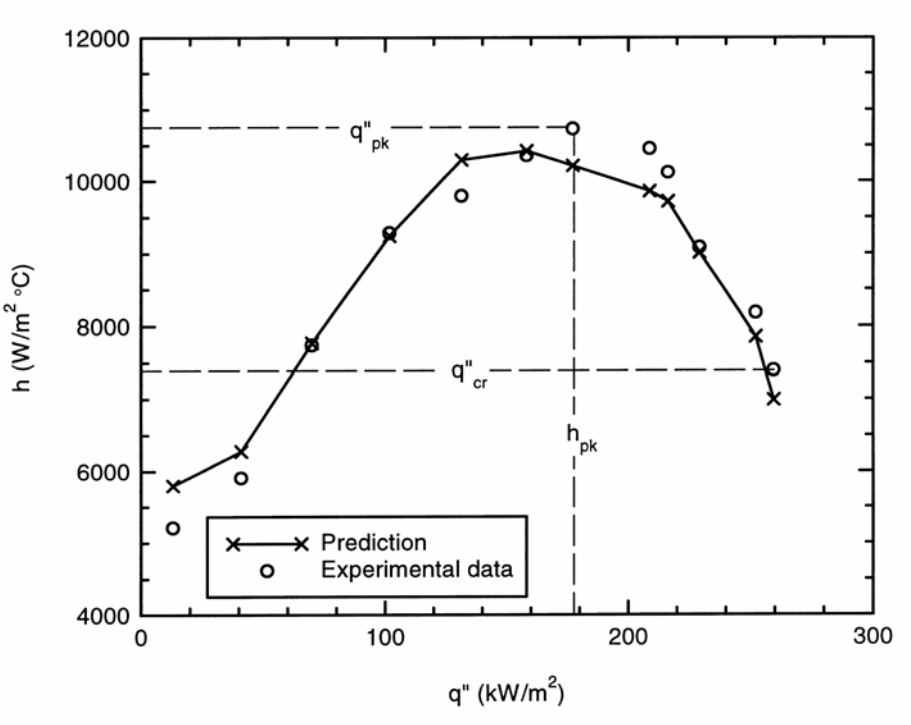

Figure 3.14 Variation of the heat transfer coefficient versus the imposed heat flux (Zhao and Liao 2000)

Zhao and Liao's (2000) experiments showed that for small and moderate heat fluxes, the whole porous structure was fully saturated with liquid except adjacent to the horizontal heated surface where evaporation took place uniformly, as shown in Figure 3.13 (a); for higher heat fluxes, a two-phase zone developed in the upper portion of the porous structure while the lower portion of the porous structure was saturated with subcooled liquid, as shown in Figure 3.13 (b). The observed heat transfer coefficient, as shown in Figure 3.14, increased during the small and moderate heat flux stage, but decreased at the high flux stage. When the imposed heat flux was further increased, a vapor blanket formed below the heated surface and the corresponding critical heat flux was reached. Furthermore, the heat transfer coefficient calculated essentially based on

Khrustalev and Faghri's (1995) approach was in good agreement with the experimental data, as shown in Figure 3.14

For LHP evaporator design, the peak heat transfer coefficient case shown in Figure 3.14 is of the most interest, since the evaporation heat transfer coefficient increases with the increasing input heat flux when $q'' < q''_{pk}$ and decreases when $q'' > q''_{pk}$, implying a optimum operation point. For occasional heat flux exceeding q''_{pk} but still significantly lower than q''_{cr}, the operation of the LHP still has a safe zone.

A design based on the peak point in Figure 3.14 can be modeled much easier than that for a higher flux, because for all the operations with $q'' < q''_{pk}$ the shape and location of the liquid-vapor interface are known and thus do not need to be calculated. As a result, the analytical model of Cao and Faghri's (1994a) should be sufficient for solving the fluid flow and heat transfer problem.

In order to model the evaporator of Singh et al.'s (2007) LHP prototype, as shown in Figure 3.15, we consider the porous flow and heat transfer problem of a unit 'cell' of the wick structure outlined in Figure 3.16. For the given geometry and boundary conditions, analytical solutions for velocity and temperature distributions are obtained following Cao and Faghri (1994a). Figure 3.17 shows the velocity and temperature results for a case of heat flux input of $q_{in} = 5\ \mathrm{W/cm^2}$, corresponding to a heat load of ~35 W applied to the evaporator shown in Figure 3.15. The modeling results indicate that the local temperature is higher adjacent to the fin and lower adjacent to the vapor channel at the surface of the wick structure, as compared with the saturation temperature, but the temperature difference is only around 1^{o}C. Such a small temperature difference contributes to a small evaporator thermal resistance, and in most situations can be ignored,

as compared with a much greater thermal resistance related to the LHP condenser operation.

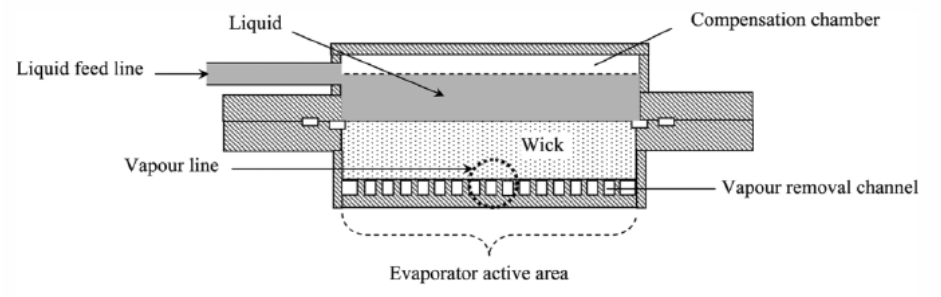

Figure 3.15 Schematic of a LHP evaporator (Singh et al. 2007)

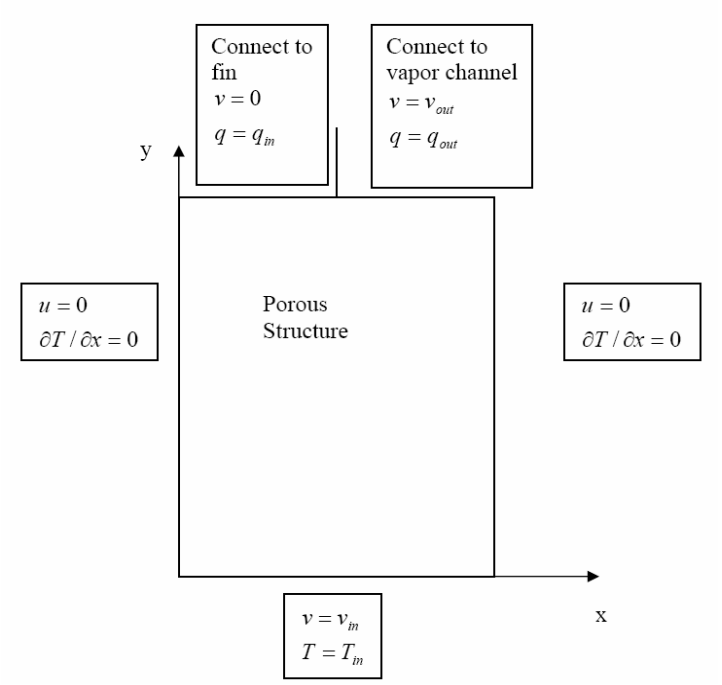

Figure 3.16 Schematic of the evaporator model showing the calculation domain and boundary conditions

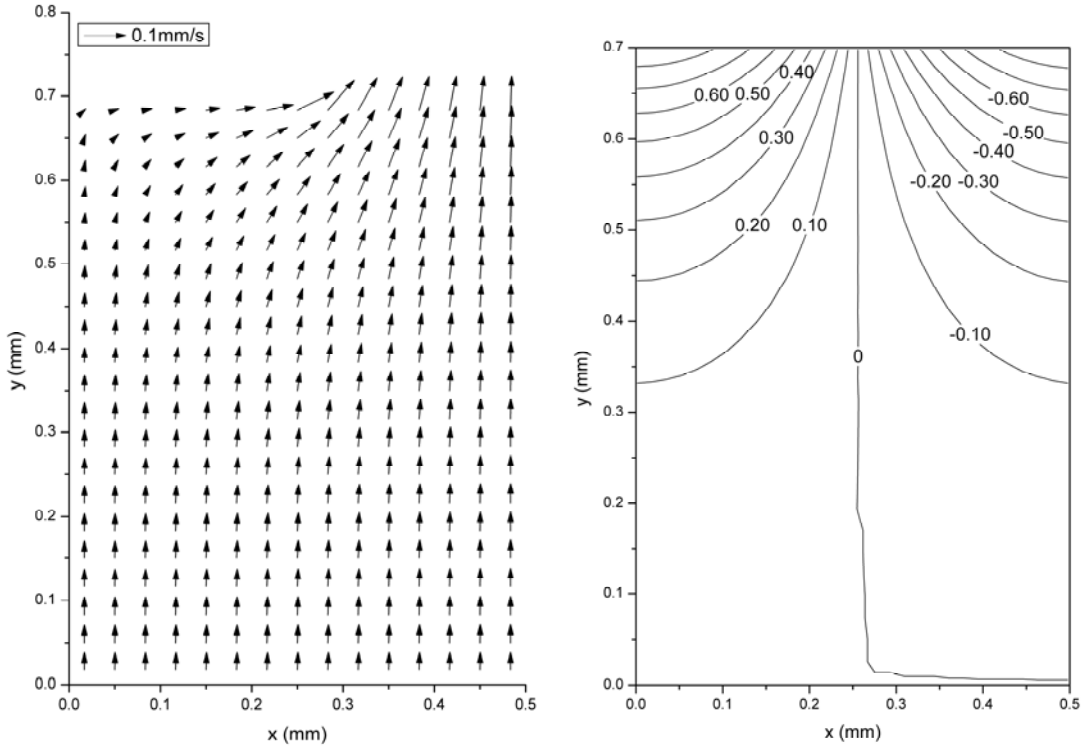

Figure 3.17 Modeling results of velocity and temperature distributions for the porous flow in the evaporator

3.4 Summary

Mathematical models have been presented in this chapter for quantitatively simulating the operations of in-tube condensation, air flow through parallel plate fins, and evaporation from saturated porous structure.

In order to thoroughly evaluate the performance of tubes in condensation heat transfer, both accurate experimental measurements and reliable numerical models that can correctly integrate appropriate experiment-based correlations are needed. In this research, a numerical model for in-tube condensation is presented comparing performances of smooth, helical and herringbone tubes with R-22 and R-410A under different operating conditions. The modeling results show that under all the conditions

investigated, a smaller diameter tube always performs better than a larger diameter tube by saving space, refrigerant and tube material. However, the validity of this observation has not been verified for microfin geometry. For tubes with the same cross sectional area, herringbone tube is the best for R-22 condensation at any mass flux below 1000 kg/s-m^2 and for R-410A condensation in small tubes or at low mass fluxes. The modeling results also show that the required total tube length for complete condensation serves as a convenient and physically sound parameter to measure the overall performance of tubes with various inner structures and under various operating conditions, while entropy generation cannot serve as a criterion to evaluate a condenser with negligible pressure drop, but can provide valuable information for measuring performance of a condenser with significant pressure drop. Since the helical and herringbone correlations used in the model have not been tested over the whole modeling range of tube size and mass flux, the modeling predictions should be used with sufficient caution.

Air flow through plate fins can be approximately modeled as developing flow between parallel plates. Analytical solutions for the heat transfer and pressure drop of this problem provide convenient tool for optimum fin spacing design, and predict results in very good agreement with the condenser design by Singh et al. (2007).

Experimental investigation (Zhao and Liao 2000) on the characteristics of capillary-driven flow and phase-change heat transfer in a porous structure heated with a finned heating plate shows that the liquid saturated wick structure provides better evaporation heat transfer performance, and allows a simpler evaporator modeling configuration, which can be analytically solved (Cao and Faghri 1994a). The modeling

results for Singh et al.'s (2007) LHP evaporator conclude that very small thermal resistance is associated with the evaporator operation.

Chapter 4

LHP Prototype Design and Modeling

4.1 LHP Prototype Design

LHP prototype design is a comprehensive process, and often involves iterations based on trial-and–error, as is shown schematically in Figure 4.1. The process of LHP prototype design usually starts from an objective that defines the purpose of the LHP to be designed. Then, various design requirements should be specified and quantified. Design requirements for a LHP used to cool notebook computer, for example, will specify the design values for operational heat load, maximum heat source temperature, ambient air temperature, space constraints on the LHP size and shape, maximum noise level, target cost, etc. The main phase of prototype design is thus to select materials and size components based on quantitative design tools. Once a prototype is designed and manufactured, it should be tested in laboratory to check if all the design requirements are satisfied. If not, necessary revisions to the prototype design have to be made, or certain design requirements have to be relaxed

As an example, let us consider designing a LHP for cooling the central processing unit (CPU) of a notebook computer. Let us assume the waste heat released by a notebook CPU is 25 to 50 W, and the heating area of the chipset is as small as 1 to 4 cm^2. The thermal management problem is further complicated by both the limited available space and the restriction to maintain the chip surface temperature below about 100^oC. These requirements, together with other constraints, such as noise level and target cost,

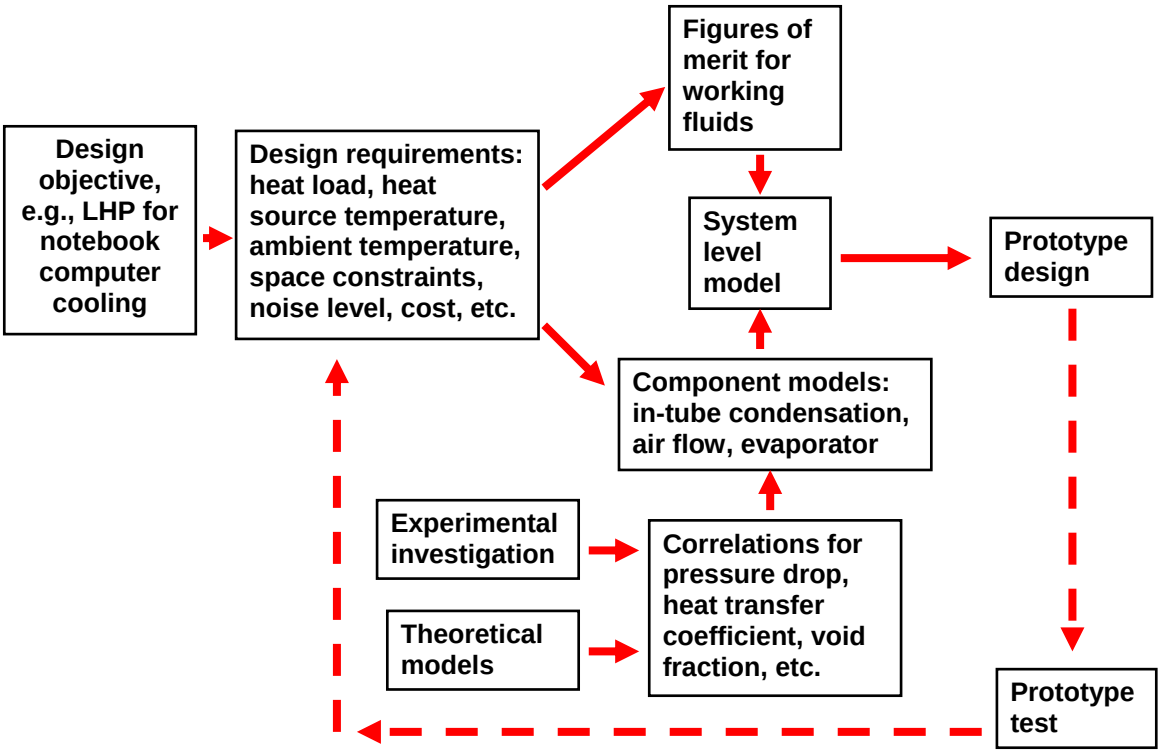

Figure 4.1 Flow chart showing LHP prototype design process

Table 4.1 Main design parameters of the LHP prototype by Singh et al. (2007)

Parameter	Value
Evaporator Shape	Flat Disk Shaped
Evaporator heating face area, cm^2	7.1
Heat Load simulator area (heater size), cm^2	3.75
Body Material	Copper
Wick Material	Nickel
Wick Effective Pore radius, µm	3-5
Vapour Line Length, mm	150
Liquid Line Length, mm	290
Vapour & Liquid Line Diameter (Internal/External), mm	2/3
Condenser Type	External Fins
Condenser Length, mm	50
Condenser Fin Surface Area, cm^2	200
Working Fluid	Water

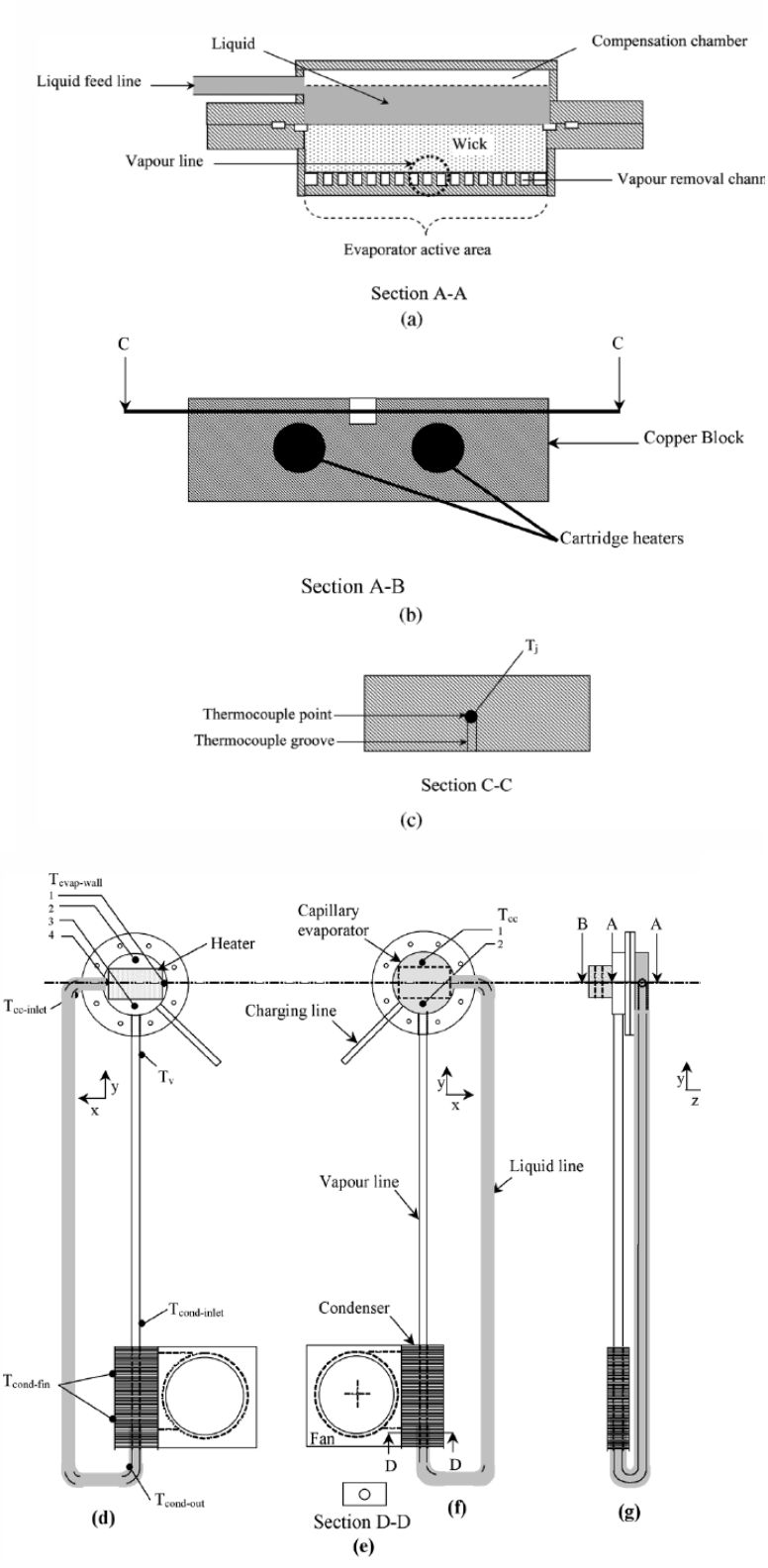

Figure 4.2 Schematic of the LHP prototype designed and tested by Singh et al. (2007)

should be carefully addressed when considering the LHP architecture and detailed component design.

Figure 4.2 shows schematically a LHP prototype designed by Singh et al. (2007) for notebook computer CPU cooling. Main design parameters are listed in Table 4.1. This LHP prototype has a flat plate evaporator and uses water as working fluid, in contrast to the conventional LHP configuration of a cylindrical evaporator with ammonia as working fluid, which was widely used in space applications (e.g. Maydanik 2005; Ku 1999).

A flat evaporator is preferable due to lower interface thermal resistance and easy integration inside the limited space of notebook computer. The flat shaped evaporator is associated with a small thickness, which is critical for notebook computer but not for space applications, and improves thermal contact between the heat source (CPU chip) and the evaporator wall.

For the thermal control of electronics in space, a low temperature working fluid like ammonia and a durable material like stainless steel for the loop container are the best options. It has been shown in Chapter 2 that ammonia has a much higher figure of merit than water or HFE-7000, no matter the capillary limit or the heat leak effect is concerned. However, in ground based electronics cooling, certain safety measures have to be observed that restrict the use of high pressure, toxic or inflammable working fluids like ammonia, acetone or different grades of alcohol. In this regard, water can be considered as the ideal working fluid, because it has efficient heat transfer characteristics, presents no hazard to people, and is fully compatible with high thermal conductive material like copper. Actually, the copper-water combination is considered very competitive and has been widely used in conventional heat pipes for ground based electronics cooling.

The material and structure of the capillary wick play an important role in LHP design, since it is the capillary pressure head that provides the driving force for circulating working fluid around the loop, and the effective thermal conductivity of the wick structure is closely related to heat leak. Using low conductive capillary structure will decrease the heat leak to the compensation chamber, but also decrease the heat transfer to the liquid-vapor interface. To balance these conflicting effects, nickel, with an intermediate value of thermal conductivity, serves as an optimum choice for the wick structure material. In addition, nickel has a great capability to be sintered in small pore sizes with relatively high porosity, so that sufficient capillary force can be generated.

4.2 LHP Prototype Modeling

Once a LHP concept is defined and the design requirements have been identified, the next step in the design process will be to model its feasibility. The prototype by Singh et al. (2007) will be used here to demonstrate the modeling tools developed in chapters 2 and 3.

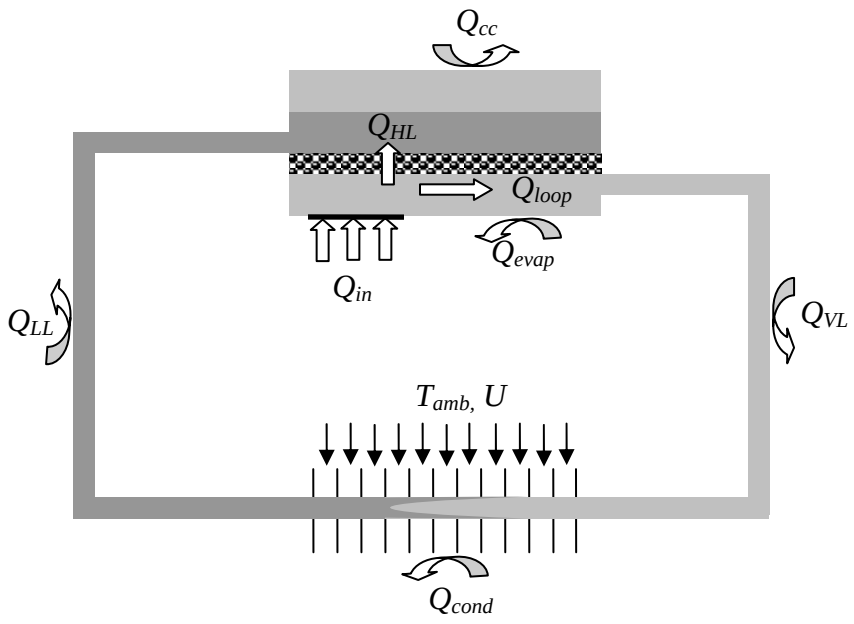

Figure 4.3 Schematic of LHP Model

For a given heat load Q_{in}, the overall energy balance is (Figure 4.3)

$$Q_{in} = Q_{loop} + Q_{HL}, \tag{4.1}$$

where $Q_{loop} = \dot{m}h_{lv}$ is the heat transferred by the circulating working fluid, and Q_{HL} is the heat leak, i.e., heat transferred backward to the compensation chamber through the conduction of the wick. For steady state operation of the LHP, Q_{in} should be equal to the total heat removal from all the components (Figure 4.3),

$$Q_{in} = Q_{cond} + Q_{evap} + Q_{VL} + Q_{LL} + Q_{cc}, \tag{4.2}$$

where $Q_{cond}, Q_{evap}, Q_{VL}, Q_{LL}, Q_{cc}$ represent heat rejections through condenser, evaporator, liquid line, vapor line, and compensation chamber, respectively. For the condenser heat rejection, only forced air convection is considered, since the natural convection and radiation contributions are much smaller than the forced convection; while for the heat losses through all other components, both natural convection and radiation are included

in the model. Heat transfer correlations for natural convection around horizontal walls with hot surface facing down and facing up (Bejan 2004), respectively, are adopted for modeling the heat losses through external surfaces of the flat evaporator and the compensation chamber, while the correlation for natural convection around horizontal cylinders (Bejan 2004) are adopted for modeling heat losses from the vapor and liquid lines. All the heat losses by radiation is approximated by

$$q'' = \varepsilon \sigma_{SB} (T_w{}^4 - T_{amb}{}^4), \tag{4.3}$$

where ε is emissivity, σ_{SB} is Stephan-Boltzmann constant, and T_w and T_{amb} are temperatures of the LHP wall and the ambient, respectively.

Heat transfer related to the condenser needs to be considered more accurately, since the condenser is the designed component for heat rejection. Heat transfer from the working fluid cross the condenser wall to the air flow can be written as

$$\begin{aligned} \frac{dQ_{cond}}{dz} &= \pi D_i h_{pc} (T_{sat} - T_w) = \pi D_o h_{air} (T_w - T_{amb}) \\ &= \dot{m} \left[(1-x) c_{pl} + x c_{pv} \right] \frac{dT_{sat}}{dz} + \dot{m} \frac{dx}{dz}, \end{aligned} \tag{4.4}$$

where D_i and D_o are the inner and outer diameters of the condenser tube, respectively, h_{pc} is the two-phase heat transfer coefficient of the working fluid inside the condenser pipe, and h_{air} is the heat transfer coefficient associate with the external air flow. For the modeling results presented in this section, the correlation by Shah and London (1978) is adopted for evaluating h_{air}, and that by Cavallini and Zecchin (1971; 1974) is used for evaluating h_{pc}, except that the Chato (1962) correlation is used for stratified flow pattern when the dimensionless vapor velocity is less than 1.0, i.e.,

$$j_g^* \equiv \frac{xG}{\sqrt{D_i g \rho_v (\rho_l - \rho_v)}} < 1.0\,, \tag{4.5}$$

based on the Breber et al.'s (1980) flow regime map. During the process of condensation, the working fluid temperature depends on its pressure, which is controlled by the frictional pressure gradient and acceleration pressure gradient. The acceleration pressure gradient is closely related to the void fraction, and the frictional pressure gradient depends upon the two-phase flow pattern. In the LHP prototype modeling considered here, the correlation by Zivi (1964) is used for evaluating void fraction and acceleration pressure gradient, and the frictional pressure drop is evaluated based on the Friedel (1979) correlation.

In all the modeling calculations, the working fluid properties are considered as functions of temperature, and the polynomial approximations given by Faghri and Zhang (2006) are adopted for calculating the temperature-dependent thermophysical properties of water.

The overall modeling process can be summarized as the following steps:

1. Start from a given temperature of vapor in the evaporator: T_{evap}
2. Assume the vapor is saturated, so that:

$$p_{evap} = p_{sat@T_{evap}}\,. \tag{4.6}$$

3. Find mass flow rate $\dot{m}$ that satisfies:

$$\dot{m} h_{lv@T_{evap}} = Q_{cond} + Q_{evap} + Q_{VL} + Q_{LL} + Q_{cc} - Q_{HL}\,. \tag{4.7}$$

4. Obtain the corresponding heat load:

$$Q_{in} = \dot{m} h_{lv@T_{evap}} + Q_{HL}\,. \tag{4.8}$$

The modeling results for the LHP prototype by Singh et al. (2007) are shown in Figs. 4.4–4.9.

In Figure 4.4, the predicted temperature of the condenser outer wall averaged over the total length of the condenser is compared with the experimental data measured by Singh et al. (2007). When the ambient temperature is fixed according to the actual experimental condition, ~24^{o}C, the condenser wall temperature increases with the heat load and decreases with the air flow rate. Although the volume flow rate of the air through the fin-tube condenser is not reported by Singh et al. (2007), Figure 4.4 indicates that an air flow rate around 0.06 – 0.07m^3/min provides the best fit to the measured data.

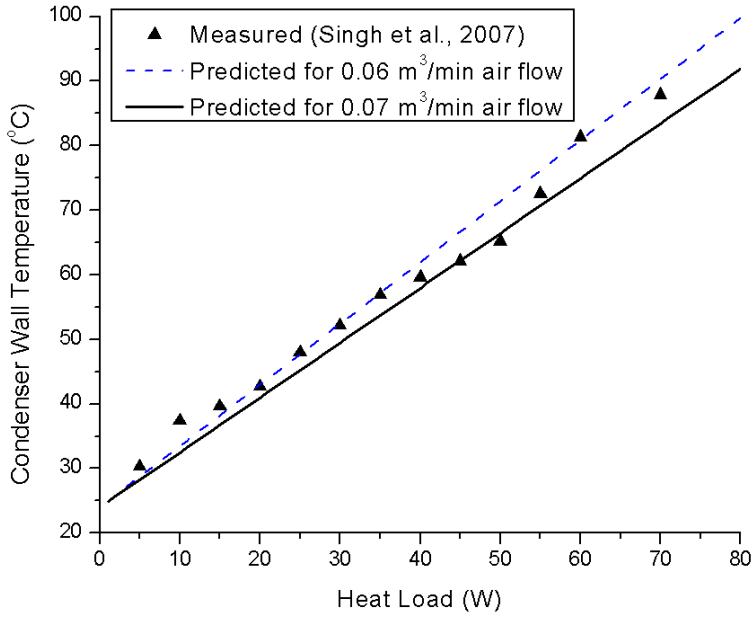

Figure 4.4 Comparison of LHP condenser temperatures between experimental data and modeling predictions

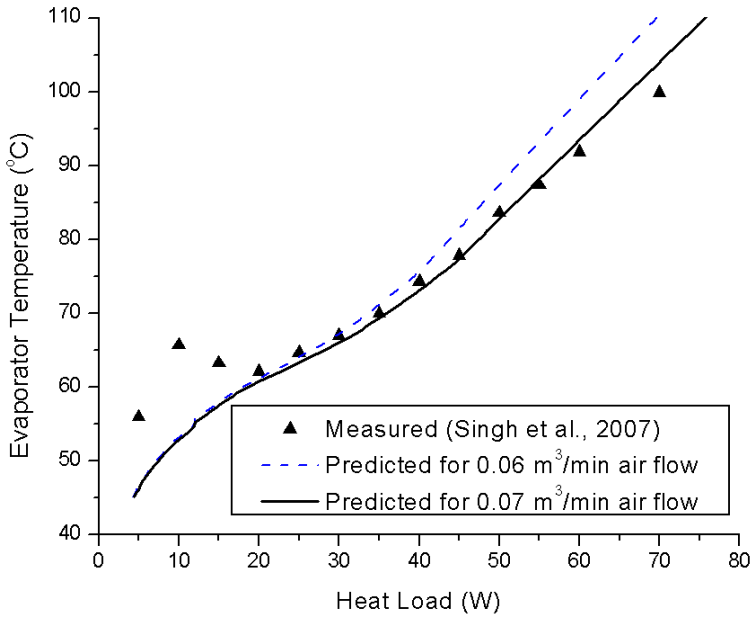

Figure 4.5 Comparison of LHP evaporator temperatures between experimental data and modeling predictions

Such an air flow rate also best fits the measured evaporator temperatures, as shown in Figure 4.5. The modeling predictions for the evaporator temperature are in good agreement with the experimental data when the applied heat load is higher than 20 W, while the discrepancy between the predicted and the measured for heat loads lower than 20 W can be explained by that at such low heat loads it is very likely that the LHP has not completely started up (working fluid has not effectively circulated inside the LHP), resulting in higher evaporator temperatures.

The predicted heat losses from the evaporator surface, compensation chamber surface, liquid line, and vapor line, as well as the heat leak to the compensation chamber are compared in Figure 4.6. It can be seen from the figure that all the heat losses increase with the applied heat load, a natural result of the increase of LHP surface temperature

with increasing heat load. It is interesting to note that the heat leak increases with the heat load at lower heat loads, while decreases at higher heat loads, resulting in a peak heat leak at around 30 W. This observation can be explained by temperature dependence of the working fluid properties. Recall the figure of merit for measuring the heat leak effect defined in Chapter 2

$$N_{HL} = \frac{\rho_v^{\,2} h_{lv}^{\,2}}{\mu_l} \sim \frac{Q_{loop}}{Q_{HL}}. \tag{4.9}$$

Equation (4.9) shows that heat leak increases along with the increasing heat load but decreases with the increasing vapor density, as a result of the increasing LHP operational temperature. At higher heat loads, the vapor density increases to a degree that the vapor density-dependence of heat leak outplays the effect of the heat load increase, causing the heat leak decreasing with applied heat load. The results shown in Figure 4.6 clearly indicates that heat leak is not an important issue at all for this LHP prototype, suggesting promising prospective of LHPs based on water-copper combination in future electronics cooling applications.

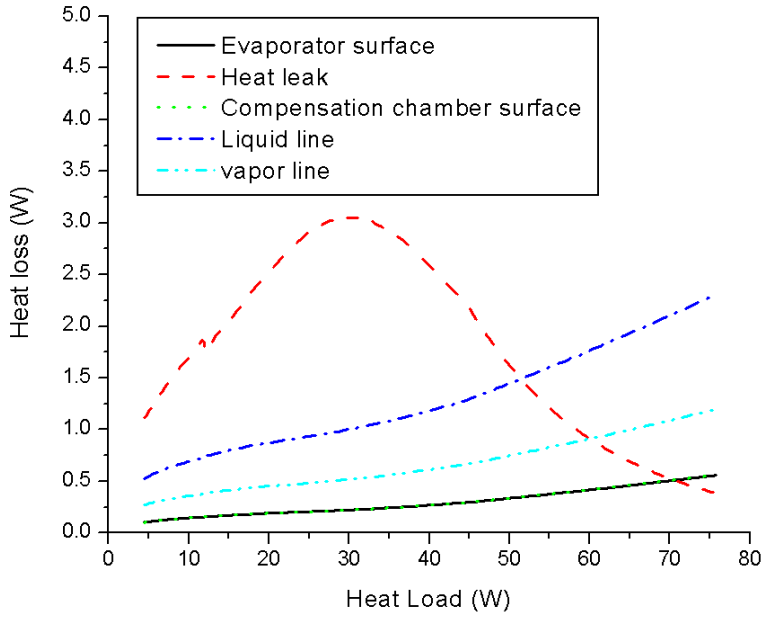

Figure 4.6 Modeling predictions for heat losses from LHP components and heat leak to compensation chamber

The predicted effective porous radius of the wick structure, which is required for driving the working fluid flow, is compared in Figure 4.7 with the actual effective porous radius used by Singh et al. (2007). It is clear that over all the range of investigated heat load, the actual wick structure can provide much higher capillary driving force than what is needed to circulate the working fluid around the loop. In other words, the LHP prototype is operated at conditions far from reaching its capillary limit.

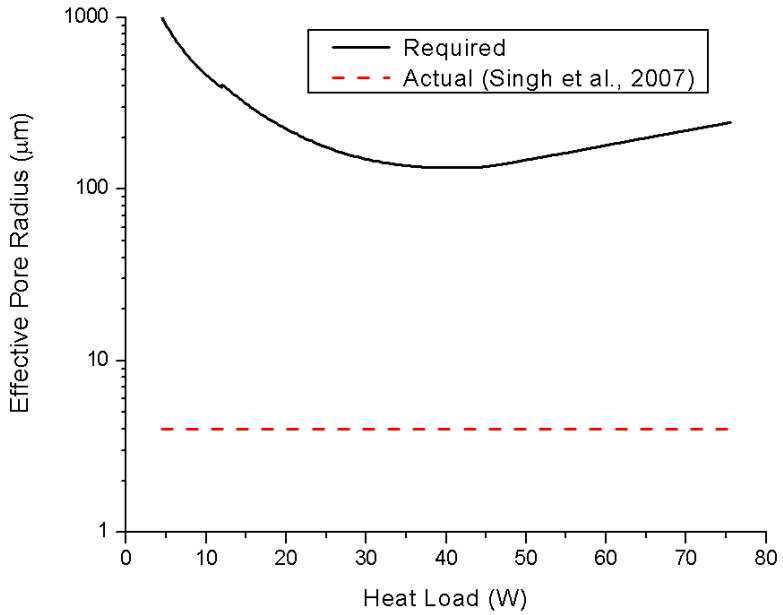

Figure 4.7 Comparison of effective porous radius between the predicted maximum value and the actual value adopted for the LHP prototype (Singh et al. 2007)

The predicted local pressure at different LHP locations as functions of the applied heat load is shown in Figure 4.8. It is clear that for all the applied heat loads, the condensation pressure drop is the most important, and the vapor line pressure drop is the second important, while all other pressure drops are practically negligible.

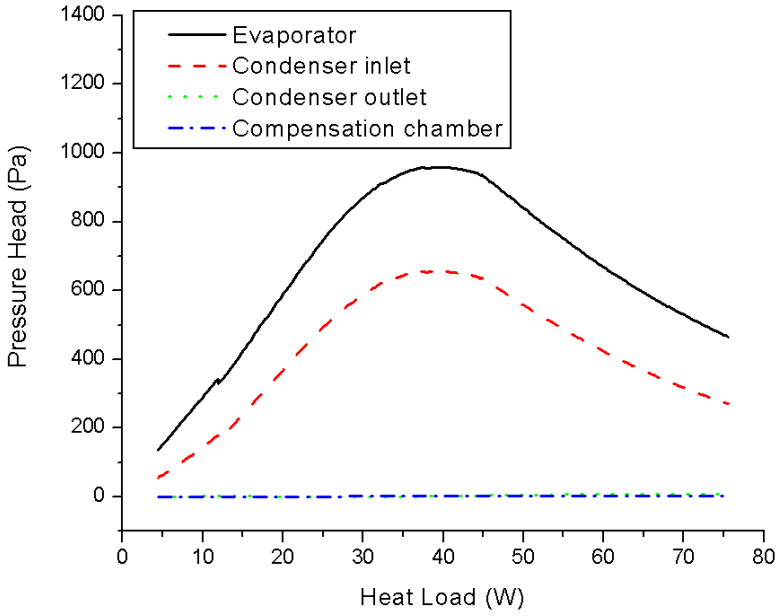

Figure 4.8 Predicted local pressure (relative to the liquid pressure at the evaporative interface in the evaporator) at different locations of the LHP prototype

Although both heat leak and capillary limit are practically not important issues for this LHP prototype, it does reach its limit at a heat load around 70 W, because the evaporator temperature reaches the allowed maximum value. Figure 4.9 shows the predicted temperatures at different LHP locations as functions of the applied heat load. It can be seen from the figure that the evaporator temperature increases at a higher rate with the increasing heat load when the applied heat load exceeds about 45 W, when the condenser is fully utilized. It is also clear from Figure 4.9 that when the LHP is operated under a heat load higher than 45 W, the temperature difference inside the air flow dominates the total temperature difference between the evaporator and the ambient temperatures. Therefore, the relatively poor heat transfer performance of the air flow is the bottleneck of the LHP prototype, and we may predict based on the modeling results

that the heat load limit can be increased to above 70 W if the fan attached to the condenser could be replaced by a stronger one that can deliver a greater air flow rate.

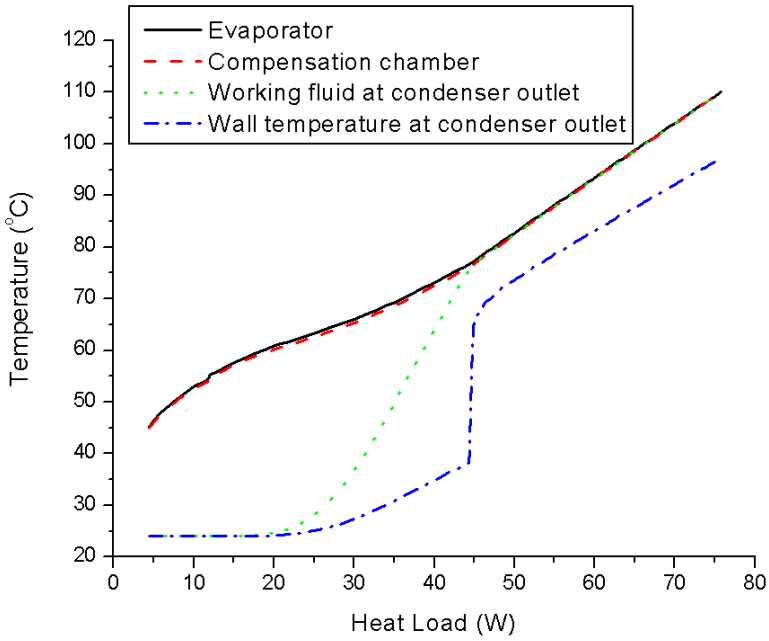

Figure 4.9 Predicted temperatures at different locations of the LHP prototype

4.3 Summary

The LHP prototype design is a comprehensive process, starting from specific design objective and quantitative requirements. The main phase of prototype design is to select materials and size components based on quantitative design tools. As an example to demonstrate the use of the modeling tools presented in Chapters 2 and 3, the LHP prototype designed and tested by Singh et al (2007) is modeled in this chapter. The modeling results show good agreement with the laboratory-measured data, and indicate that the LHP prototype is operated under conditions far from either reaching capillary limit or generating significant heat leak to compensation chamber, but it reaches

maximum evaporator temperature at about 70 W heat load. It is also suggested by the model that air flow is the bottleneck of this prototype, and its heat load limit may be increased by employing a stronger fan and/or greater finned surface area.

Chapter 5

Analytical Models for Annular Two-Phase Flow

5.1 Introduction

Gas/vapor-liquid two-phase flow in tubes exists extensively in engineering systems, including heat pipes and loop heat pipes. In order to solve the hydrodynamic and heat transfer problems related to two-phase flow, correlations of void fraction, frictional pressure gradient, acceleration pressure gradient, and heat transfer coefficient are needed, in addition to the conservation laws of mass, momentum, and energy (e.g. Wallis 1969; Hewitt & Hall-Taylor 1970; Chisholm 1983). In the literature, various correlations have been proposed, dominantly based on experimental investigations, and significant difference exists between different correlations. One reason for such a difference is that different correlations are based on different working fluids and operational conditions, and thus applicable to different situations. In practice, it is often a real challenge for engineers to deal with new working fluids or new operational conditions when not all the needed correlations are available.

Alternatively, developing theoretical models provides a powerful approach to obtain widely applicable correlations. Such an approach has been proved very successful for single-phase convection flows (e.g. Bejan 2004). However, similarly successful theoretical models for two-phase flows have not been established yet.

The most widely used two-phase flow models are the homogeneous flow model, which approximates the two-phase flow by a single-phase flow that averages the actual two phase flow, and the separated flow model, which assumes a uniform velocity for

each phase. These models not only sacrifice the modeling accuracy by oversimplifying assumptions, but also are incomplete by themselves. It is required by the homogeneous flow model to define average thermodynamic and hydrodynamic properties for the two-phase fluids so that they may be treated as a single-phase flow. However, no meaningful definitions of the average properties, particularly the viscosity of the two-phase fluids, are provided or recommended by the framework of the homogeneous flow model. In engineering practice, various ways to define average viscosity have been proposed (Owens 1962; Dukler et al. 1964; Cicchitti et al. 1960; McAdams et al. 1942), but none of them has a solid physical foundation. As for the separated flow model, the assumption of uniform velocity and temperature for each phase breaks the inherent connection of velocity, shear stress, temperature, and heat flux between the two phases. Consequently, the most important information carried by the derivatives of velocity and temperature for calculating frictional pressure gradient and heat transfer coefficient has been lost. As a result, empirical correlations, e.g. the Lockhart & Martinelli (1949) correlations for frictional pressure drop and void fraction, have to be supplied to "fill the gaps in the theory" (Wallis 1969).

Due to the complex nature of two-phase flows, it seems impossible to develop a theoretical model that is universally applicable to all flow regimes. Since annular flow is the predominant flow pattern in various engineering devices, such as evaporators, condensers, natural gas pipelines, and steam heating systems (Wallis 1969; Hewitt & Hall-Taylor 1970), it is especially important to develop annular flow models. Here we propose analytical models for gas/vapor-liquid annular flow in a horizontal tube.

In our model, the velocity and temperature distributions (including the derivative information) for the gas/vapor and liquid phases are represented by the exact solutions to the governing equations for laminar flow regime and by the universal profiles for turbulent flow regime. As a result, void fraction, frictional pressure gradient, acceleration pressure gradient, and heat transfer coefficient are derived on a self-contained and self-consistent basis, eliminating the need for defining ambiguous fluid properties (e.g. the two-phase viscosity in the homogeneous flow model) or appealing to empirical correlations to complete a model (e.g. the separated flow model).

It should be noted that in various annular flow systems in the real world, both the gas/vapor and liquid phases can be laminar (viscous) or turbulent, and the flows can be with phase change or without phase change. These cases will be analyzed in detail in the following sections.

Figure 5.1 shows schematically the velocity profile over a cross-section for annular gas/vapor-liquid flow in a horizontal tube with an inner radius r_0. The gas/vapor phase flows in the core region ($r < r_1$), while the liquid phase flows between the gas/vapor core and the tube wall ($r_1 < r < r_0$). Note that the modeling results for cases without phase change are also applicable to liquid-liquid annular flows, e.g., heavy oil transport problem, although the core phase is always denoted by subscript '*v*' to keep the symbol consistency throughout this chapter.

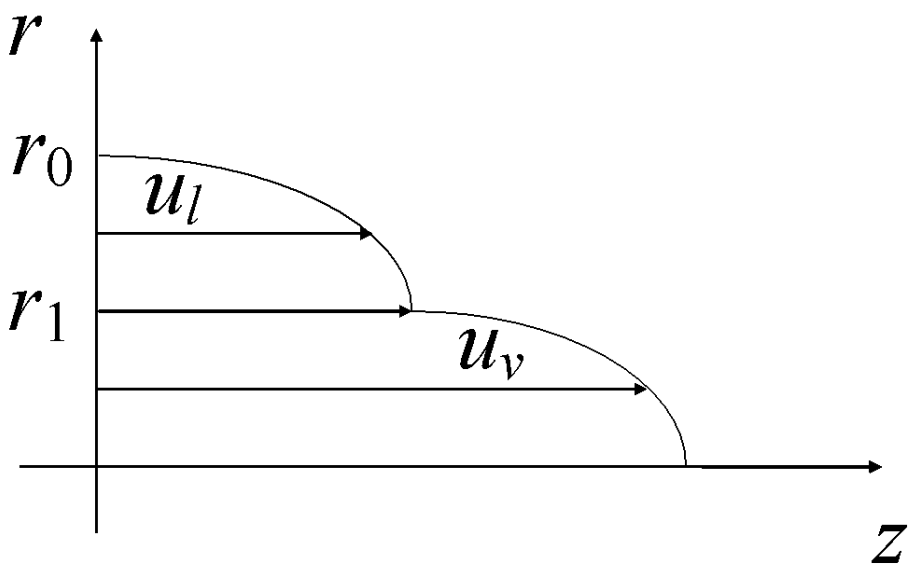

Figure 5.1 Schematic of velocity distribution over a cross-section of gas/vapor-liquid annular flow in a horizontal round tube.

5.2 Convective Annular Flow of Laminar Gas and Liquid

5.2.1. Formulation of the problem

5.2.1.1 *Hydrodynamic problem*

For fully developed laminar gas and liquid flows, the velocity distributions are governed by the following equations (Bejan 2004)

$$\frac{d^2u_l}{dr^2}+\frac{1}{r}\frac{du_l}{dr}=\frac{1}{\mu_l}\frac{dp}{dz},\ \frac{d^2u_v}{dr^2}+\frac{1}{r}\frac{du_v}{dr}=\frac{1}{\mu_v}\frac{dp}{dz}. \tag{5.1}$$

The total derivative operators indicate that liquid velocity u_l and gas velocity u_v depend upon *r*-coordinate only, whereas pressure *p* depends upon *z*-coordinate only. Velocity

conditions for non-slip at wall and symmetry about central line are satisfied by boundary conditions

$$u_l\Big|_{r=r_0} = 0\,,\ \frac{du_v}{dr}\Big|_{r=0} = 0\,. \tag{5.2}$$

At the gas-liquid interface, the continuity of velocity and shear stress requires

$$u_l\Big|_{r=r_1} = u_v\Big|_{r=r_1}\,,\ \mu_l \frac{du_l}{dr}\Big|_{r=r_1} = \mu_v \frac{du_v}{dr}\Big|_{r=r_1}\,. \tag{5.3}$$

Axial force balance for a differential segment *dz* of the two-phase fluids yields

$$\pi r_0^{\,2}(-dp) = 2\pi r_0 \tau_0 dz\,,\ -\frac{dp}{dz} = \frac{2\tau_0}{r_0}. \tag{5.4}$$

Submitting (5.2)-(5.4) into (5.1), the exact solution of the velocity distributions are obtained as

$$u_l = \frac{\tau_0 r_0}{2\mu_l}\left(1-\frac{r^2}{r_0^{\,2}}\right),\ u_v = \frac{\tau_0 r_0}{2\mu_l}\left[1-\frac{r_1^{\,2}}{r_0^{\,2}} + \frac{\mu_l}{\mu_v}\left(\frac{r_1^{\,2}}{r_0^{\,2}} - \frac{r^2}{r_0^{\,2}}\right)\right]. \tag{5.5}$$

The mass flow rates of the liquid and gas phases are obtained by integrating the product of density and velocity over the corresponding cross-sectional areas

$$\dot{m}_l = 2\pi\int_{r_1}^{r_0} \rho_l u_l r dr = \frac{\pi\tau_0 r_0^{\,3}\rho_l}{4\mu_l}\left(1-\frac{r_1^{\,2}}{r_0^{\,2}}\right)^2, \tag{5.6}$$

$$\dot{m}_v = 2\pi\int_0^{r_1} \rho_v u_v r dr = \frac{\pi\tau_0 r_0^{\,3}\rho_v}{4\mu_l}\left[\left(\frac{\mu_l}{\mu_v}-2\right)\frac{r_1^{\,4}}{r_0^{\,4}} + \frac{2r_1^{\,2}}{r_0^{\,2}}\right]. \tag{5.7}$$

Since quality *x* and void fraction α are defined by

$$x \equiv \frac{\dot{m}_v}{\dot{m}_l + \dot{m}_v}\,,\ \alpha \equiv \frac{r_1^{\,2}}{r_0^{\,2}}\,, \tag{5.8}$$

a relation between quality and void fraction is given by dividing (5.7) by (5.6)

$$\hat{x} \equiv \frac{x}{1-x} = \frac{\dot{m}_v}{\dot{m}_l} = \frac{2\alpha}{\hat{\rho}(1-\alpha)} + \frac{\hat{\mu}\alpha^2}{\hat{\rho}(1-\alpha)^2}, \tag{5.9}$$

where $\hat{\rho}$ and $\hat{\mu}$ are density ratio and viscosity ratio, respectively,

$$\hat{\rho} \equiv \frac{\rho_l}{\rho_v}, \ \hat{\mu} \equiv \frac{\mu_l}{\mu_v}. \tag{5.10}$$

Solving α from (5.9) yields an explicit expression for void fraction as a function of quality, density ratio and viscosity ratio

$$\alpha = \frac{1 + \hat{x}\hat{\rho} - \sqrt{1 + \hat{x}\hat{\rho}\hat{\mu}}}{2 + \hat{x}\hat{\rho} - \hat{\mu}}, \tag{5.11}$$

Combining (5.6) with the definition of quality, the mass flux is expressed by

$$G \equiv \frac{\dot{m}_l + \dot{m}_v}{\pi r_0^2} = \frac{\dot{m}_l}{(1-x)\pi r_0^2} = \frac{r_0 \tau_0 \rho_l}{4\mu_l} \frac{(1-\alpha)^2}{(1-x)}. \tag{5.12}$$

Consequently, the wall shear stress and the pressure gradient can be evaluated by

$$\tau_0 = \frac{4G\mu_l}{r_0\rho_l} \frac{(1-x)}{(1-\alpha)^2}, \ -\frac{dp}{dz} = \frac{2\tau_0}{r_0} = \frac{8G\mu_l}{r_0^2\rho_l} \frac{(1-x)}{(1-\alpha)^2}. \tag{5.13}$$

For single-phase liquid flow with the total mass flow rate, we have

$$x = 0, \ \alpha = 0, \ \left(-\frac{dp}{dz}\right)_{l0} = \frac{8G\mu_l}{r_0^2\rho_l}. \tag{5.14}$$

Therefore, the frictional multiplier for the annular two-phase flow is obtained following (5.13) and (5.14)

$$\phi_{l0}^2 \equiv \frac{(-dp/dz)_f}{(-dp/dz)_{l0}} = \frac{(1-x)}{(1-\alpha)^2}. \tag{5.15}$$

Note that the frictional pressure gradient is identical to the total pressure gradient, as is clear from the momentum balance shown in (5.4).

Substituting the first equation of (5.13) into (5.5), the laminar velocity profiles can be expressed in terms of the total mass flux by

$$u_l = \frac{2G}{\rho_l}\frac{(1-x)}{(1-\alpha)^2}(1-\frac{r^2}{r_0^2})\,,\ u_v = \frac{2G\hat{\mu}}{\rho_l}\frac{(1-x)}{(1-\alpha)^2}\left(C_0-\frac{r^2}{r_0^2}\right)\,,\ C_0 = \alpha+\frac{1-\alpha}{\hat{\mu}}\,. \quad (5.16)$$

5.2.1.2. *Heat transfer problem with constant wall heat flux*

The heat transfer problem of fully developed gas and liquid in a round tube is governed by the following energy equations (Bejan 2004)

$$\frac{\partial^2 T_l}{\partial r^2}+\frac{1}{r}\frac{\partial T_l}{\partial r} = \frac{\rho_l c_{pl} u_l}{k_l}\frac{\partial T_l}{\partial z}\,,\ \frac{\partial^2 T_v}{\partial r^2}+\frac{1}{r}\frac{\partial T_v}{\partial r} = \frac{\rho_v c_{pv} u_v}{k_v}\frac{\partial T_v}{\partial z}\,, \quad (5.17)$$

subject to the boundary conditions and connection conditions as follows

$$T_l\big|_{r=r_0} = T_0\,,\ k_l\frac{\partial T_l}{\partial r}\Big|_{r=r_0} = q_0\,,\ \frac{\partial T_v}{\partial r}\Big|_{r=0} = 0\,,\ T_l\big|_{r=r_1} = T_v\big|_{r=r_1}\,. \quad (5.18)$$

Energy balance for a differential segment *dz* of the two-phase fluids yields

$$\dot{m}_l c_{pl} dT_m + \dot{m}_v c_{pv} dT_m = 2\pi r_0 q_0 dz\,,\ \frac{dT_m}{dz} = \frac{2q_0}{Gr_0 c_{pl}(1-x)(1+\hat{x}/\hat{c}_p)}\,, \quad (5.19)$$

where $\hat{c}_p \equiv c_{pl}/c_{pv}$.

For fully developed convection heat transfer problem with constant heat flux at the tube wall, we may assume (Bejan 2004)

$$\frac{\partial T_l}{\partial z} = \frac{\partial T_v}{\partial z} = \frac{dT_m}{dz}\,, \quad (5.20)$$

Substituting (5.16) and (5.18)-(5.20) into (5.17), the exact temperature distributions in gas and liquid phases are obtained as follows

$$T_l = T_0 + C_1\frac{r_0 q_0}{k_l}\left(\frac{r^2}{r_0^2}-\frac{r^4}{4r_0^4}-\frac{3}{4}\right)+C_2\frac{r_0 q_0}{k_l}\ln\frac{r}{r_0}\,,\ T_v = T_0 + C_3\frac{r_0 q_0}{k_l}\left(\frac{C_0 r^2}{r_0^2}-\frac{r^4}{4r_0^4}\right)+C_4\frac{r_0 q_0}{k_l}\,,$$

(5.21)

where

$$C_1 = \frac{1}{(1+\hat{x}/\hat{c}_p)(1-\alpha)^2} = \frac{\hat{\rho}\hat{c}_p}{\hat{\rho}\hat{c}_p(1-\alpha)^2 + (\hat{\mu}-2)\alpha^2 + 2\alpha},\ C_2 = 1 - C_1, \tag{5.22}$$

$$C_3 = \frac{\hat{\mu}}{\hat{\rho}\hat{c}_p}C_1,\ C_4 = \frac{1}{2}C_2 \ln\alpha + (C_1 - \hat{k}C_0C_3)\alpha - \frac{1}{4}(C_1 - \hat{k}C_3)\alpha^2 - \frac{3}{4}C_1, \tag{5.23}$$

and $\hat{k} \equiv k_l / k_v$. It can be readily verified that the heat flux across the gas-liquid interface is continuous. This physically correct consequence is a demonstration of the exactness of the temperature solution.

Evaluating the stream-wall temperature difference by

$$T_m - T_0 = \frac{\int_{r_1}^{r_0} \rho_l c_{pl} u_l (T_l - T_0) 2\pi r dr + \int_0^{r_1} \rho_v c_{pv} u_v (T_v - T_0) 2\pi r dr}{c_{pl}\dot{m}_l + c_{pv}\dot{m}_v}, \tag{5.24}$$

the Nusselt number for laminar gas-liquid annular flow can be obtained by

$$\mathrm{Nu}_l \equiv \frac{2r_0 h}{k_l} = \frac{2r_0 q_0}{k_l(T_0 - T_m)} = \left(N_1 + N_2 + N_3\right)^{-1}, \tag{5.25}$$

where *h* is heat transfer coefficient and

$$N_1 = C_1^2\left(\frac{11}{48} - \frac{3}{4}\alpha + \frac{7}{8}\alpha^2 - \frac{5}{12}\alpha^3 + \frac{1}{16}\alpha^4\right), \tag{5.26}$$

$$N_2 = C_1C_2\left(\frac{3}{8} - \frac{\alpha}{2} + \frac{1}{8}\alpha^2 - \frac{1}{4}\alpha^2\ln\alpha + \frac{1}{2}\alpha\ln\alpha\right), \tag{5.27}$$

$$N_3 = -\hat{k}C_3^{\,2}\left(\frac{1}{2}C_0^{\,2}\alpha^2 - \frac{5}{12}C_0\alpha^3 + \frac{1}{16}\alpha^4\right) - C_3C_4\left(C_0\alpha - \frac{1}{2}\alpha^2\right). \tag{5.28}$$

It can be readily verified that (5.25) approaches to the following limits of Nusselt number

$$\mathrm{Nu}_l\big|_{x=0} = \frac{48}{11},\ \mathrm{Nu}_v\big|_{x=1} \equiv \frac{2r_0 h\big|_{x=1}}{k_v} = \frac{48}{11}. \tag{5.29}$$

These are the classical results for single phase convection flow under constant wall flux.

For heat transfer problem of laminar gas-liquid annular flow subject to other types of thermal boundary condition, e.g. constant wall temperature or externally convective surrounding fluid, the analyzing process is similar, but numerical approach may be needed to solve the heat transfer coefficient, because even for single-phase laminar flow under constant wall temperature or surrounded by isothermal fluid, close-formed solution to heat transfer coefficient does not exist (Bejan 2004).

5.2.1.3. *Applicable domain*

The formulation presented in the above is only applicable to horizontal annular flow of laminar gas and liquid. In this subsection, we investigate the conditions under which the gas and liquid flows are laminar or turbulent.

It is well known that for single-phase flow of liquid or gas in a round tube, the corresponding Reynolds numbers are defined by

$$\mathrm{Re}_{l0} \equiv \frac{2r_0 G}{\mu_l},\ \mathrm{Re}_{v0} \equiv \frac{2r_0 G}{\mu_v} = \hat{\mu}\mathrm{Re}_{l0}, \tag{5.30}$$

and the transition between laminar flow to turbulent flow occurs at a critical Reynolds number Re_{cr}, i.e.

$$\mathrm{Re}_{l0} = \mathrm{Re}_{cr},\ \mathrm{Re}_{v0} = \mathrm{Re}_{cr}, \mathrm{Re}_{cr} \cong 2000. \tag{5.31}$$

In gas-liquid annular flow, the Reynolds number for liquid phase can be defined based on hydraulic diameter and mean liquid velocity,

$$\mathrm{Re}_l \equiv \frac{D_h \rho_l \bar{u}_l}{\mu_l},\ D_h = \frac{4\pi\left(r_0^2 - r_1^2\right)}{2\pi r_0} = 2r_0(1-\alpha),\ \bar{u}_l = \frac{\dot{m}_l}{\rho_l \pi\left(r_0^2 - r_1^2\right)} = \frac{G(1-x)}{\rho_l(1-\alpha)}, \tag{5.32}$$

i.e.,

$$\mathrm{Re}_l = (1-x)\mathrm{Re}_{l0}, \tag{5.33}$$

and a liquid transition line (LTL) between laminar flow and turbulent flow is defined accordingly by

$$\mathrm{Re}_l = \mathrm{Re}_{cr}, \mathrm{Re}_{l0} = \frac{\mathrm{Re}_{cr}}{1-x}. \tag{5.34}$$

For the gas phase in gas-liquid annular flow, since the gas feels the surrounding liquid flow as a "wall", it is reasonable to define the gas Reynolds number based on the mean gas velocity minus the "wall" velocity, i.e., the liquid velocity at the gas-liquid interface,

$$\mathrm{Re}_v \equiv \frac{2r_1\rho_v(\bar{u}_v - u_1)}{\mu_v},\ \bar{u}_v = \frac{\dot{m}_v}{\rho_v \pi r_1^2} = \frac{Gx}{\rho_v \alpha},\ u_1 \equiv u_l\big|_{r=r_1} = \frac{2G(1-x)}{\rho_l(1-\alpha)}. \tag{5.35}$$

Therefore,

$$\mathrm{Re}_v = \sqrt{\alpha}\left[\frac{x}{\alpha} - \frac{2(1-x)}{\hat{\rho}(1-\alpha)}\right]\mathrm{Re}_{v0}. \tag{5.36}$$

As a result, a gas (vapor) transition line (VTL) between laminar flow and turbulent flow is defined by

$$\mathrm{Re}_v = \mathrm{Re}_{cr}, \mathrm{Re}_{v0} = \frac{\mathrm{Re}_{cr}}{\sqrt{\alpha}\left[\frac{x}{\alpha} - \frac{2(1-x)}{\hat{\rho}(1-\alpha)}\right]}. \tag{5.37}$$

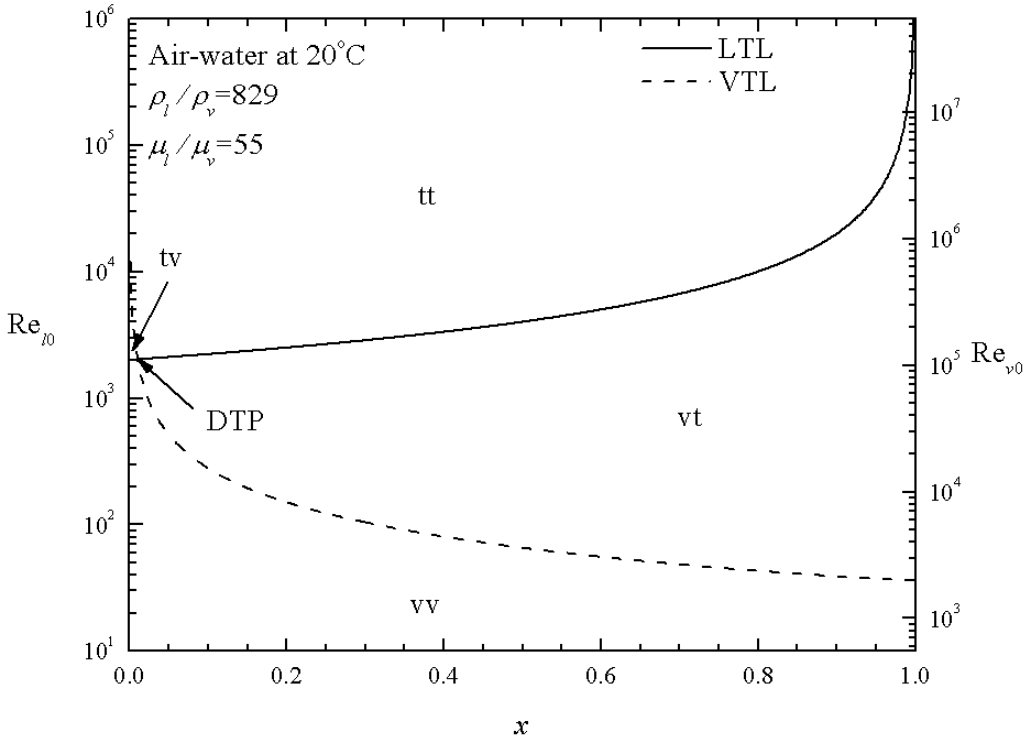

Figure 5.2 Annular flow domains (vv, vt, tv, and tt) formed by laminar-turbulent transition lines (LTL and VTL) for air-water system.

As an example, Figure 5.2 shows the transition lines, LTL and VTL, for air-water annular flow at 20°C. LTL and VTL divide the Re_{l0} - x plane into 4 domains: vv, vt, tv, and tt. Here we follow a widely used terminology system (e.g. Lockhart & Martinelli 1949) in two-phase flow studies by denoting, for instance, the laminar (viscous) liquid and turbulent gas domain by vt. It is obvious that vv is the domain to which the analytical model presented in subsections 5.2.1.1 and 5.2.1.2 is applicable. Furthermore, we define the intersection point of LTL and VTL as double transition point (DTP), reflecting the fact that at this point both the gas and liquid phases have a laminar-turbulent transition. In

the real fluid flow systems, the laminar-turbulent transition occurs at a range of Reynolds number instead of a precise single value Re_{cr}. Consequently, LTL and VTL will be two zones with finite widths, and the DTP will occupy a small region. The meaning and defining criteria of the above defined transition lines, domains, and double transition point are summarized in Table 5.1.

Table 5.1 Abbreviation, full description and defining criteria for transition lines, domains, and double transition point.

Abbreviation	Full description	Defining criteria
DTP	Double transition point	$\mathrm{Re}_l = \mathrm{Re}_v = \mathrm{Re}_{cr}$
LTL	Liquid transition line	$\mathrm{Re}_l = \mathrm{Re}_{cr}$
VTL	Gas transition line	$\mathrm{Re}_v = \mathrm{Re}_{cr}$
vv	Laminar liquid and laminar gas	$\mathrm{Re}_l < \mathrm{Re}_{cr}$ and $\mathrm{Re}_v < \mathrm{Re}_{cr}$
vt	Laminar liquid and turbulent gas	$\mathrm{Re}_l < \mathrm{Re}_{cr}$ and $\mathrm{Re}_v > \mathrm{Re}_{cr}$
tv	Turbulent liquid and laminar gas	$\mathrm{Re}_l > \mathrm{Re}_{cr}$ and $\mathrm{Re}_v < \mathrm{Re}_{cr}$
tt	Turbulent liquid and turbulent gas	$\mathrm{Re}_l > \mathrm{Re}_{cr}$ and $\mathrm{Re}_v > \mathrm{Re}_{cr}$

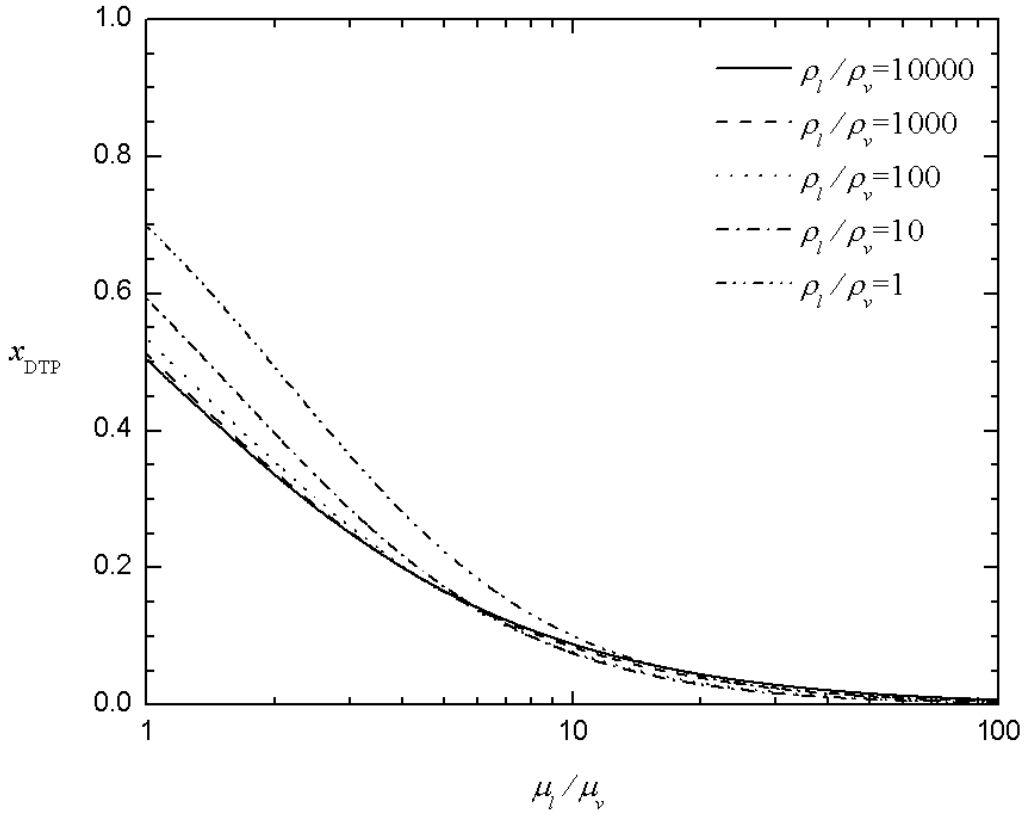

Figure 5.3 Quality of the double transition point (DTP) as a function of viscosity ratio and density ratio.

Figure 5.2 shows that for the air-water system the tv domain is a region with very small quality values, a condition that is most favorable for bubbly flow regime and certainly not favorable for the annular flow regime, implying that tv type annular flow may never occur in the real air-water system. This implication is consistent with the comment by Wallis (1969) that "in annular flow the gas is seldom viscous if the liquid is turbulent". Figure 5.3 shows the quality of the DTP as a function of viscosity ratio and density ratio, and reveals that as long as the liquid viscosity is an order higher than the

gas, the DTP quality will be less than 0.1, and thus the tv type annular flow is unlikely to occur in the real world.

Finally, , we may provide a physical explanation for the unfavorableness of the tv type gas-liquid annular flow and the favorableness of the bubbly flow at very low qualities, based on what we learned from Figures 5.2 and 5.3. Since the void fraction is positively correlated to quality, when quality is low, the gas flow in the gas-liquid annular flow has a small size, compared with the tube size, associating with a Reynolds number smaller than the critical Reynolds number. For gas flow with such a Reynolds number, there are two scenarios. In the first scenario, the liquid flow in the annular flow is laminar. Therefore, there is no fluctuation at the liquid-gas interface, and the gas flow can stay as undisturbed laminar flow, resulting in the stable vv type annular flow. In the other scenario, the liquid flow is turbulent, and the interface has already been disturbed by the eddy motion related to the liquid flow. As a result, although the gas flow will not generate eddy by itself, it cannot stay laminar due to the interface fluctuation. In other words, the tv type gas-liquid annular flow is dynamically unstable. Moreover, since the size of the gas flow is very small, it is very likely that it is comparable or even smaller than the liquid eddy size. If this is the case, the gas flow will be torn up and entrained into the liquid flow as bubbles, resulting in bubbly flow.

5.2.2. Results and discussion

In this subsection, the results of the analytical model presented in subsections 5.2.1.1 and 5.2.1.2 are compared with prevailing correlations of void fraction, frictional

pressure drop, and heat transfer in the literature. All the comparisons are based on the air-water system at 20^{o}C.

5.2.2.1. *Void fraction*

Figure 5.4 shows a comparison of the prediction of (5.11) with seven existing void fraction correlations (Table 5.2). These α - x correlations are dependent upon density ratio and viscosity ratio only, i.e., independent upon flow conditions, e.g. Reynolds number or mass flux. It is clear from Figure 5.4 that the void fraction given by (5.11) is significantly lower than all the predictions of the seven correlations, indicating that all the examined empirical correlations significantly overestimate void fraction for laminar gas-liquid annular flow.

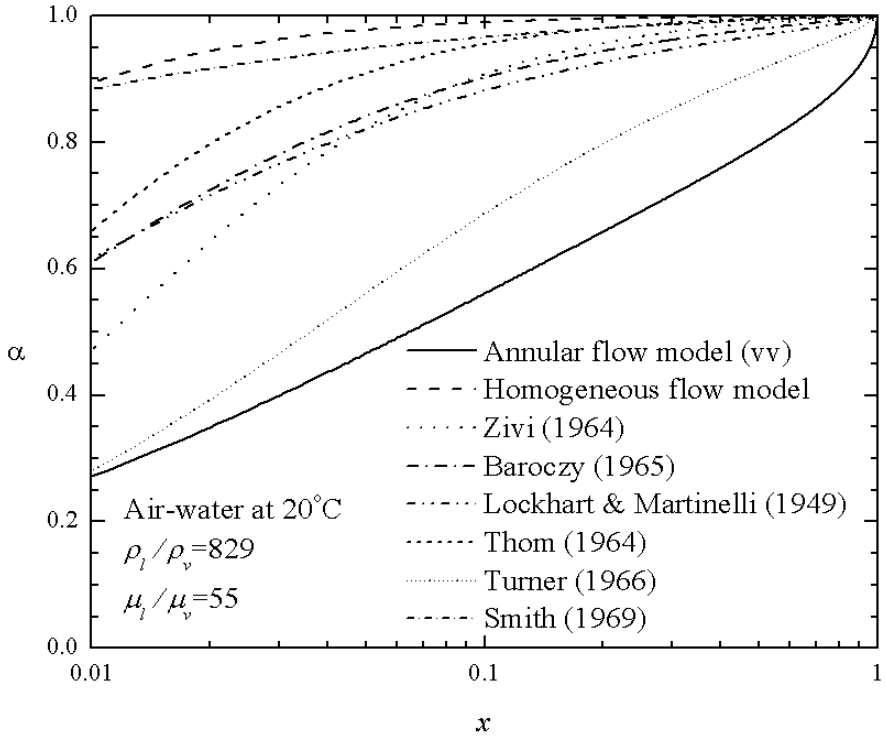

Figure 5.4 Comparison of prediction of (5.11) with empirical correlations of void fraction.

Table 5.2 Void fraction correlations.

Correlation	α
Annular flow model	Equation (5.11)
Homogeneous flow model	$\left(1+\hat{x}^{-1}\hat{\rho}^{-1}\right)^{-1}$
Zivi (1964)	$\left(1+\hat{x}^{-1}\hat{\rho}^{-2/3}\right)^{-1}$
Baroczy (1965)	$\left(1+\hat{x}^{-0.74}\hat{\rho}^{-0.65}\hat{\mu}^{0.13}\right)^{-1}$
Lockhart & Martinelli (1949)	$\left(1+0.28\hat{x}^{-0.64}\hat{\rho}^{-0.36}\hat{\mu}^{0.07}\right)^{-1}$
Thom (1964)	$\left(1+\hat{x}^{-1}\hat{\rho}^{-0.89}\hat{\mu}^{0.18}\right)^{-1}$
Turner (1966)	$\left(1+\hat{x}^{-0.72}\hat{\rho}^{-0.40}\hat{\mu}^{0.08}\right)^{-1}$
Smith (1969)	$\left\{1+\hat{x}^{-1}\hat{\rho}^{-1}\left[0.4+0.6\sqrt{\left(0.4+\hat{x}\hat{\rho}\right)\left(0.4+\hat{x}\right)^{-1}}\right]\right\}^{-1}$

5.2.2.2. *Frictional pressure drop*

Figure 5.5 shows a comparison of the prediction of (5.15) with six existing frictional multiplier correlations (Table 5.3). It is clear from Figure 5.5 that the frictional multiplier predicted by the analytical model is significantly different from the predictions of the empirical correlations. Relatively, the predictions of Dukler et al. (1964), McAdams et al. (1942), and Lockhart & Martinelli (1949) are better than those of Owens (1962), Cicchitti et al. (1960), and Friedel (1979) for laminar air-water annular flow at room temperature. In the result shown in Figure 5.5, the effects of Froude number and Weber number on the Friedel (1979) correlation are neglected.

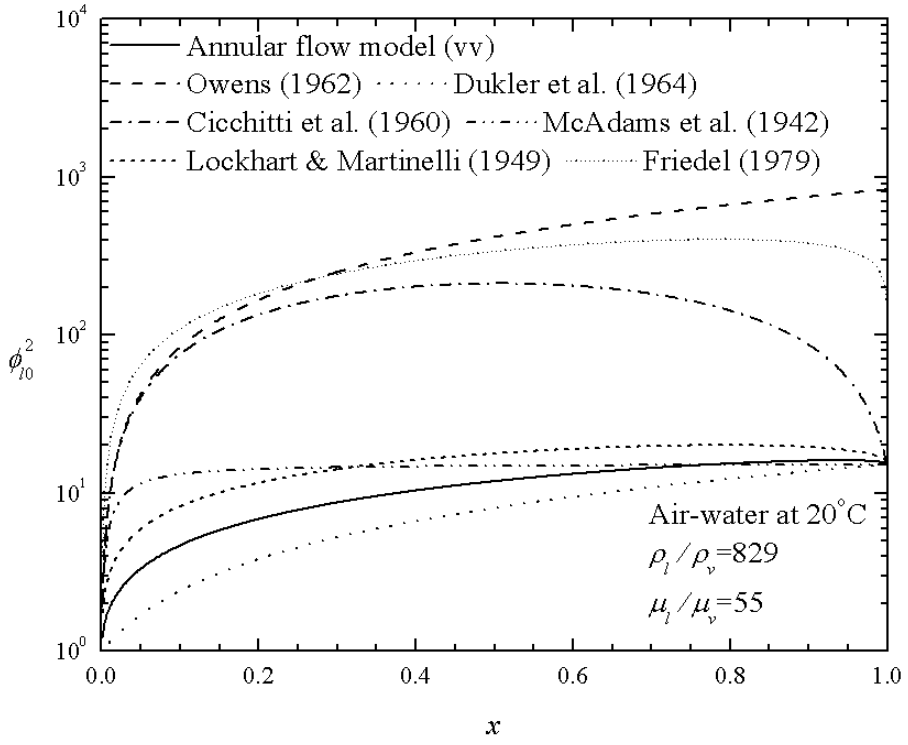

Figure 5.5 Comparison of prediction of (5.15) with empirical correlations of frictional pressure drop.

Table 5.3 Frictional multiplier correlations for the vv domain.

Correlation	ϕ_{l0}^2
Annular flow model	Equation (5.15)
Owens (1962)	$1+x\left(\hat{\rho}-1\right)$
Dukler et al. (1964)	$1+x\left(\hat{\rho}\hat{\mu}^{-1}-1\right)$
Cicchitti et al. (1960)	$\left[1+x\left(\hat{\rho}-1\right)\right]\left[1-x\left(1-\hat{\mu}^{-1}\right)\right]$
McAdams et al. (1942)	$\left[1+x\left(\hat{\rho}-1\right)\right]\left[1+x\left(\hat{\mu}-1\right)\right]^{-1}$
Lockhart & Martinelli (1949)	$\left(1-x\right)\left(1+5\sqrt{\hat{x}\hat{\rho}\hat{\mu}^{-1}}+\hat{x}\hat{\rho}\hat{\mu}^{-1}\right)$
Friedel (1979)	$\left(1-x\right)^2+x^2\hat{\rho}\hat{\mu}^{-1}+3.23x^{0.78}\left(1-x\right)^{0.224}\hat{\rho}^{0.91}\hat{\mu}^{-0.19}\left(1-\hat{\mu}^{-1}\right)^{0.7}$

5.2.2.3. *Heat transfer*

Since we cannot find any heat transfer correlation for gas-liquid two-phase flows without phase change, we compare in Figure 5.6 the prediction of (5.25) with two popular correlations that established through phase change two-phase flows, viz., the Shah (1979) and the Cavallini & Zecchin (1971) correlations (Table 5.4). Both the correlations are in a form of a generalization of the classical heat transfer correlation of turbulent single-phase flow. Consequently, Nusselt numbers predicted by the two correlations depend on Reynolds number of the flow. In obtaining the results of the two correlations shown in Figure 5.6, a somewhat arbitrary value of $\mathrm{Re}_{v0} = 2000$ is used. It

should be emphasized that a different pick of Reynolds number will not substantially change the trend of the curves, although the absolute value of Nusselt number will be different.

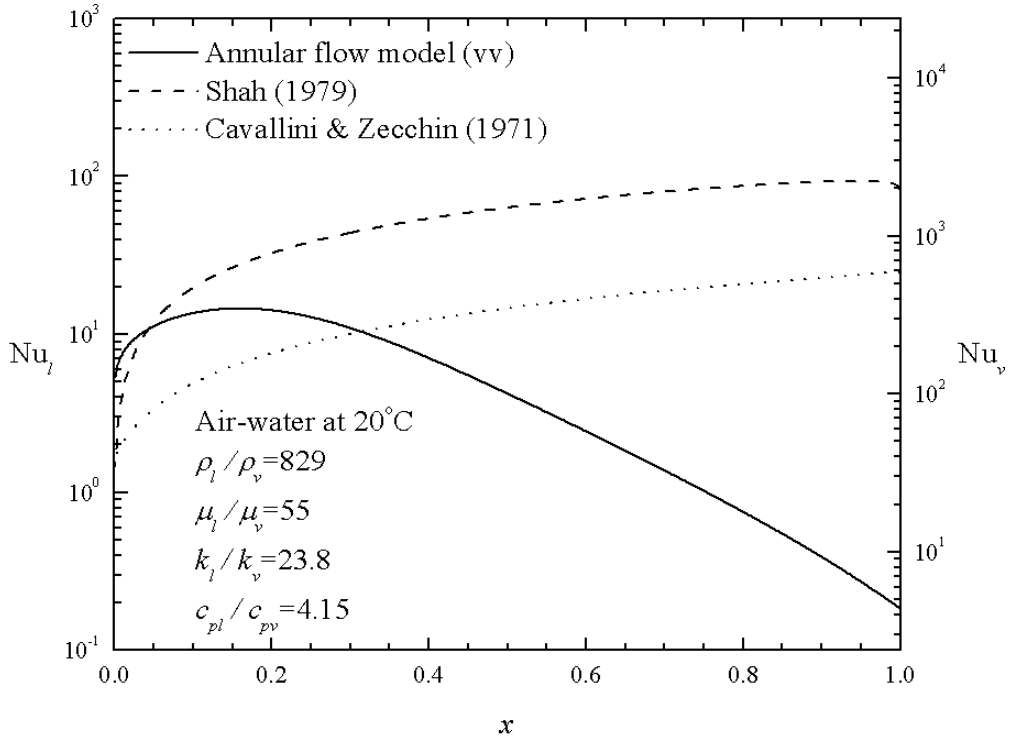

Figure 5.6 Comparison of prediction of (5.25) with empirical correlations of heat transfer.

It is clear from Figure 5.6 that the Nusselt number predicted by the analytical model has significantly different trend than those predicted by the empirical correlations. Therefore, we conclude that the Shah (1979) and the Cavallini & Zecchin (1971) correlations cannot give reliable heat transfer predictions for laminar gas-liquid annular flow without phase change.

Table 5.4 Heat transfer correlations.

Correlation	Nu_l
Annular flow model	Equation (5.25)
Shah (1979)	$0.023\,\mathrm{Re}_{l0}^{0.8}\,\mathrm{Pr}_l^{0.4}\left[(1-x)^{0.8}+3.8x^{0.76}(1-x)^{0.04}\left(p/p_{cr}\right)^{-0.38}\right]$
Cavallini & Zecchin (1971)	$0.05\,\mathrm{Re}_{l0}^{0.8}\,\mathrm{Pr}_l^{0.33}\left[(1-x)+x\sqrt{\hat{\rho}}\right]^{0.8}$

5.2.3. Conclusions

An analytical model for convective annular flow of laminar gas and liquid in a horizontal tube is presented. The model is based on exact solutions of velocity and temperature distributions within the gas and liquid phases, and predicts void fraction, frictional pressure gradient, and heat transfer coefficient on a self-contained and self-consistent basis. In terms of physically reasonable definition of Reynolds numbers for the gas and liquid phases in annular flow, the applicable domain of the analytical model is determined. Moreover, it has been shown that annular flow of turbulent liquid and laminar gas is unlikely to occur in the real world, as long as the liquid viscosity is an order higher than the gas. In terms of the air-water system at room temperature as an example, modeling results show that the prevailing empirical correlations of void fraction, frictional pressure drop, and heat transfer for two-phase flow are generally inapplicable to horizontal annular flows of laminar gas and liquid.

5.3 Condensing/Evaporating Annular Flow of Laminar Vapor and Liquid

5.3.1. Formulation of the problem

5.3.1.1 *Hydrodynamic problem*

When phase change (condensation or evaporation) occurs in the laminar vapor-liquid annular flow, the liquid velocity u_l and vapor velocity u_v depend upon both *r*-coordinate and *z*-coordinate, and thus (5.1) is not sufficient to describe the local momentum balance.

For both the liquid flow and vapor flow, let us start from the steady and axisymmetric continuity equation and Navier-Stokes equations

$$\frac{\partial u_j}{\partial z}+\frac{1}{r}\frac{\partial (rv_j)}{\partial r}=0\,, \tag{5.38}$$

$$\rho_j u_j\frac{\partial u_j}{\partial z}+\rho_j v_j\frac{\partial u_j}{\partial r}=-\frac{\partial p}{\partial z}+\mu_j\left[\frac{\partial^2 u_j}{\partial z^2}+\frac{1}{r}\frac{\partial}{\partial r}\left(r\frac{\partial u_j}{\partial r}\right)\right], \tag{5.39}$$

$$\rho_j u_j\frac{\partial v_j}{\partial z}+\rho_j v_j\frac{\partial v_j}{\partial r}=-\frac{\partial p}{\partial r}+\mu_j\left[\frac{\partial^2 v_j}{\partial z^2}+\frac{1}{r}\frac{\partial}{\partial r}\left(r\frac{\partial v_j}{\partial r}\right)-\frac{v_j}{r^2}\right], \tag{5.40}$$

where *j*=*l*, *v*. Exact distributions of velocity and pressure are governed by the above equations subject to the boundary conditions (5.2) and connection conditions (5.3). Such a problem cannot be solved analytically, and we consider in the following an integral solution.

Following the classical boundary layer analysis (Schlichting 1968), if we assume that the *z*-direction characteristic length *L* is much greater than that of the *r*-direction

$$r_0 << L \tag{5.41}$$

we have the following results from scale analysis (Bejan 2004)

$$\frac{\partial^2 u_j}{\partial z^2}<<\frac{1}{r}\frac{\partial}{\partial r}\left(r\frac{\partial u_j}{\partial r}\right),\ \frac{(\partial p/\partial r)(dr/dz)}{\partial p/\partial z}<<1\,. \tag{5.42}$$

Consequently, (5.39) can be simplified as

$$\rho_j u_j \frac{\partial u_j}{\partial z} + \rho_j v_j \frac{\partial u_j}{\partial r} = -\frac{dp}{dz} + \frac{\mu_j}{r}\frac{\partial}{\partial r}\left(r \frac{\partial u_j}{\partial r} \right). \tag{5.43}$$

Multiplying the continuity equation (5.38) by $\rho_j u_j$ and adding it to (5.43) yields

$$\frac{\partial}{\partial z}\left(\rho_j {u_j}^2\right) + \frac{1}{r}\frac{\partial}{\partial r}\left(r \rho_j u_j v_j\right) = -\frac{dp}{dz} + \frac{\mu_j}{r}\frac{\partial}{\partial r}\left(r \frac{\partial u_j}{\partial r} \right). \tag{5.44}$$

Integrating (5.44) over the cross sectional area and using Leibnitz's integral formula, we have

$$\frac{d}{dz}\left(\int_0^{r_1} \rho_v {u_v}^2 r dr + \int_{r_1}^{r_0} \rho_l {u_l}^2 r dr \right) + \left(r \rho_v u_v v_v \right)\Big|_0^{r_1} + \left(r \rho_l u_l v_l \right)\Big|_{r_1}^{r_0} = -\frac{{r_0}^2}{2}\frac{dp}{dz} + \left(r \mu_v \frac{\partial u_v}{\partial r} \right)\Big|_0^{r_1} + \left(r \mu_l \frac{\partial u_l}{\partial r} \right)\Big|_{r_1}^{r_0}. \tag{5.45}$$

Since

$$v_v\Big|_{r=0} = v_l\Big|_{r=r_0} = 0,\ u_v\Big|_{r=r_1} = u_l\Big|_{r=r_1},\ \frac{\partial u_v}{\partial r}\Big|_{r=0} = 0, \mu_v \frac{\partial u_v}{\partial r}\Big|_{r=r_1} = \mu_l \frac{\partial u_l}{\partial r}\Big|_{r=r_1}, \mu_l \frac{\partial u_l}{\partial r}\Big|_{r=r_0} = -\tau_0, \tag{5.46}$$

from the boundary and connection conditions and

$$\rho_v v_v\Big|_{r=r_1} = \rho_l v_l\Big|_{r=r_1}, \tag{5.47}$$

from the mass conservation at the phase change surface (Faghri and Zhang 2006), (5.45) is reduced to

$$-\frac{dp}{dz} = \frac{2\tau_0}{r_0} + \frac{2}{{r_0}^2}\frac{d}{dz}\left(\int_0^{r_1} \rho_v {u_v}^2 r dr + \int_{r_1}^{r_0} \rho_l {u_l}^2 r dr \right), \tag{5.48}$$

As a result, the total pressure drop can be divided into a frictional component and an acceleration component

$$-\frac{dp}{dz}=\left(-\frac{dp}{dz}\right)_f+\left(-\frac{dp}{dz}\right)_a, \tag{5.49}$$

where

$$\left(-\frac{dp}{dz}\right)_f=\frac{2\tau_0}{r_0}, \tag{5.50}$$

$$\left(-\frac{dp}{dz}\right)_a=\frac{2}{r_0^{\,2}}\frac{d}{dz}\left(\int_0^{r_1}\rho_v u_v^{\,2} r dr+\int_{r_1}^{r_0}\rho_l u_l^{\,2} r dr\right). \tag{5.51}$$

Taking the parabolic velocity profile of laminar annular flow without phase change, (5.16), which satisfy the necessary boundary and connection conditions (5.2)-(5.3), as an approximate velocity solution for laminar annular flow with phase change, and noting G is a constant for steady flow, (5.50) and (5.51) yield

$$\left(-\frac{dp}{dz}\right)_f=\frac{8G\mu_l}{r_0^{\,2}\rho_l}\frac{(1-x)}{(1-\alpha)^2},\ \phi_{l0}^2\equiv\frac{(-dp/dz)_f}{(-dp/dz)_{l0}}=\frac{(1-x)}{(1-\alpha)^2}\ , \tag{5.52}$$

$$\left(-\frac{dp}{dz}\right)_a=\frac{G^2}{\rho_l}\frac{dx}{dz}\frac{d}{dx}\left\{\frac{4(1-x)^2}{3(1-\alpha)}\left[1+\frac{\hat{\mu}^2\alpha\left(3C_0^2-3C_0\alpha+\alpha^2\right)}{\hat{\rho}(1-\alpha)^3}\right]\right\}, \tag{5.53}$$

where α should be evaluated by (5.11). These are the integral approximate solutions to the frictional and acceleration pressure gradients for condensing/evaporating annular flow of laminar vapor and liquid.

5.3.1.2. *Heat transfer problem with constant wall heat flux*

The central task of convection heat transfer analysis is to solve heat transfer coefficient, which relates wall heat flux to a convenient temperature difference. For phase change heat transfer, the difference between the saturation temperature of the working fluid and the wall temperature is generally selected to define heat transfer coefficient, i.e.

$$h_{pc} \equiv \frac{q_0}{T_0 - T_{sat}}. \tag{5.54}$$

Note such defined heat transfer coefficient is substantially different from that defined for heat transfer without phase change, e.g. in (5.25), which is based on the temperature difference of the wall and the mean stream $h_{npc} \equiv \frac{q_0}{T_0 - T_m}$.

For heat transfer with constant heat flux at wall, it is reasonable to assume (Bejan 2004)

$$\frac{\partial T_v}{\partial z} = \frac{\partial T_l}{\partial z} = \frac{dT_{sat}}{dz}. \tag{5.55}$$

Assuming that the phase change (condensation or evaporation) takes place at the liquid-vapor interface, the heat flux at the interface can be obtained from an overall energy balance of the interface and vapor phase

$$q_1 = \frac{\dot{m} h_{lv} dx + \dot{m}_v c_{pv} dT_{sat}}{2\pi r_1 dz} = \frac{G\pi r_0^2 \left(h_{lv} dx/dz + x c_{pv} dT_{sat}/dz\right)}{2\pi r_1} = \frac{G r_0 \left(\xi + x\right) c_{pv} dT_{sat}/dz}{2\alpha^{1/2}}, \tag{5.56}$$

where ξ is latent-sensible heat ratio defined by

$$\xi \equiv \frac{h_{lv} dx/dz}{c_{pv} dT_{sat}/dz}. \tag{5.57}$$

Since in most engineering applications, the saturation temperature decreases with the *z*-coordinate as a result of the total pressure drop, ξ is positive for condensing flow and negative for evaporating flow.

For condensing/evaporating laminar annular flow, the liquid temperature is governed by the steady and axisymmetric energy equation

$$\rho_l c_{pl} u_l \frac{\partial T_l}{\partial z} + \rho_l c_{pl} v_l \frac{\partial T_l}{\partial r} = k_l \left[\frac{\partial^2 T_l}{\partial z^2} + \frac{1}{r} \frac{\partial}{\partial r} \left(r \frac{\partial T_l}{\partial r} \right) \right], \tag{5.58}$$

Since (5.58) is too complicated to solve analytically, it needs to be simplified first. Following the classical boundary layer analysis (Schlichting 1968), if we assume that the *z*-direction characteristic length *L* is much greater than that of the *r*-direction, $r_0 << L$, it can be readily shown from scale analysis (Bejan 2004) that

$$\frac{\partial^2 T_l}{\partial z^2} << \frac{1}{r}\frac{\partial}{\partial r}\left(r\frac{\partial T_l}{\partial r}\right). \tag{5.59}$$

Consequently, (5.58) can be simplified as

$$\rho_l c_{pl} u_l \frac{\partial T_l}{\partial z} + \rho_l c_{pl} v_l \frac{\partial T_l}{\partial r} = \frac{k_l}{r}\frac{\partial}{\partial r}\left(r\frac{\partial T_l}{\partial r}\right), \tag{5.60}$$

As this equation is still difficult to solve analytically, we consider analytical solution to a special case that the second term on the left hand side of (5.60), the radial convection term, is negligible, as compared to the first term, the axial convection term. Such a treatment is justified, because in most engineering applications the radial convection is much less important than the axial convection. The validity of this assumption can be readily verified once the approximated solutions to the axial velocity and temperature are obtained and the radial velocity is solved from the continuity equation.

With the above assumptions, the liquid temperature is governed by

$$\rho_l c_{p_l} u_l \frac{\partial T_l}{\partial z} = \frac{k_l}{r}\frac{\partial}{\partial r}\left(r\frac{\partial T_l}{\partial r}\right), \tag{5.61}$$

subject to the boundary conditions

$$T_l\Big|_{r=r_1} = T_{sat},\ k_l \frac{dT_l}{dr}\Big|_{r=r_1} = q_1. \tag{5.62}$$

Substituting (5.16), (5.55) and (5.62) into (5.61), the heat flux and temperature at the wall can be found to be

$$q_0 = k_l \frac{\partial T_l}{\partial r}\Big|_{r=r_0} = 2r_0 G c_{pl} \frac{dT_{sat}}{dz}\left\{\frac{1-x}{4} + \frac{\xi + x}{4\hat{c}_p}\right\}, \tag{5.63}$$

$$T_0 = T_{sat} + \frac{2r_0{}^2 G c_{pl}}{k_l}\frac{dT_{sat}}{dz}\left\{\frac{1-x}{(1-\alpha)^2}\left[\left(\frac{2}{16} - \frac{\alpha}{4} + \frac{\alpha^2}{16}\right) + \left(\frac{\alpha}{4} - \frac{\alpha^2}{8}\right)\ln\alpha\right] - \frac{(\xi + x)}{8\hat{c}_p}\ln\alpha\right\}. \tag{5.64}$$

Finally, the Nusselt number for laminar annular flow with phase change is obtained as

$$\mathrm{Nu}_l \equiv \frac{2r_0 h_{pc}}{k_l} = \frac{2r_0 q_0}{k_l(T_0 - T_{sat})} = \frac{8 + \dfrac{8(\xi + x)}{\hat{c}_p(1-x)}}{\dfrac{(3-\alpha)}{(1-\alpha)} + \dfrac{2\alpha(2-\alpha)\ln\alpha}{(1-\alpha)^2} - \dfrac{2(\xi + x)\ln\alpha}{\hat{c}_p(1-x)}}. \tag{5.65}$$

If the latent-sensible heat ratio is large, we have

$$\mathrm{Nu}_l \cong \mathrm{Nu}_l\Big|_{\xi\to\infty} = \frac{4}{-\ln\alpha}, \tag{5.66}$$

where α should be evaluated by (5.11).

Figure 5.7 shows the results of (5.65) in terms of the Nusselt number as a function of the latent-sensible heat ratio, for saturated water at 100^{o}C and saturated R-134a at 50^{o}C, respectively. The predicted Nusselt number for phase change case increases monotonically with quality, in distinct contrast with the no phase change case shown in Figure 5.6. The main reason for this difference is the different definitions of heat transfer coefficient and hence Nusselt number. For the phase change case, the heat transfer coefficient is defined based on wall-interface temperature difference, and the deceasing thickness of the liquid layer with increasing quality results in the increasing Nusselt number.

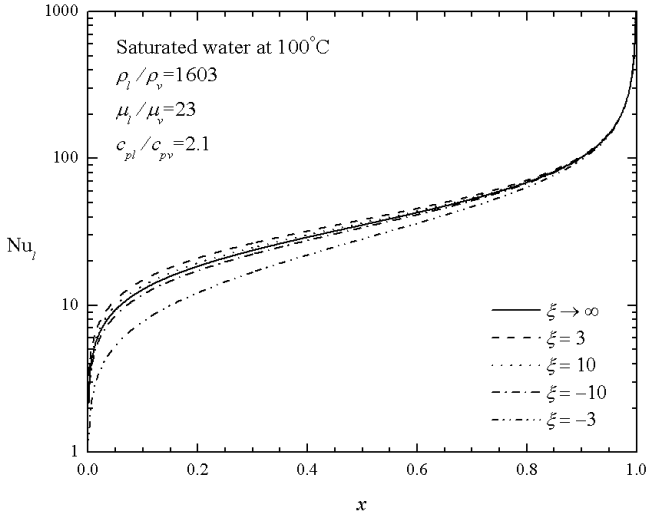

(a)

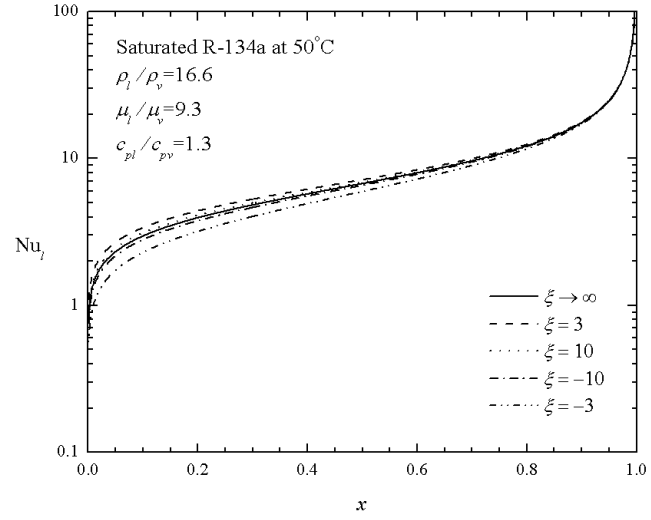

(b)

Figure 5.7 Nusselt number for laminar annular flow with phase change as a function of vapor quality and latent-sensible heat ratio.

It is clear from Figure 5.7 that (5.66) provides a very good approximation to (5.65) as long as the absolute value of the latent-sensible heat ratio is higher than 10, for both the condensing case (positive ξ) and the evaporating case (negative ξ). In most engineering applications, the latent-sensible heat ratio is very large, and (5.66) can be used to calculate phase change heat transfer.

5.3.1.3. *Applicable domain*

The applicable domain, vv, of the formulation presented in this section is defined by (5.34) and (5.37), and shown in Figure 5.8 for saturated water at 100^{o}C and saturated R-134a at 50^{o}C, respectively. Similar to the air-water system shown in Figure 5.2, the tv domain of annular flow with turbulent liquid and laminar vapor is corresponding to very low quality, and thus unlikely exists in the real engineering systems.

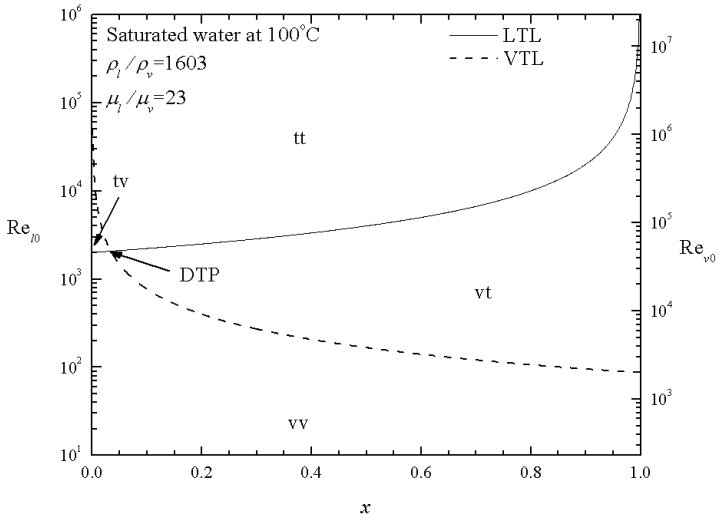

(a)

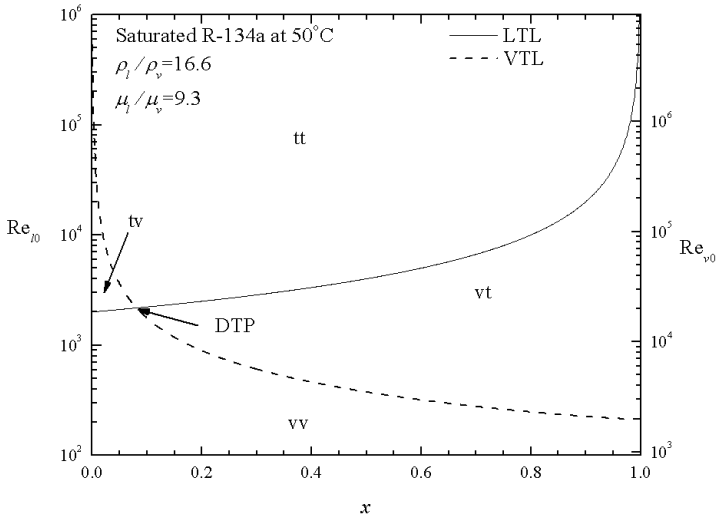

(b)

Figure 5.8 Annular flow domains (vv, vt, tv, and tt) formed by laminar-turbulent transition lines (LTL and VTL) for saturated water and R-134a.

5.3.2. Results and discussion

In this subsection, the results of the analytical model in section 5.3.1 are compared with prevailing correlations of void fraction, frictional pressure gradient, acceleration pressure gradient, and heat transfer in the literature. All the comparisons are based on the thermophysical properties of saturated water at 100^{o}C and saturated R-134a at 50^{o}C.

5.3.2.1. *Void fraction*

Figure 5.9 shows a comparison of the prediction of (5.11) with seven existing void fraction correlations (Table 5.2). For both water and R-134a cases, the void fraction given by (5.11) is significantly lower than almost all the predictions of the seven correlations, indicating that all the examined empirical correlations significantly overestimate void fraction for laminar vapor-liquid annular flow.

5.3.2.2. *Frictional pressure drop*

Figure 5.10 shows a comparison of the prediction of (5.15) with six existing frictional multiplier correlations (Table 5.3). It is clear from Figure 5.10 that the frictional multiplier predicted by the analytical model is significantly different from the predictions of the empirical correlations.

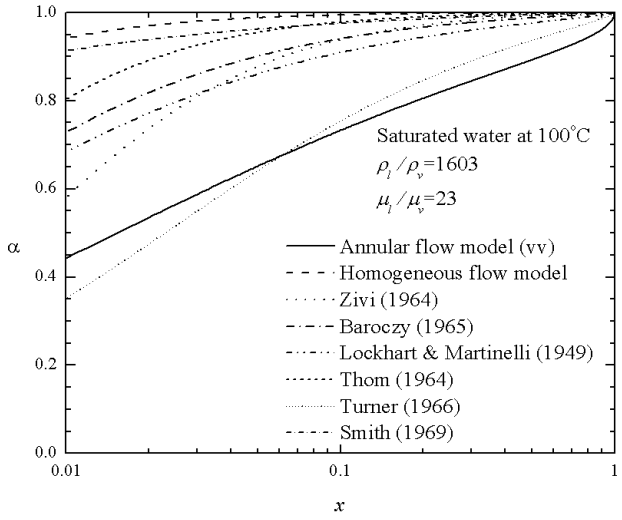

(a)

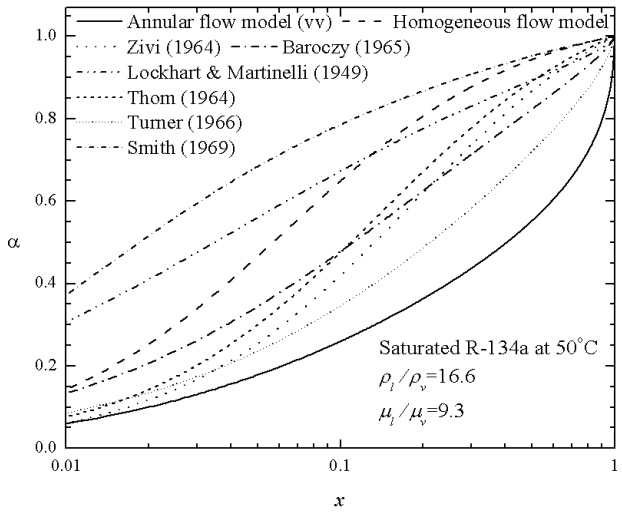

(b)

Figure 5.9 Comparison of prediction of (5.11) with empirical correlations of void fraction for saturated water and R-134a.

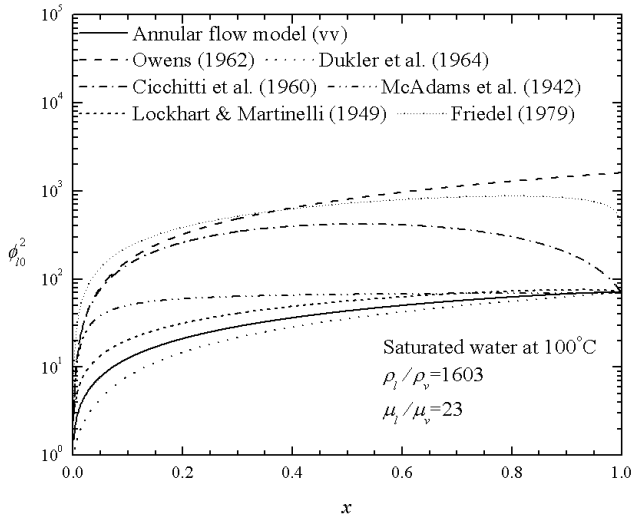

(a)

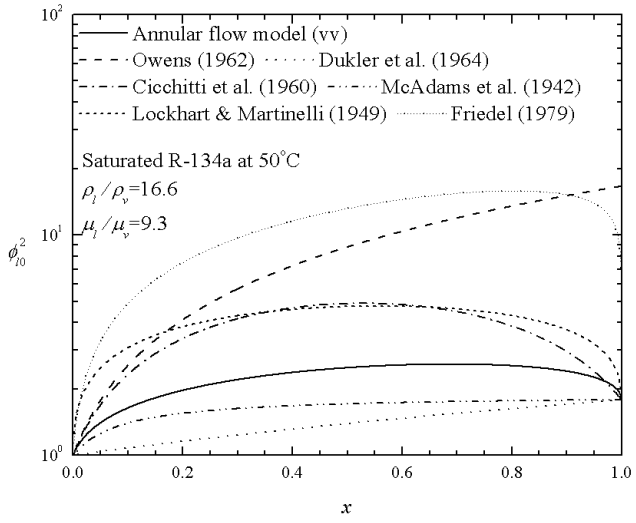

(b)

Figure 5.10 Comparison of prediction of (5.15) with empirical correlations of frictional pressure drop for saturated water and R-134a.

5.3.2.3. *Acceleration pressure drop*

Figure 5.11 shows a comparison of acceleration pressure gradients predicted by (5.53) and by the homogeneous and separated flow models (Table 5.5). It is clear that the homogeneous flow model cannot capture the quality dependence of the acceleration pressure gradient, while the separated flow model systematically underestimates the acceleration pressure gradient in laminar annular flow, for both the saturated water and R-134a cases examined here.

Table 5.5 Acceleration pressure gradient correlations.

Correlation	$\left(-\frac{dp}{dz}\right)_a$
Annular flow model	Equation (5.53)
Homogeneous flow model (e.g. Hewitt & Hall-Taylor 1970)	$\frac{G^2}{\rho_l}\frac{dx}{dz}\left(\hat{\rho}-1\right)$
Separated flow model (e.g. Hewitt & Hall-Taylor 1970)	$\frac{G^2}{\rho_l}\frac{dx}{dz}\frac{d}{dx}\left[\frac{\hat{\rho}x^2}{\alpha}+\frac{(1-x)^2}{(1-\alpha)}\right]$

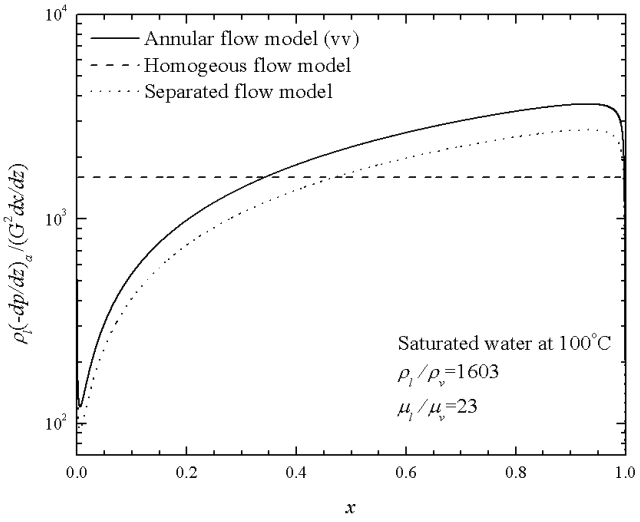

(a)

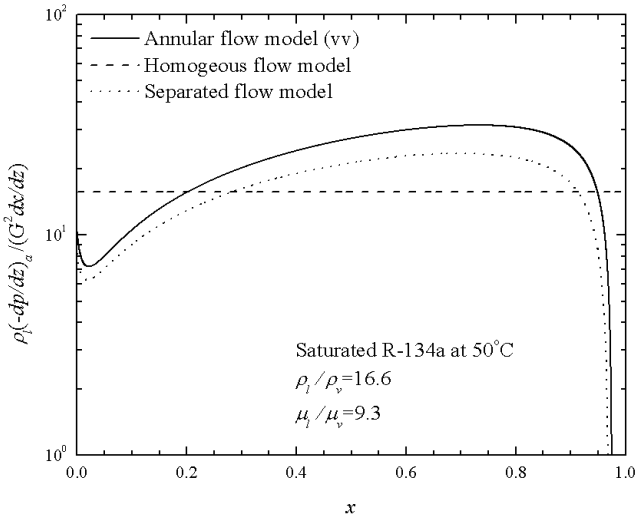

(b)

Figure 5.11 Comparison of acceleration pressure gradient predicted by (5.53) and those by the homogeneous and separated flow models for saturated water and R-134a.

5.3.2.4. *Heat transfer*

In Figure 5.12 the prediction of (5.66) is compared with two popular correlations that established through phase change two-phase flows, viz., the Shah (1979) and the Cavallini & Zecchin (1971) correlations (Table 5.4). Both the correlations are in a form of a generalization of the classical heat transfer correlation of turbulent single-phase flow. Consequently, Nusselt numbers predicted by the two correlations depend on Reynolds number of the flow. In obtaining the results of the two correlations shown in Figure 5.12, a somewhat arbitrary value of $\mathrm{Re}_{v0} = 2000$ is used. A different pick of Reynolds number will not substantially change the trend of the curves, although the absolute value of Nusselt number will be different. Note that the heat transfer coefficient of turbulent single-phase flow is defined based on wall-stream temperature difference, which is fundamentally different from the heat transfer coefficient defined bases on wall-interface (saturation) temperature difference and generally used for phase change two-phase flows, and the physical basis for the two empirical correlations is highly questionable. Nevertheless, Figure 5.12 shows that the Nusselt number predicted by the analytical model of laminar vapor-liquid annular flow has similar trend as those predicted by the empirical correlations.

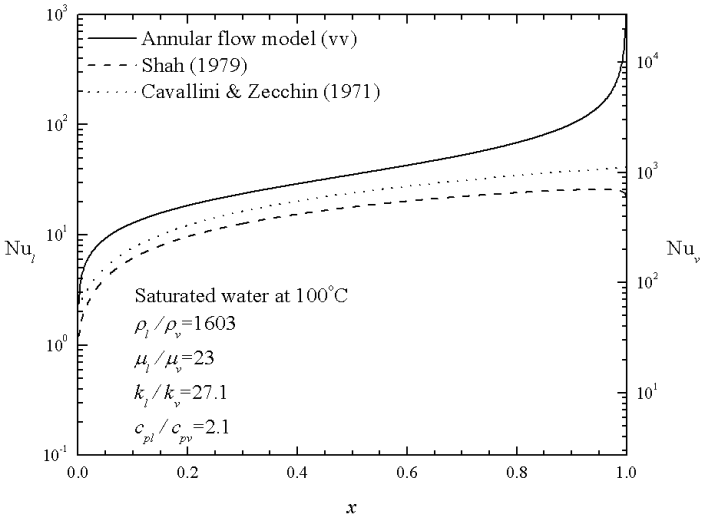

(a)

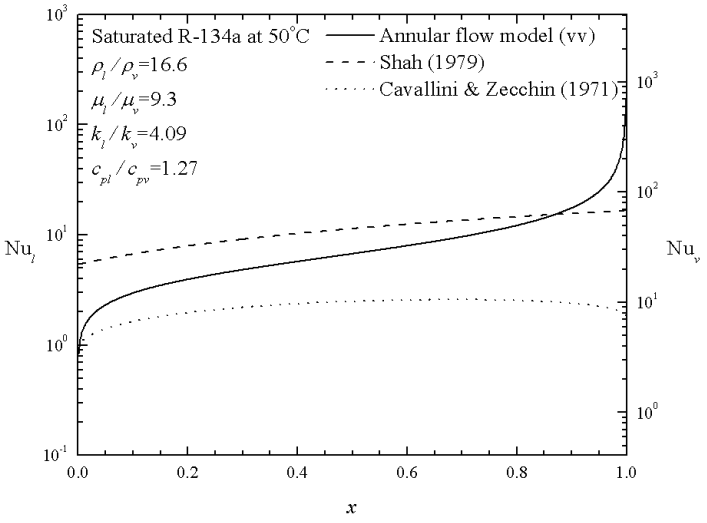

(b)

Figure 5.12 Comparison of Nusselt number predicted by (5.66) and those by empirical correlations of heat transfer for saturated water and R-134a.

5.3.3. Conclusions

An analytical model for condensing/evaporating annular flow of laminar vapor and liquid in a horizontal tube is presented. The model is based on approximation solutions of velocity and temperature distributions within the vapor and liquid phases, and predicts void fraction, frictional pressure gradient, acceleration pressure gradient, and heat transfer coefficient on a self-contained and self-consistent basis. In terms of physically reasonable definition of Reynolds numbers for the vapor and liquid phases in annular flow, the applicable domain of the analytical model is determined. In terms of saturated water at 100^{o}C and saturated R-134a at 50^{o}C as two examples, modeling results are compared with the predictions of the prevailing empirical correlations of void fraction, frictional pressure drop, acceleration pressure drop, and heat transfer for two-phase flow, and it is shown that the empirical correlations examined are generally inapplicable to horizontal annular flows of laminar vapor and liquid.

5.4 Convective Annular Flow of Turbulent Gas and Laminar Liquid

5.4.1. Formulation of the problem

5.4.1.1 *Hydrodynamic problem*

In this section, we consider the case of annular flow of turbulent gas and laminar liquid without phase change. Since there is turbulent flow involved in the gas flow, the pressure at a certain cross section and the gas velocity are no longer steady. In most engineering practices, however, the main interest is in the time-average values of the pressure and velocity instead of their transient variations from the average values. In this

section, the pressure and gas velocity should be understood in such a time-average fashion.

Following a similar procedure as in the boundary layer analysis (e.g. Bejan 2004), we can assume that the pressure is independent upon the *r*-coordinate, and thus a function of *z* only.

In order to solve the liquid velocity, we start from the axial force balance for a differential segment *dz* of the two-phase fluids cylinder of radius *r*

$$\pi r^2(-dp) = 2\pi r\tau dz\ ,\ -\frac{dp}{dz} = \frac{2\tau}{r} = \frac{2\tau_1}{r_1} = \frac{2\tau_0}{r_0}\ , \tag{5.67}$$

where $r_1 \le r \le r_0$. Assuming the liquid is Newtonian, (5.67) gives

$$\frac{du_l}{dr} = \frac{-\tau_0}{\mu_l r_0} r\ . \tag{5.68}$$

Integrating (5.68) and using the nonslip boundary condition at wall, $u_l\Big|_{r=r_0} = 0$, the exact solution of the liquid velocity is found to be

$$u_l = \frac{\tau_0 r_0}{2\mu_l}(1-\frac{r^2}{r_0^{\ 2}}). \tag{5.69}$$

This is identical to the liquid velocity for the laminar gas-liquid annular flow shown in (5.5), and the mass flow rate of the liquid phase can be obtained accordingly

$$\dot{m}_l = 2\pi\int_{r_1}^{r_0}\rho_l u_l r dr = \frac{\pi\tau_0 r_0^{\ 3}\rho_l}{4\mu_l}(1-\alpha)^2\ , \tag{5.70}$$

In terms of the definition of quality, the total mass flux can be expressed by

$$G = \frac{\dot{m}_l}{(1-x)\pi r_0^{\ 2}} = \frac{r_0\tau_0\rho_l}{4\mu_l}\frac{(1-\alpha)^2}{(1-x)}\ . \tag{5.71}$$

Therefore

$$\tau_0 = \frac{4G\mu_l}{\mathrm{r}_0\rho_l}\frac{(1-x)}{(1-\alpha)^2},\ -\frac{dp}{dz} = \frac{2\tau_0}{r_0} = \frac{8G\mu_l}{\mathrm{r}_0^{\,2}\rho_l}\frac{(1-x)}{(1-\alpha)^2}, u_l = \frac{2G}{\rho_l}\frac{(1-x)}{(1-\alpha)^2}(1-\frac{r^2}{r_0^{\,2}}), \quad (5.72)$$

and the frictional multiplier for the annular flow of turbulent gas and laminar liquid can be expressed by

$$\phi_{l0}^2 \equiv \frac{(-dp/dz)_f}{(-dp/dz)_{l0}} = \frac{(1-x)}{(1-\alpha)^2}\ . \quad (5.73)$$

This is in exact the same form as (5.15), except that the void fraction should be determined based on the mass flow rates of the laminar liquid flow, (5.70), and the turbulent gas flow, which will be determined next.

For the turbulent gas flow, it is impossible to solve velocity from the transient Navier-Stokes equation. Instead, we adopt the universal turbulent velocity profile proposed by Prandtl and Taylor (Schlichting 1960), which is also called the law of the wall (Bejan 2004), based on the mixing length assumption (Prandtl, 1969) to express the gas velocity by

$$u_v^+ = y_v^+ \quad \text{for } y_v^+ < y_{VSL}^+,\ u_v^+ = A\ln y_v^+ + B \quad \text{for } y_v^+ > y_{VSL}^+, \quad (5.74)$$

where

$$u_v^+ = \frac{u_v - u_l\big|_{r=r_1}}{u_v^\tau},\ y_v^+ = \frac{(r_1 - r)\rho_v u_v^\tau}{\mu_v},\ u_v^\tau = \left(\frac{\tau_1}{\rho_v}\right)^{\frac{1}{2}} = \left(\frac{\tau_0\alpha^{\frac{1}{2}}}{\rho_v}\right)^{\frac{1}{2}}, \quad (5.75)$$

and $A \cong 2.5$, $B \cong 5.5$, $y_{VSL}^+ \cong 11.6$. Accordingly, the mass flow rate of the gas flow is found to be

$$\dot{m}_v = \int_0^{r_1}\rho_v u_v 2\pi r dr = 2\pi\mu_v r_1\int_0^{R_v^+} u_v^+(1-\frac{y_v^+}{R_v^+})dy_v^+ = \pi\mu_v r_1 A\left(R_v^+\ln R_v^+ + b_1 R_v^+ + b_2 + \frac{b_3}{R_v^+}\right), \quad (5.76)$$

where

$$b_1 = \frac{B}{A} - \frac{3}{2} \cong 0.7\,, \tag{5.77}$$

$$b_2 = \frac{y_{VSL}^{+2}}{A} - 2y_{VSL}^{+}\left(\ln y_{VSL}^{+} + \frac{B}{A} - 1\right) \cong -30.88\,, \tag{5.78}$$

$$b_3 = y_{VSL}^{+2}\ln y_{VSL}^{+} - \frac{2y_{VSL}^{+3}}{3A} + y_{VSL}^{+2}\left(\frac{B}{A} - \frac{1}{2}\right) \cong 142.32\,, \tag{5.79}$$

and R_v^+ is the dimensionless interface radius, which is defined by

$$R_v^+ \equiv \frac{r_1\rho_v u_v^\tau}{\mu_v} = \frac{r_0\tau_0^{\frac{1}{2}}\rho_v^{\frac{1}{2}}\alpha^{\frac{3}{4}}}{\mu_v} = \left[\frac{2\,\mathrm{Re}_{v0}\,\hat{\mu}(1-x)}{\hat{\rho}}\right]^{\frac{1}{2}}\frac{\alpha^{\frac{3}{4}}}{(1-a)}\,, \tag{5.80}$$

where

$$\mathrm{Re}_{v0} \equiv \frac{2r_0 G}{\mu_v}\,. \tag{5.81}$$

Dividing (5.76) by (5.70) yields an implicit relation for solving the void fraction

$$R_v^+\ln R_v^+ + b_1 R_v^+ + b_2 + \frac{b_3}{R_v^+} = \frac{\mathrm{Re}_v}{2A} = \frac{\mathrm{Re}_{v0}\sqrt{\alpha}}{2A}\left[\frac{x}{\alpha} - \frac{2(1-x)}{\hat{\rho}(1-\alpha)}\right]. \tag{5.82}$$

(5.82) shows that for the annular flow of turbulent gas and laminar liquid, the void fraction depends upon Reynolds number, which is a fundamental difference from the laminar annular flow case, as shown in (5.11). For given x and Re_{v0}, the void fraction in the vt domain can be solved from (5.82) by applying appropriate numerical algorithm, e.g., the secant method.

5.4.1.2. *Heat transfer problem with constant wall heat flux*

The temperature distribution in the liquid phase can be determined in the same way as in section 5.2.1.2. The heat transfer problem of fully developed liquid flow in a

round tube is governed by the following energy equation and boundary conditions (Bejan 2004)

$$\frac{\partial^2 T_l}{\partial r^2}+\frac{1}{r}\frac{\partial T_l}{\partial r}=\frac{\rho_l c_{pl} u_l}{k_l}\frac{\partial T_l}{\partial z},\ T_l\Big|_{r=r_0}=T_0,\ k_l\frac{\partial T_l}{\partial r}\Big|_{r=r_0}=q_0. \tag{5.83}$$

Energy balance for a differential segment *dz* of the two-phase fluids yields

$$\dot{m}_l c_{pl} dT_m+\dot{m}_v c_{pv} dT_m=2\pi r_0 q_0 dz,\ \frac{dT_m}{dz}=\frac{2q_0}{Gr_0 c_{pl}(1-x)(1+\hat{x}/\hat{c}_p)}, \tag{5.84}$$

where $\hat{c}_p \equiv c_{pl}/c_{pv}$. For fully developed convection heat transfer problem with constant heat flux at the tube wall, we may assume (Bejan 2004)

$$\frac{\partial T_l}{\partial z}=\frac{\partial T_v}{\partial z}=\frac{dT_m}{dz}, \tag{5.85}$$

Substituting (5.84) and (5.85) into (5.83), and using the liquid velocity shown in (5.75), the exact temperature distribution in the liquid phase is obtained as follows

$$T_l=T_0+C_1\frac{r_0 q_0}{k_l}\left(\frac{r^2}{r_0^{\,2}}-\frac{r^4}{4r_0^{\,4}}-\frac{3}{4}\right)+C_2\frac{r_0 q_0}{k_l}\ln\frac{r}{r_0}, \tag{5.86}$$

where

$$C_1=\frac{1}{(1+\hat{x}/\hat{c}_p)(1-\alpha)^2},\ C_2=1-C_1. \tag{5.87}$$

Since it is impossible to solve the temperature distribution in the turbulent gas flow, the gas temperature is assumed based on the mixing length assumption (Prandtl 1969) to follow a universal profile (Bejan 2004)

$$T_v^+=\mathrm{Pr}_v\, y_v^+ \quad \text{for } y_v^+<y_{CSL}^+,\ T_v^+=A_T\ln y_v^+ + B_T \quad \text{for } y_v^+>y_{CSL}^+, \tag{5.88}$$

where

$$T_v^+ = \frac{\left(T_l\big|_{r=r_1} - T_v\right)\rho_v c_{pv} u_v^\tau}{q_1},\ A_T \cong 2.195,\ B_T \cong 13.2\,\mathrm{Pr}_v - 5.66,\ y_{CSL}^+ \cong 13.2, \qquad (5.89)$$

and Pr_v is Prandtl number of the gas. On the basis of (5.85), energy balance for the gas flow and for the two phases yields

$$\frac{dT_m}{dz} = \frac{2q_0}{Gr_0 c_{pl}(1 - x + x/\hat{c}_p)} = \frac{2r_1 q_1}{G{r_0}^2 c_{pv} x},\ q_1 = \frac{q_0}{\left(1 + \hat{c}_p/\hat{x}\right)\alpha^{\frac{1}{2}}}. \qquad (5.90)$$

Combining (5.86)-(5.90), the gas temperature is found to be

$$\begin{aligned} T_v = T_0 &+ C_1 \frac{r_0 q_0}{k_l}\left(\alpha - \frac{\alpha^2}{4} - \frac{3}{4}\right) + C_2 \frac{r_0 q_0}{2k_l}\ln\alpha \\ &+ \frac{q_0}{\left(1 + \hat{c}_p/\hat{x}\right)\tau_0^{\frac{1}{2}}\rho_v^{\frac{1}{2}} c_{pv}\alpha^{\frac{3}{4}}}\left[A_T \ln\left(\frac{(r_1 - r)\tau_0^{\frac{1}{2}}\rho_v^{\frac{1}{2}}\alpha^{\frac{1}{4}}}{\mu_v}\right) + B_T\right]. \end{aligned} \qquad (5.91)$$

Evaluating the stream-wall temperature difference by

$$T_m - T_0 = \frac{\int_{r_1}^{r_0} \rho_l c_{pl} u_l (T_l - T_0) 2\pi r dr + \int_0^{r_1} \rho_v c_{pv} u_v (T_v - T_0) 2\pi r dr}{c_{pl}\dot{m}_l + c_{pv}\dot{m}_v}, \qquad (5.92)$$

the Nusselt number for annular flow of turbulent gas and laminar liquid can be expressed by

$$\mathrm{Nu}_l \equiv \frac{2r_0 h_{npc}}{k_l} = \frac{2r_0 q_0}{k_l(T_0 - T_m)} = \left(N_1 + N_2 + N_3 + N_4 + N_5 + N_6\right)^{-1}, \qquad (5.93)$$

where h_{npc} is the heat transfer coefficient for no phase change case and

$$N_1 = C_1^2\left(\frac{11}{48} - \frac{3}{4}\alpha + \frac{7}{8}\alpha^2 - \frac{5}{12}\alpha^3 + \frac{1}{16}\alpha^4\right), \qquad (5.94)$$

$$N_2 = C_1 C_2\left(\frac{3}{8} - \frac{\alpha}{2} + \frac{1}{8}\alpha^2 - \frac{1}{4}\alpha^2\ln\alpha + \frac{1}{2}\alpha\ln\alpha\right), \qquad (5.95)$$

$$N_3 = \frac{-(1-\alpha)R_v^{+2}\left[C_1\left(\alpha - \frac{\alpha^2}{4} - \frac{3}{4}\right) + \frac{C_2}{2}\ln\alpha\right]}{4A\hat{\mu}\alpha\left(\hat{c}_p/\hat{x}+1\right)\left(R_v^+\ln R_v^+ + b_1 R_v^+ + b_2 + \frac{b_3}{R_v^+}\right)}, \tag{5.96}$$

$$N_4 = \frac{-\left[C_1\left(\alpha - \frac{\alpha^2}{4} - \frac{3}{4}\right) + \frac{C_2}{2}\ln\alpha\right]}{2\left(\hat{c}_p/\hat{x}+1\right)}, \tag{5.97}$$

$$N_5 = \frac{A_T\hat{k}(1-\alpha)\left(R_v^+\ln R_v^+ + b_{T1}R_v^+ + b_{T2} + \frac{b_{T3}}{R_v^+}\right)}{4A\hat{\mu}\,\mathrm{Pr}_v\,\alpha\left(\hat{c}_p/\hat{x}+1\right)^2\left(R_v^+\ln R_v^+ + b_1 R_v^+ + b_2 + \frac{b_3}{R_v^+}\right)}, \tag{5.98}$$

$$N_6 = \frac{\hat{k}\left(N_7\,\mathrm{Pr}_v + N_8 A_T\right)}{\mathrm{Pr}_v\,\alpha\left(\hat{c}_p/\hat{x}+1\right)^2 R_v^+\left(R_v^+\ln R_v^+ + b_1 R_v^+ + b_2 + \frac{b_3}{R_v^+}\right)}, \tag{5.99}$$

$$b_{T1} = \frac{B_T}{A_T} - \frac{3}{2}, \tag{5.100}$$

$$b_{T2} = \frac{\mathrm{Pr}_v}{A_T}y_{CSL}^{+2} - 2y_{CSL}^+\left(\ln y_{CSL}^+ + \frac{B_T}{A_T} - 1\right), \tag{5.101}$$

$$b_{T3} = y_{CSL}^{+2}\left(\ln y_{CSL}^+ + \frac{B_T}{A_T} - \frac{1}{2}\right) - \frac{2\,\mathrm{Pr}_v\,y_{CSL}^{+3}}{3A_T}, \tag{5.102}$$

$$\begin{aligned} N_7 = {} & y_{CSL}^{+2}\ln y_{CSL}^+ - y_{VSL}^{+2}\ln y_{VSL}^+ - \frac{2}{3R_v^+}\left(y_{CSL}^{+3}\ln y_{CSL}^+ - y_{VSL}^{+3}\ln y_{VSL}^+\right) \\ & + \left(\frac{B}{A} - \frac{1}{2}\right)\left(y_{CSL}^{+2} - y_{VSL}^{+2}\right) - \frac{2}{3R_v^+}\left(\frac{B}{A} - \frac{1}{3}\right)\left(y_{CSL}^{+3} - y_{VSL}^{+3}\right) \\ & + \frac{2}{3A}y_{VSL}^{+3} - \frac{1}{2AR_v^+}y_{VSL}^{+4}, \end{aligned} \tag{5.103}$$

$$N_8 = R_v^+ \ln^2 R_v^+ + \left(\frac{B}{A} + \frac{B_T}{A_T} - 3\right) R_v^+ \ln R_v^+ + \left(\frac{BB_T}{AA_T} - \frac{3B}{2A} - \frac{3B_T}{2A_T} + \frac{7}{2}\right) R_v^+ + \frac{y_{CSL}^{+2}}{R_v^+}\left[\ln^2 y_{CSL}^+ + \left(\frac{B}{A} + \frac{B_T}{A_T} - 1\right)\left(\ln y_{CSL}^+ - \frac{1}{2}\right) + \frac{BB_T}{AA_T}\right] - 2y_{CSL}^+\left[\ln^2 y_{CSL}^+ + \left(\frac{B}{A} + \frac{B_T}{A_T} - 2\right)\left(\ln y_{CSL}^+ - 1\right) + \frac{BB_T}{AA_T}\right]. \quad (5.104)$$

5.4.1.3. *Applicable domain*

The formulation presented in sections 5.4.1.1 and 5.4.1.2 is only applicable to horizontal annular flow of turbulent gas and laminar liquid, i.e., the vt domain, defined by

$$\mathrm{Re}_l \equiv (1-x)\mathrm{Re}_{l0} < \mathrm{Re}_{cr} \text{ and } \mathrm{Re}_v \equiv \sqrt{\alpha}\left[\frac{x}{\alpha} - \frac{2(1-x)}{\hat{\rho}(1-\alpha)}\right]\mathrm{Re}_{v0} > \mathrm{Re}_{cr}. \quad (5.105)$$

In contrast to that the liquid transition line (LTL), $\mathrm{Re}_{l0} = \mathrm{Re}_{cr}/(1-x)$, is uniquely defined in the $\mathrm{Re}_{l0} \sim x$ plane, the gas transition line (VTL) is dependent upon void fraction, which is determined by (5.82) for the vt domain and by (5.9) for the vv domain. It is interesting to check if the two equations give the same void fraction for laminar-turbulent transition and thus the same VTL. Submitting $\mathrm{Re}_v = \mathrm{Re}_{cr} \cong 2000$ and $A \cong 2.5$ into (5.82) yields $R_v^+ \cong 83.7$, and (5.80) can be rewritten as

$$\frac{x}{1-x} = \frac{2\alpha}{\hat{\rho}(1-\alpha)} + \frac{\mathrm{Re}_{cr}}{R_v^{+2}} \frac{\hat{\mu}\alpha^2}{\hat{\rho}(1-\alpha)^2} \cong \frac{2\alpha}{\hat{\rho}(1-\alpha)} + \frac{0.57\hat{\mu}\alpha^2}{\hat{\rho}(1-\alpha)^2}. \quad (5.106)$$

Comparing (5.106) with (5.9), we can see the difference in the coefficient of the second term of the right hand side. This difference actually shows the incompatibility of the theory caused by the approximation of the universal turbulent profile. For most engineering systems, however, the difference between VTL-vt based on (5.82) and VTL-

vv based on (5.9) is negligible, as shown in Figure 5.13, for air-water system at room temperature as an example. Considering that laminar-turbulent transition does not occur at a precise Reynolds number, the VTL-vv based on (5.9) is accurate enough to partition different domains of annular flow for various engineering applications.

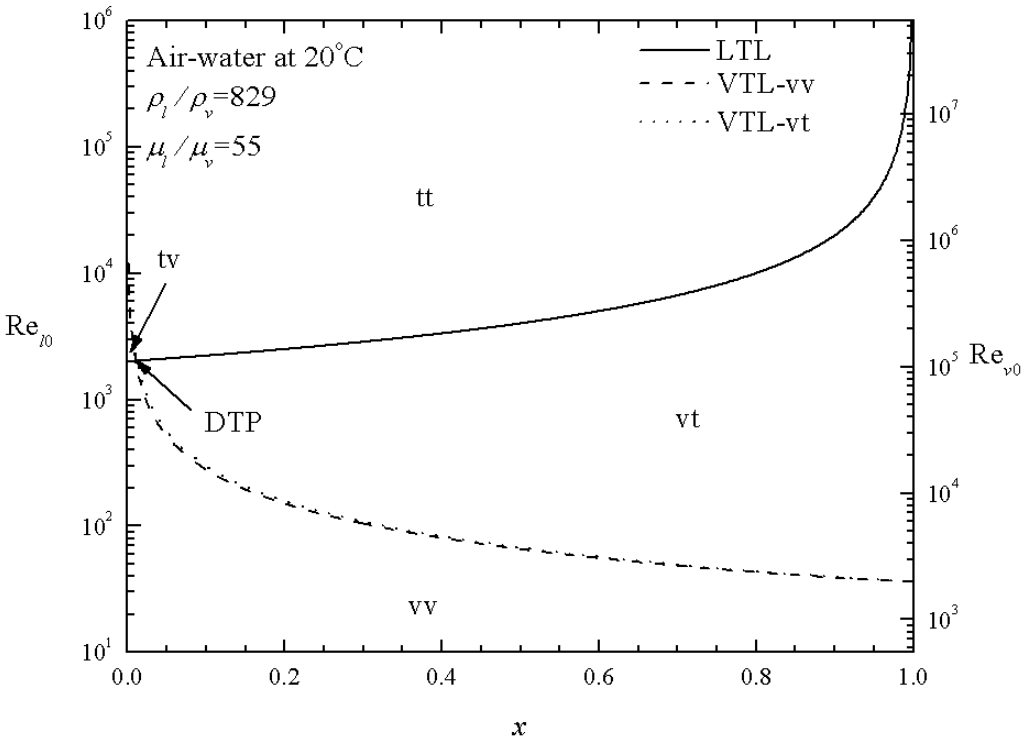

Figure 5.13 Annular flow domains (vv, vt, tv, and tt) formed by laminar-turbulent transition lines (LTL and VTL) for air-water system.

5.4.2. Results and discussion

In this subsection, the results of the analytical model presented in subsections 5.4.1.1 and 5.4.1.2 are compared with prevailing correlations of void fraction, frictional pressure drop, and heat transfer in the literature. All the comparisons are based on the air-water system at 20^{o}C.

5.4.2.1. *Void fraction*

Figure 5.14 shows a comparison of the prediction of (5.82) with seven existing void fraction correlations (Table 5.2). Although (5.82) predicts that void fraction for annular flow in the vt domain is a function of Reynolds number, the empirical α - x correlations examined here are dependent upon density ratio and viscosity ratio only, i.e., independent upon Reynolds number. It is clear from Figure 5.14 that the void fractions given by (5.82) for Re_{l0} = 500, 1000, 2000, and 4000, respectively, are close to the prediction of the Turner (1966) correlation, and significantly lower than the predictions of all the other six correlations, suggesting these six correlations significantly overestimate the void fraction for horizontal annular flow in the vt domain.

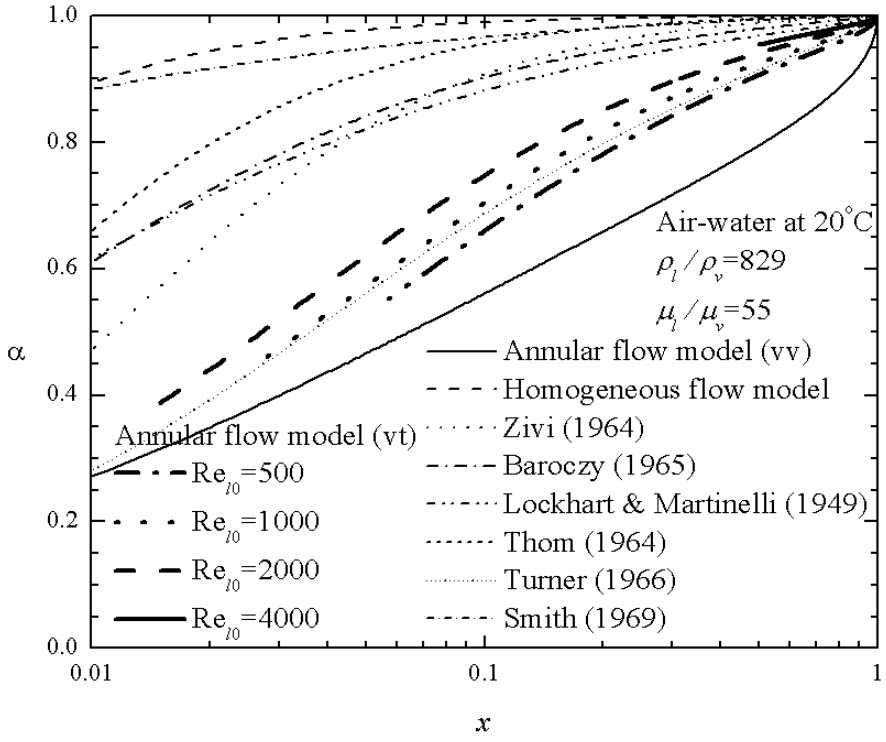

Figure 5.14 Comparison of prediction of (5.82) with empirical correlations of void fraction.

5.4.2.2. *Frictional pressure drop*

Figure 5.15 shows a comparison of the prediction of (5.73) with two popular frictional multiplier correlations (Table 5.6) for Re_{l0} = 500, 1000, 2000, and 4000, respectively, in the vt domain. It is clear from Figure 5.15 that the frictional multiplier predicted by the analytical model is significantly different from the predictions of the empirical correlations. All the perditions of the Lockhart & Martinelli (1949) correlation are lower, while those of the Friedel (1979) correlation are higher than the corresponding analytical results. Moreover, both the two empirical correlation predict that the frictional pressure drop decreases when Reynolds number increases, while the annular flow model predicts

the opposite, i.e., the frictional pressure drop increase with the Reynolds number. Figure 5.15 also shows that the frictional pressure drop in the vt domain is higher than that in the vv domain.

Table 5.6 Frictional multiplier correlations for the vt domain.

Correlation	ϕ_{l0}^2
Annular flow model	Equations (5.73) and (5.82)
Lockhart & Martinelli (1949)	$\phi_{l0}^2 = (1-x)\left(1+\frac{12}{X_{vt}}+\frac{1}{X_{vt}^2}\right),\ X_{vt}^2 = \frac{16\,\mathrm{Re}_{v0}^{0.75}(1-x)}{0.079\hat{\rho}\sqrt{\hat{\mu}}x^{1.75}}$
Friedel (1979)	$\phi_{l0}^2 = (1-x)^2 + \frac{16x^2\hat{\rho}\hat{\mu}}{0.079\,\mathrm{Re}_{v0}^{0.75}} + 3.23x^{0.78}(1-\mathrm{x})^{0.224}\hat{\rho}^{0.91}\hat{\mu}^{-0.19}(1-\hat{\mu}^{-1})^{0.7}$

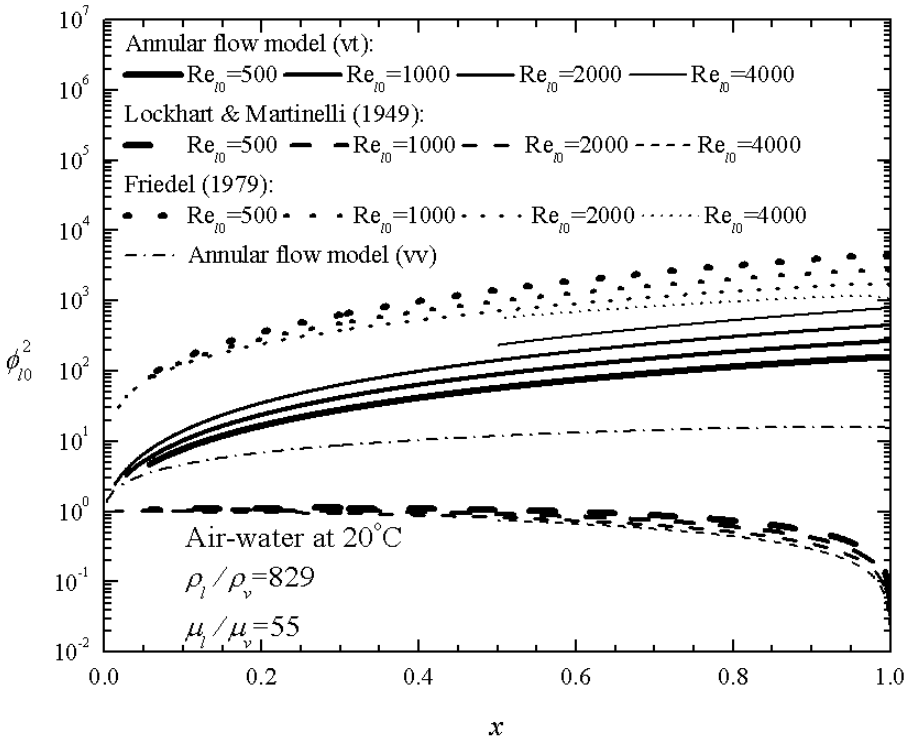

Figure 5.15 Comparison of prediction of (5.73) with empirical correlations of frictional pressure drop for two-phase flow in the vt domain.

5.4.2.3. *Heat transfer*

Since we cannot find any heat transfer correlation for gas-liquid two-phase flows without phase change, we compare in Figure 5.16 the prediction of (5.93) with two popular correlations that established through phase change two-phase flows, viz., the Shah (1979) and the Cavallini & Zecchin (1971) correlations (Table 5.4), for Re_{l0} = 500, 1000, 2000, and 4000, respectively, in the vt domain.. Both the correlations are in a form of a generalization of the classical heat transfer correlation of turbulent single-phase flow.

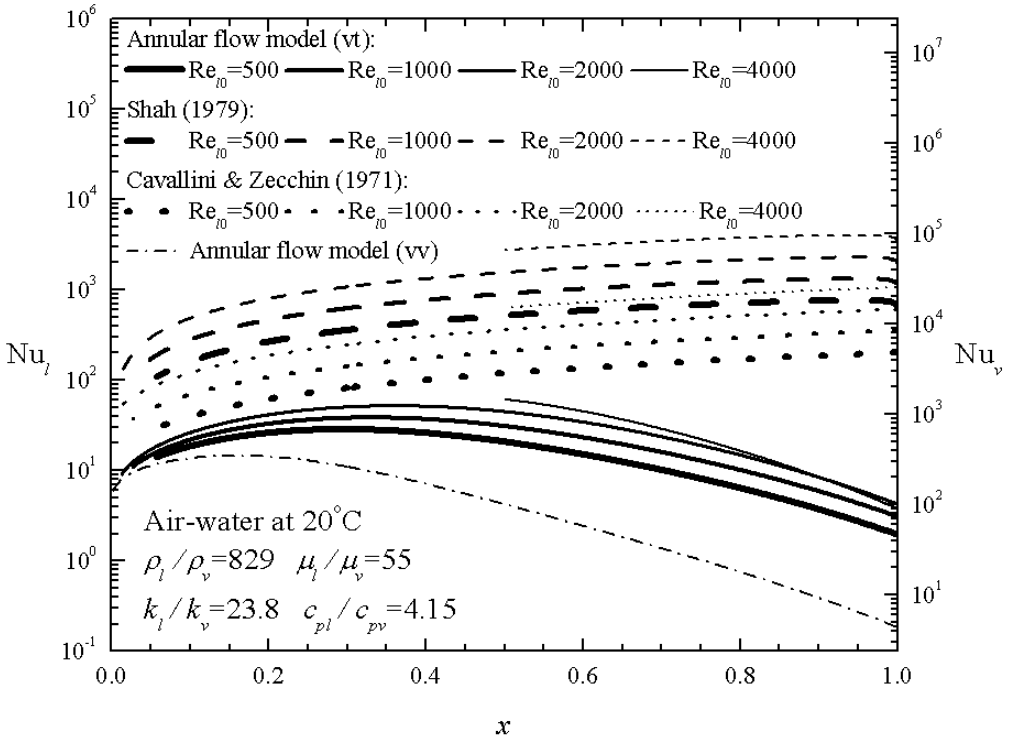

Figure 5.16 Comparison of prediction of (5.93) with empirical correlations of heat transfer.

It is clear from Figure 5.16 that the Nusselt numbers predicted by the analytical model are significantly smaller and in different trend, as compared with those predicted by the empirical correlations. Therefore, we conclude that the Shah (1979) and the Cavallini & Zecchin (1971) correlations cannot give reliable heat transfer predictions for horizontal annular flow of turbulent gas and laminar liquid without phase change. Figure 5.16 also shows that the heat transfer in the vt domain is better than the vv domain.

5.4.3. Conclusions

An analytical model for convective annular flow of turbulent gas and laminar liquid in a horizontal tube is presented. The model is based on exact solutions of velocity and temperature distributions for the liquid phase and universal turbulent velocity and temperature profiles for the gas phase, and predicts void fraction, frictional pressure gradient, and heat transfer coefficient on a self-contained and self-consistent basis. In terms of physically reasonable definition of Reynolds numbers for the gas and liquid phases in annular flow, the applicable domain of the analytical model is determined. In terms of the air-water system at room temperature as an example, modeling results show that the prevailing empirical correlations of void fraction, frictional pressure drop, and heat transfer for two-phase flow are generally inapplicable to horizontal annular flows of turbulent gas and laminar liquid, except that the Turner (1966) correlation provide fairly good approximation to the void fraction of annular flow in the vt domain with Re_{l0} between 500 and 1000.

5.5 Condensing/Evaporating Annular Flow of Turbulent Vapor and Laminar Liquid

5.5.1. Formulation of the problem

5.3.1.1 *Hydrodynamic problem*

When phase change (condensation or evaporation) occurs in the annular flow of turbulent vapor and laminar liquid, the liquid velocity u_l and vapor velocity u_v depend upon both *r*-coordinate and *z*-coordinate. In addition, since the vapor flow is turbulent, both the pressure and the vapor velocity are unsteady. However, for most engineering applications,

the main interest is in the time-average values of the pressure and velocity, which we consider as steady and still are denoted by p and u_v.

Following the classical boundary layer analysis (Schlichting 1968), if we assume that the z-direction characteristic length L is much greater than that of the r-direction, $r_0 << L$, the momentum balances, Navier-Stokes equations, for the liquid and vapor phases can be written respectively by (Bejan 2004)

$$\rho_l u_l \frac{\partial u_l}{\partial z} + \rho_l v_l \frac{\partial u_l}{\partial r} = -\frac{dp}{dz} + \frac{\mu_l}{r}\frac{\partial}{\partial r}\left(r\frac{\partial u_l}{\partial r}\right), \tag{5.107}$$

$$\rho_v u_l \frac{\partial u_v}{\partial z} + \rho_v v_v \frac{\partial u_v}{\partial r} = -\frac{dp}{dz} + \frac{1}{r}\frac{\partial}{\partial r}\left[r(\mu_v + \rho_v \varepsilon_M)\frac{\partial u_v}{\partial r}\right], \tag{5.108}$$

where ε_M is momentum eddy diffusivity, and the continuity equations for the two phases are

$$\frac{\partial u_l}{\partial z} + \frac{1}{r}\frac{\partial (r v_l)}{\partial r} = 0\,,\ \frac{\partial u_v}{\partial z} + \frac{1}{r}\frac{\partial (r v_v)}{\partial r} = 0\,. \tag{5.109}$$

Multiplying the continuity equations by the product of the corresponding density and velocity and adding it to the Navier-Stokes equations yields

$$\frac{\partial}{\partial z}\left(\rho_l {u_l}^2\right) + \frac{1}{r}\frac{\partial}{\partial r}\left(r\rho_l u_l v_l\right) = -\frac{dp}{dz} + \frac{\mu_l}{r}\frac{\partial}{\partial r}\left(r\frac{\partial u_l}{\partial r}\right), \tag{5.110}$$

$$\frac{\partial}{\partial z}\left(\rho_v {u_v}^2\right) + \frac{1}{r}\frac{\partial}{\partial r}\left(r\rho_v u_v v_v\right) = -\frac{dp}{dz} + \frac{1}{r}\frac{\partial}{\partial r}\left[r(\mu_v + \rho_v \varepsilon_M)\frac{\partial u_v}{\partial r}\right]. \tag{5.111}$$

Integrating (5.110) and (5.111) over the cross sectional area and using Leibnitz's integral formula, we have

$$\frac{d}{dz}\left(\int_0^{r_1}\rho_v {u_v}^2 r dr+\int_{r_1}^{r_0}\rho_l {u_l}^2 r dr\right)+\left(r\rho_v u_v v_v\right)\Big|_0^{r_1}+\left(r\rho_l u_l v_l\right)\Big|_{r_1}^{r_0}=-\frac{{r_0}^2}{2}\frac{dp}{dz}$$
$$+\left[r\left(\mu_v+\rho_v\varepsilon_M\right)\frac{\partial u_v}{\partial r}\right]\Big|_0^{r_1}+\left(r\mu_l\frac{\partial u_l}{\partial r}\right)\Big|_{r_1}^{r_0}. \tag{5.112}$$

The boundary and connection conditions of the problem give

$$v_v\Big|_{r=0}=v_l\Big|_{r=r_0}=0,\ u_v\Big|_{r=r_1}=u_l\Big|_{r=r_1},\ \frac{\partial u_v}{\partial r}\Big|_{r=0}=0,\mu_v\frac{\partial u_v}{\partial r}\Big|_{r=r_1}=\mu_l\frac{\partial u_l}{\partial r}\Big|_{r=r_1},\mu_l\frac{\partial u_l}{\partial r}\Big|_{r=r_0}=-\tau_0. \tag{5.113}$$

The mass conservation at the phase change surface yields (Faghri and Zhang 2006)

$$\rho_v v_v\Big|_{r=r_1}=\rho_l v_l\Big|_{r=r_1}. \tag{5.114}$$

The liquid vapor interface is a surface joining the laminar liquid flow and the laminar (vicious) sublayer of the turbulent vapor boundary layer yields

$$\varepsilon_M\Big|_{r=r_1}=0. \tag{5.115}$$

Substituting (5.113)-(5.115) into (5.112), we have

$$-\frac{dp}{dz}=\frac{2\tau_0}{r_0}+\frac{2}{{r_0}^2}\frac{d}{dz}\left(\int_0^{r_1}\rho_v {u_v}^2 r dr+\int_{r_1}^{r_0}\rho_l {u_l}^2 r dr\right), \tag{5.116}$$

which shows the total pressure drop can be divided into a frictional component and an acceleration component

$$-\frac{dp}{dz}=\left(-\frac{dp}{dz}\right)_f+\left(-\frac{dp}{dz}\right)_a, \tag{5.117}$$

where

$$\left(-\frac{dp}{dz}\right)_f=\frac{2\tau_0}{r_0}, \tag{5.118}$$

$$\left(-\frac{dp}{dz}\right)_a=\frac{2}{{r_0}^2}\frac{d}{dz}\left(\int_0^{r_1}\rho_v {u_v}^2 r dr+\int_{r_1}^{r_0}\rho_l {u_l}^2 r dr\right). \tag{5.119}$$

Taking the velocity distributions, (5.72) and (5.74), of annular flow of turbulent gas and laminar liquid without phase change as approximate velocities for the phase change case, and noting G is a constant for steady flow, (5.118) and (5.119) yield

$$\left(-\frac{dp}{dz}\right)_f = \frac{8G\mu_l}{r_0^{\,2}\rho_l}\frac{(1-x)}{(1-\alpha)^2},\ \phi_{l0}^2 \equiv \frac{(-dp/dz)_f}{(-dp/dz)_{l0}} = \frac{(1-x)}{(1-\alpha)^2}\ , \tag{5.120}$$

$$\left(-\frac{dp}{dz}\right)_a = \frac{G^2}{\rho_l}\frac{dx}{dz}\frac{d}{dx}\{M_1+M_2+M_3+M_4\}, \tag{5.121}$$

where

$$M_1 = \frac{4(1-x)^2}{3(1-\alpha)}, \tag{5.122}$$

$$M_2 = \frac{4\alpha(1-x)^2}{\hat{\rho}(1-\alpha)^2}, \tag{5.123}$$

$$M_3 = \frac{8\alpha^{\frac{1}{2}}(1-x)A}{(1-\alpha)\mathrm{Re}_{v0}}\left(R_v^+\ln R_v^+ + b_1R_v^+ + b_2 + \frac{b_3}{R_v^+}\right), \tag{5.124}$$

$$M_4 = \frac{8\hat{\rho}R_v^+A^2}{\mathrm{Re}_{v0}^2}\left(R_v^+\ln^2 R_v^+ + b_1R_v^+\ln R_v^+ + b_4R_v^+ + b_5 + \frac{b_6}{R_v^+}\right), \tag{5.125}$$

$$b_4 = \frac{B^2}{A^2} - \frac{3B}{A} + \frac{7}{2} \cong 1.74, \tag{5.126}$$

$$b_5 = -2\left[y_{VSL}^+\ln^2 y_{VSL}^+ + 2\left(\frac{B}{A}-1\right)y_{VSL}^+\left(\ln y_{VSL}^+ - 1\right) + \frac{B^2}{A^2}y_{VSL}^+ - \frac{1}{3A}y_{VSL}^{+3}\right] \cong 83.79, \tag{5.127}$$

$$b_6 = y_{VSL}^{+2}\ln^2 y_{VSL}^+ + \left(\frac{2B}{A}-1\right)y_{VSL}^{+2}\left(\ln y_{VSL}^+ - \frac{1}{2}\right) + \frac{B^2}{A^2}y_{VSL}^{+2} - \frac{1}{2A^2}y_{VSL}^{+4} \cong 903.71, \tag{5.128}$$

b_1, b_2, b_3 and R_v^+ are given by (5.77)-(5.81), and α should be evaluated by (5.82). These are the integral approximate solutions to the frictional and acceleration pressure gradients for condensing/evaporating annular flow of turbulent vapor and laminar liquid.

5.5.1.2. *Heat transfer problem with constant wall heat flux*

The difference of the present problem from the problem discussed in subsection 5.3.1.2 is that the vapor flow we are dealing with is turbulent. However, the overall effect of the turbulent vapor flow on heat transfer actually goes through the vapor mass flow rate, and has been captured by the void fraction. Therefore, the formulation of the current problem is exactly the same as that presented in subsection 5.3.1.2, except that the void fraction should be evaluated by (5.82). In the following, only main assumptions and results are outlined, and subsection 5.3.1.2 should be referred for the derivation details.

For phase change heat transfer, the difference between the saturation temperature of the working fluid and the wall temperature is generally selected to define heat transfer coefficient, i.e.

$$h_{pc} \equiv \frac{q_0}{T_0 - T_{sat}}. \tag{5.129}$$

For heat transfer with constant heat flux at wall, it is reasonable to assume (Bejan 2004)

$$\frac{\partial T_v}{\partial z} = \frac{\partial T_l}{\partial z} = \frac{dT_{sat}}{dz}. \tag{5.130}$$

Assuming that the phase change (condensation or evaporation) takes place at the liquid-vapor interface, the heat flux at the interface can be obtained from an overall energy balance of the interface and vapor phase

$$q_1 = \frac{\dot{m}h_{lv}dx + \dot{m}_v c_{pv} dT_{sat}}{2\pi r_1 dz} = \frac{G\pi r_0^2 \left(h_{lv}dx/dz + xc_{pv}dT_{sat}/dz\right)}{2\pi r_1} = \frac{Gr_0\left(\xi + x\right)c_{pv}dT_{sat}/dz}{2\alpha^{1/2}}, \tag{5.131}$$

where ξ is latent-sensible heat ratio defined by

$$\xi \equiv \frac{h_{lv} dx/dz}{c_{pv} dT_{sat}/dz}. \tag{5.132}$$

Since in most engineering applications, the saturation temperature decreases with the *z*-coordinate as a result of the total pressure drop, ξ is positive for condensing flow and negative for evaporating flow.

The Nusselt number for annular flow of turbulent vapor and laminar liquid with phase change can be obtained as

$$\mathrm{Nu}_l \equiv \frac{2r_0 h_{pc}}{k_l} = \frac{2r_0 q_0}{k_l (T_0 - T_{sat})} = \frac{8 + \dfrac{8(\xi + x)}{\hat{c}_p (1-x)}}{\dfrac{(3-\alpha)}{(1-\alpha)} + \dfrac{2\alpha(2-\alpha)\ln\alpha}{(1-\alpha)^2} - \dfrac{2(\xi + x)\ln\alpha}{\hat{c}_p (1-x)}}, \tag{5.133}$$

and if the latent-sensible heat ratio is large, we have

$$\mathrm{Nu}_l \cong \mathrm{Nu}_l\Big|_{\xi \to \infty} = \frac{4}{-\ln\alpha}. \tag{5.134}$$

In (5.133) and (5.134) α should be evaluated by (5.82).

Figure 5.17 shows the results of (5.133) in terms of the Nusselt number as a function of vapor quality and the latent-sensible heat ratio, for saturated water at 100^{o}C and saturated R-134a at 50^{o}C, respectively. The predicted Nusselt number for phase change case increases monotonically with quality, in distinct contrast with the no phase change case shown in Figure 5.16. The main reason for this difference is the different definitions of heat transfer coefficient and hence Nusselt number. For the phase change case, the heat transfer coefficient is defined based on wall-interface temperature difference, and the deceasing thickness of the liquid layer with increasing quality results in the increasing Nusselt number.

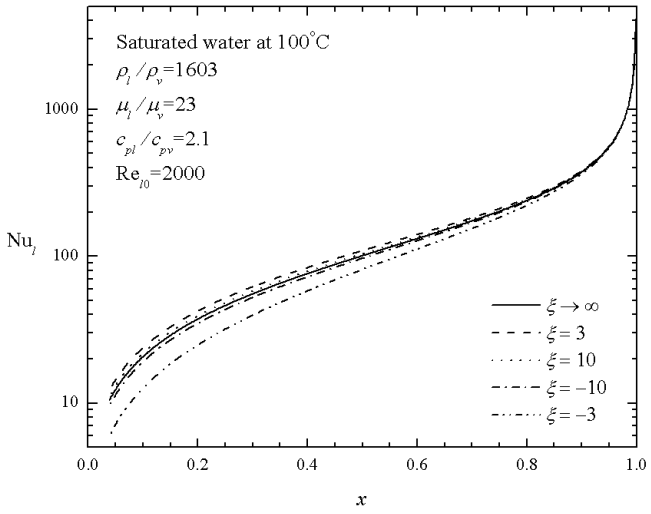

(a)

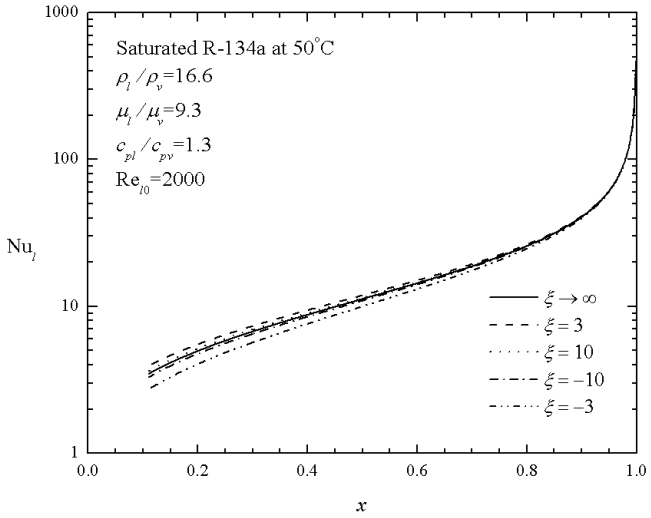

(b)

Figure 5.17 Nusselt number for annular flow of turbulent vapor and laminar liquid with phase change as a function of vapor quality and latent-sensible heat ratio.

It is clear from Figure 5.17 that (5.134) provides a very good approximation to (5.133) as long as the absolute value of the latent-sensible heat ratio is higher than 10, for both the condensing case (positive ξ) and the evaporating case (negative ξ). In most engineering applications, the latent-sensible heat ratio is very large, and (5.134) can be used to calculate phase change heat transfer for annular flow of turbulent vapor and laminar liquid.

5.5.1.3. *Applicable domain*

The applicable domain, vt, of the formulation presented in this section is defined by (5.105), and shown in Figure 5.18 for saturated water at 100^{o}C and saturated R-134a at 50^{o}C, respectively. Similar to the air-water system shown in Figure 5.13, the tv domain of annular flow with turbulent liquid and laminar vapor is corresponding to very low quality, and thus unlikely exists in the real engineering systems. Figure 5.18 also shows the difference between VTL-vt based on (5.82) and VTL-vv based on (5.9) for saturated water is much smaller than that for and saturated R-134a, which can be explained by the much higher density ratio of the water, resulting in a negligible second term on the right hand side of (5.106). Considering that laminar-turbulent transition does not occur at a precise Reynolds number, the VTL-vv based on (5.9) is accurate enough to partition different domains of annular flow for various engineering applications.

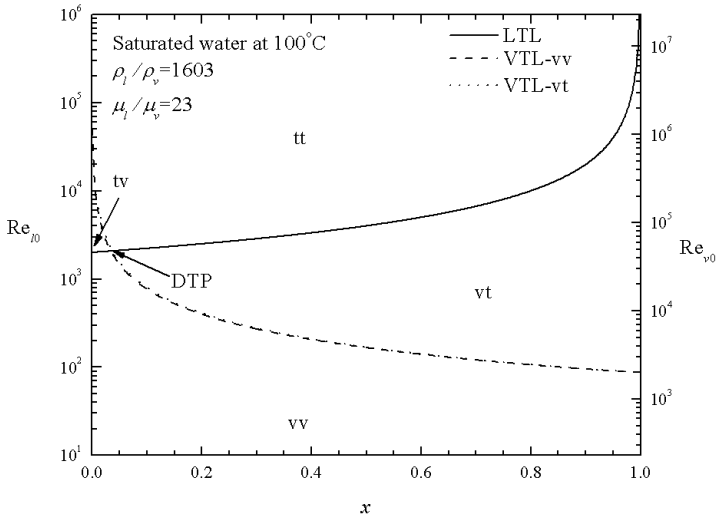

(a)

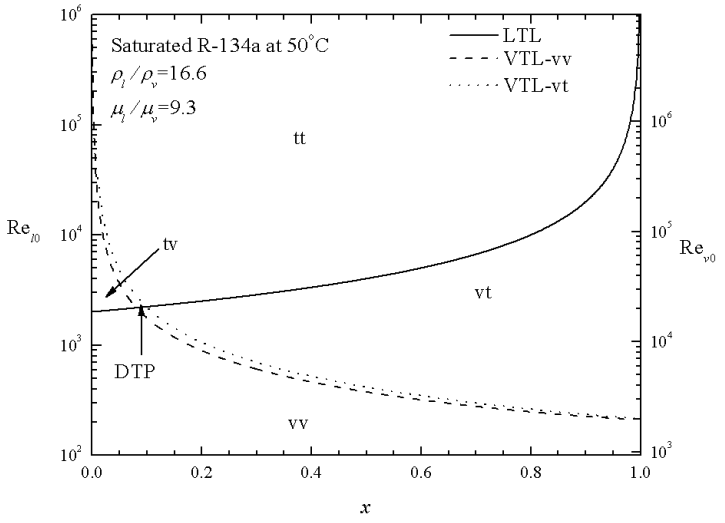

(b)

Figure 5.18 Annular flow domains (vv, vt, tv, and tt) formed by laminar-turbulent transition lines (LTL and VTL) for saturated water and R-134a.

5.5.2. Results and discussion

In this subsection, the results of the analytical model in section 5.5.1 are compared with prevailing correlations of void fraction, frictional pressure gradient, acceleration pressure gradient, and heat transfer in the literature. All the comparisons are based on the thermophysical properties of saturated water at 100^{o}C and saturated R-134a at 50^{o}C.

5.5.2.1. *Void fraction*

Figure 5.19 shows a comparison of the prediction of (5.82) with seven existing void fraction correlations (Table 5.2). For both water and R-134a cases, the void fraction given by (5.82) is significantly lower than the predictions of all but the Turner (1966) correlations. The turner (1966) correlation best fits the result of (5.82) for the vt annular flow of water with Re_{l0}=500 and that of R-134a with Re_{l0}=4000, but cannot correctly captures the dependence of void fraction in the vt domain upon the Reynolds number.

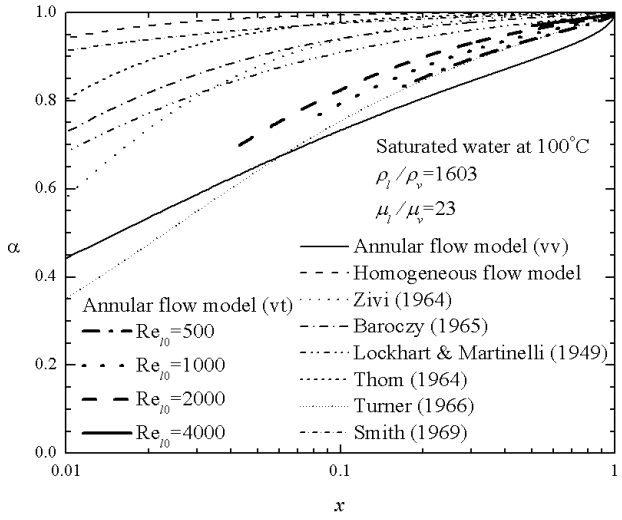

(a)

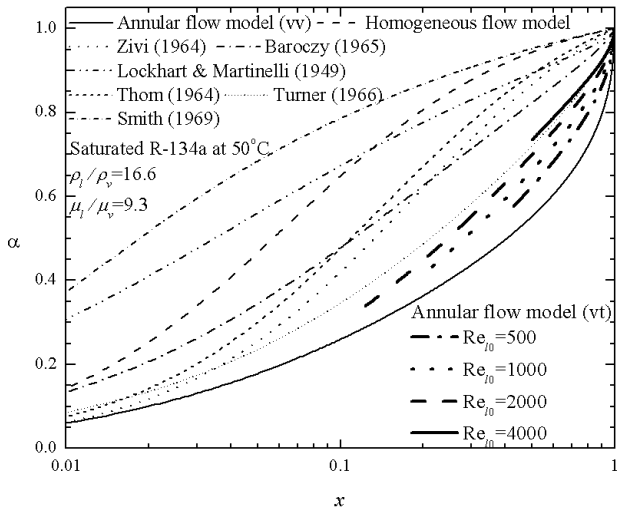

(b)

Figure 5.19 Comparison of prediction of (5.82) with empirical correlations of void fraction for saturated water and R-134a.

5.5.2.2. *Frictional pressure drop*

Figure 5.20 shows a comparison of the prediction of (5.73) with two popular frictional multiplier correlations (Table 5.6) for Re_{l0} = 500, 1000, 2000, and 4000, respectively, in the vt domain. It is clear from Figure 5.20 that the frictional multiplier predicted by the analytical model is significantly different from the predictions of the empirical correlations. All the perditions of the Lockhart & Martinelli (1949) correlation are lower, while those of the Friedel (1979) correlation are higher than the corresponding analytical results. Moreover, both the two empirical correlations predict that the frictional pressure drop decreases when Reynolds number increases, while the annular flow model predicts the opposite, i.e., the frictional pressure drop increase with the Reynolds number. Figure 5.20 also shows that the frictional pressure drop in the vt domain is higher than that in the vv domain.

5.5.2.3. *Acceleration pressure drop*

Figure 5.21 shows a comparison of acceleration pressure gradients predicted by (5.121) and by the homogeneous and separated flow models (Table 5.5), for Re_{l0} = 500, 1000, 2000, and 4000, respectively, in the vt domain. It is clear that the homogeneous flow model cannot capture the quality dependence of the acceleration pressure gradient, while the separated flow model systematically underestimates the acceleration pressure gradient in annular flow of turbulent vapor and laminar liquid, for both the saturated water and R-134a cases examined here. It is also shown in Figure 5.21 that the dependence of the acceleration pressure gradient on the Reynolds number is very weak for water.

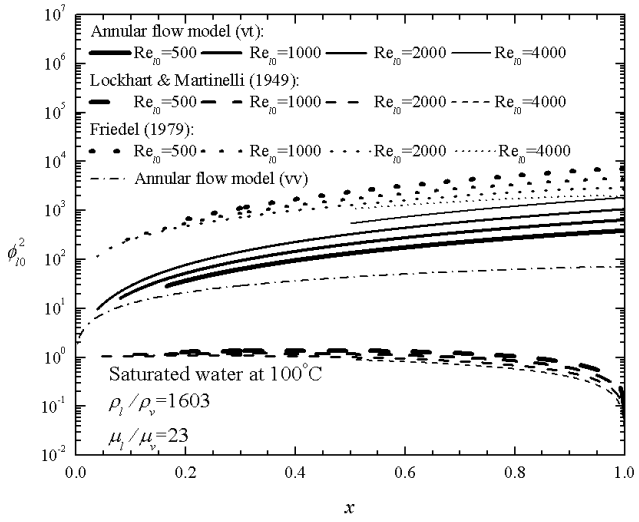

(a)

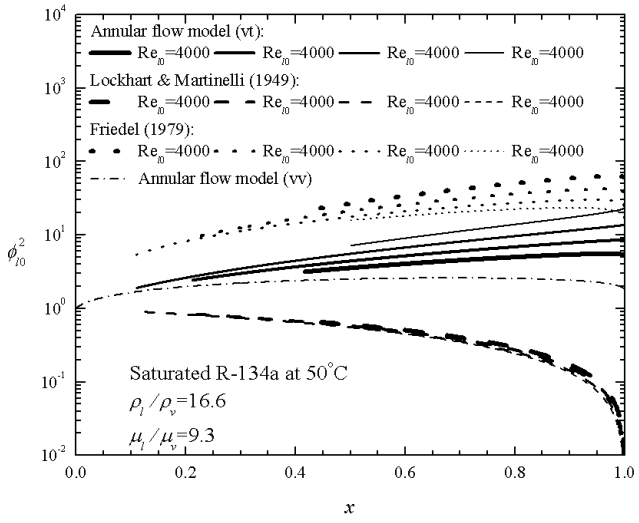

(b)

Figure 5.20 Comparison of prediction of (5.73) with empirical correlations of frictional pressure drop for saturated water and R-134a.

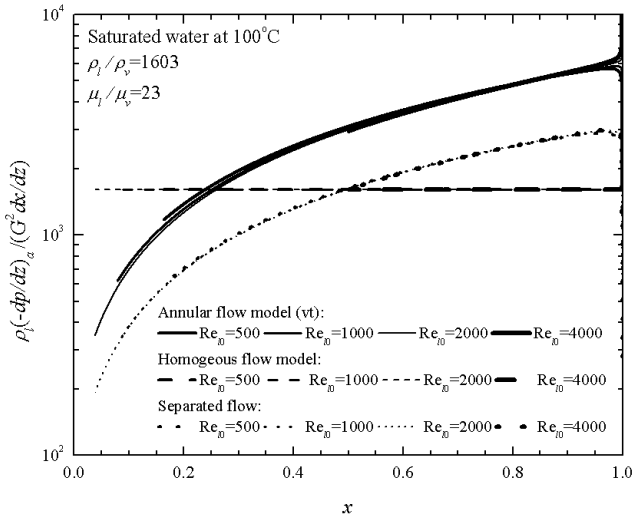

(a)

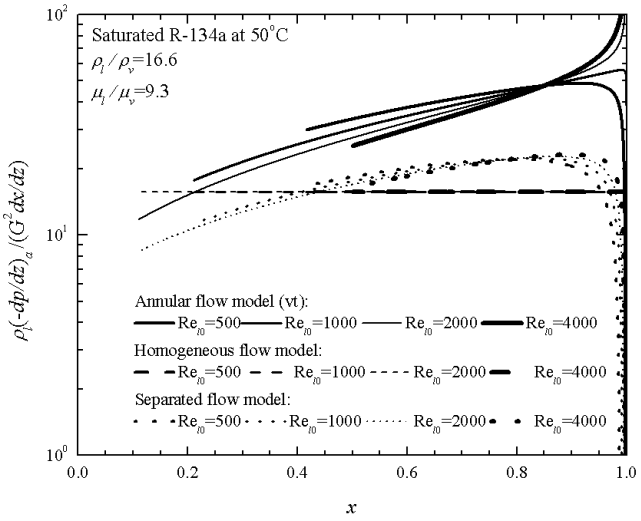

(b)

Figure 5.21 Comparison of acceleration pressure gradient predicted by (5.121) and those by the homogeneous and separated flow models for saturated water and R-134a.

5.5.2.4. *Heat transfer*

In Figure 5.22 the prediction of (5.134) is compared with two popular correlations that established through phase change two-phase flows, viz., the Shah (1979) and the Cavallini & Zecchin (1971) correlations (Table 5.4), for Re_{l0} = 500, 1000, 2000, and 4000, respectively, in the vt domain. Both the correlations are in a form of a generalization of the classical heat transfer correlation of turbulent single-phase flow. Note that the heat transfer coefficient of turbulent single-phase flow is defined based on wall-stream temperature difference, which is fundamentally different from the heat transfer coefficient defined bases on wall-interface (saturation) temperature difference and generally used for phase change two-phase flows, and the physical basis for the two empirical correlations is highly questionable. Nevertheless, Figure 5.22 shows that although the Nusselt numbers predicted by the analytical model for annular flow of turbulent vapor and laminar liquid are generally in similar trends as those predicted by the empirical correlations, significant quantitative differences exist between the modeling results and the empirical correlations. Figure 5.22 also shows that the phase change heat transfer in the vt domain is better than that in the vv domain, similar to the no phase change situation shown in Figure 5.16.

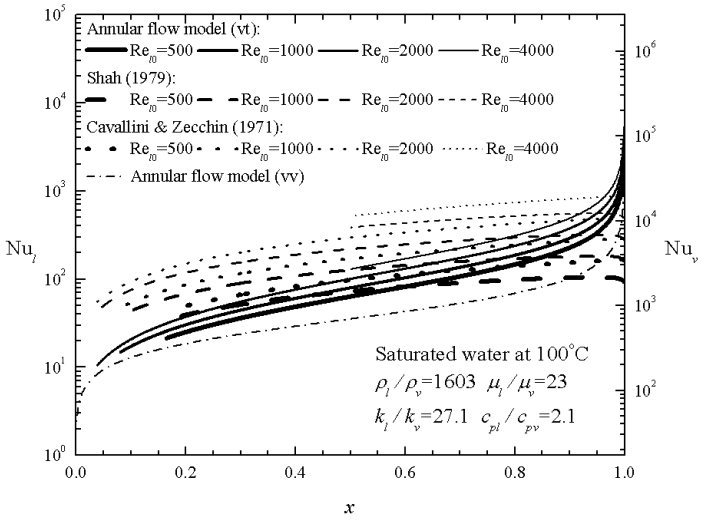

(a)

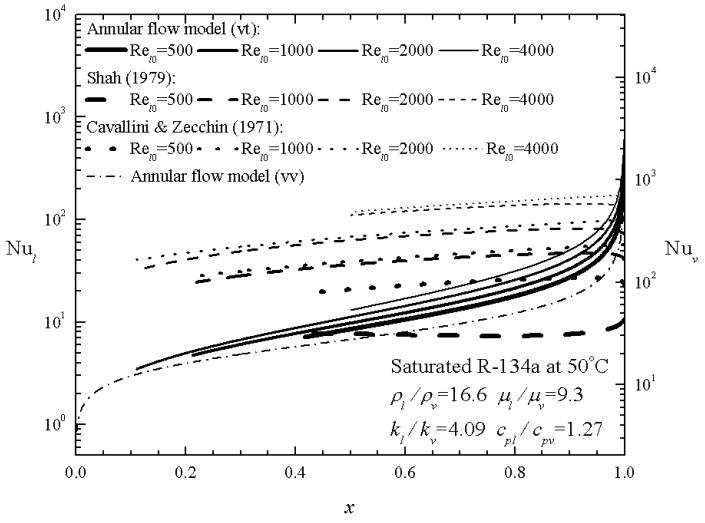

(b)

Figure 5.22 Comparison of Nusselt number predicted by (5.134) and those by empirical correlations of heat transfer for saturated water and R-134a.

5.5.3. Conclusions

An analytical model for condensing/evaporating annular flow of turbulent vapor and laminar liquid in a horizontal tube is presented. The model is based on approximation solutions of velocity and temperature distributions within the vapor and liquid phases, and predicts void fraction, frictional pressure gradient, acceleration pressure gradient, and heat transfer coefficient on a self-contained and self-consistent basis. In terms of physically reasonable definition of Reynolds numbers for the vapor and liquid phases in annular flow, the applicable domain of the analytical model is determined. In terms of saturated water at 100^{o}C and saturated R-134a at 50^{o}C as two examples, modeling results are compared with the predictions of the prevailing empirical correlations of void fraction, frictional pressure drop, acceleration pressure drop, and heat transfer for two-phase flow, and it is shown that the empirical correlations examined are generally inapplicable for horizontal annular flows of turbulent vapor and laminar liquid.

5.6 Convective Annular Flow of Turbulent Gas and Liquid

5.6.1. Formulation of the problem

5.6.1.1 *Hydrodynamic problem*

In this section, we consider the case of annular flow of turbulent gas and liquid without phase change. For the turbulent liquid and gas flows, it is impossible to solve velocity from the transient Navier-Stokes equation. Here we adopt the law of the wall (Bejan 2004) based on the mixing length assumption (Prandtl, 1969) to represent both the liquid and gas velocities.

For the liquid flow, we assume

$$u_l^+ = y_l^+ \ \text{ for } y_l^+ < y_{VSL}^+ \ , \ u_l^+ = A\ln y_l^+ + B \ \text{ for } y_l^+ > y_{VSL}^+ , \tag{5.135}$$

where

$$u_l^+ = \frac{u_l}{u_l^\tau} , y_l^+ = \frac{(r_0 - r)\rho_l u_l^\tau}{\mu_l} , \ u_l^\tau = \sqrt{\frac{\tau_0}{\rho_l}} , \tag{5.136}$$

and $A \cong 2.5$, $B \cong 5.5$, $y_{VSL}^+ \cong 11.6$.

For the gas flow, we assume

$$u_v^+ = A\ln y_v^+ + B' , \tag{5.137}$$

where

$$u_v^+ = \frac{u_v}{u_v^\tau} , y_v^+ = \frac{(y_1 + r_1 - r)\rho_v u_v^\tau}{\mu_v} , \ u_v^\tau = \sqrt{\frac{\tau_0}{\rho_v}} , \tag{5.138}$$

and y_1 and B' are two constants to be determined for matching the velocity and shear tress at the gas-liquid interface. Both the liquid and gas velocities are scaled in terms of the wall shear stress, in consistence with Prandtl's assumption of constant apparent shear stress, which is the foundation of the law the wall (Bejan 2004).

The continuity of the shear stress at the interface requires

$$\mu_l \frac{du_l}{dr}\Big|_{r=r_1} = \mu_v \frac{du_v}{dr}\Big|_{r=r_1} , \tag{5.139}$$

which yields

$$y_1 = (r_0 - r_1)\frac{\sqrt{\hat{\rho}}}{\hat{\mu}} . \tag{5.140}$$

The continuity of the velocity at the interface gives

$$B' = \frac{A}{\sqrt{\hat{\rho}}}\left\{\frac{B}{A} - (\sqrt{\hat{\rho}} - 1)\ln\left[\left(1 - \sqrt{\alpha}\right)R_l^+\right]\right\} , \tag{5.141}$$

where R_l^+ is the dimensionless tube radius, defined by

$$R_l^+ = \frac{r_0\sqrt{\tau_0\rho_l}}{\mu_l}. \tag{5.142}$$

As a result, the velocity distributions can be written as

$$u_l = \sqrt{\frac{\tau_0}{\rho_l}}\left(1-\frac{r}{r_0}\right)R_l^+ \quad \text{for } r_0\left(1-\frac{y_{VSL}^+}{R_l^+}\right) \le r \le r_0, \tag{5.143}$$

$$u_l = A\sqrt{\frac{\tau_0}{\rho_l}}\left\{\ln\left[\left(1-\frac{r}{r_0}\right)R_l^+\right]+\frac{B}{A}\right\} \quad \text{for } r_1 \le r \le r_0\left(1-\frac{y_{VSL}^+}{R_l^+}\right), \tag{5.144}$$

$$u_v = A\sqrt{\frac{\tau_0}{\rho_l}}\left\{\sqrt{\hat{\rho}}\ln\left[1+\frac{\left(\sqrt{\alpha}-\dfrac{r}{r_0}\right)\hat{\mu}}{\left(1-\sqrt{\alpha}\right)\sqrt{\hat{\rho}}}\right]+\ln\left[\left(1-\sqrt{\alpha}\right)R_l^+\right]+\frac{B}{A}\right\} \quad \text{for } r \le r_1. \tag{5.145}$$

Accordingly, the mass flow rate of the liquid flow is found to be

$$\dot{m}_l = \pi r_0^{\,2}\sqrt{\tau_0\rho_l}A\left[\begin{array}{l}\left(\ln R_l^+ + \dfrac{B}{A}-\dfrac{1}{2}\right)\left(\eta^2-\alpha\right)+(1-\alpha)\ln\left(1-\sqrt{\alpha}\right)\\ -\left(1-\eta^2\right)\ln(1-\eta)-\eta+\sqrt{\alpha}+\dfrac{R_l^+}{A}\left(\dfrac{1}{3}-\eta^2+\dfrac{2}{3}\eta^3\right)\end{array}\right], \tag{5.146}$$

where

$$\eta = 1-\frac{y_{VSL}^+}{R_l^+}. \tag{5.147}$$

Since the viscous sublayer in the turbulent flow is almost always much thinner than the tube radius, it is safe to approximate η by 1, and thus (5.146) is simplified to

$$\dot{m}_l = \pi r_0^{\,2}\sqrt{\tau_0\rho_l}A(1-\alpha)\left(\ln R_l^+ + a_1\right), \tag{5.148}$$

where

$$a_1 = \frac{B}{A}-\frac{1}{2}+\ln\left(1-\sqrt{\alpha}\right)-\frac{1}{1+\sqrt{\alpha}}. \tag{5.149}$$

Integrating (5.145), the mass flow rate of the gas flow is found to be

$$\dot{m}_v = \frac{\pi r_0^{\,2}\sqrt{\tau_0 \rho_l}\, A\alpha}{\hat{\rho}}\left(\ln R_l^{\,+} + a_2\right), \tag{5.150}$$

where

$$a_2 = \ln\left(1-\sqrt{\alpha}\right) + \frac{B}{A} - \sqrt{\hat{\rho}}\left[\frac{s^2}{\alpha}\ln\left(1-\frac{\sqrt{\alpha}}{s}\right) + \frac{s}{\alpha}\sqrt{\alpha} + \frac{1}{2}\right], \tag{5.151}$$

$$s = \frac{(1-\sqrt{\alpha})\sqrt{\hat{\rho}}}{\hat{\mu}} + \sqrt{\alpha}\,. \tag{5.152}$$

As a result, a void fraction-quality relation is given by dividing (5.150) by (5.148)

$$\hat{x} \equiv \frac{x}{1-x} = \frac{\alpha\left(\ln R_l^{\,+} + a_2\right)}{(1-\alpha)\hat{\rho}\left(\ln R_l^{\,+} + a_1\right)}, \tag{5.153}$$

and the mass flux is obtained by adding (5.148) to (5.150)

$$G = \sqrt{\tau_0 \rho_l}\, A\left[(1-\alpha)\left(\ln R_l^{\,+} + a_1\right) + \frac{\alpha}{\hat{\rho}}\left(\ln R_l^{\,+} + a_2\right)\right]. \tag{5.154}$$

Since the frictional pressure drop for single-phase turbulent flow cannot be expressed in a universally accepted form, using frictional multiplier for turbulent two-phase flow is no longer convenient for the tt domain. Instead, two-phase friction factor based on liquid properties can be expressed by

$$f_l \equiv \frac{2\rho_l \tau_0}{G^2} = \frac{8 r_0^2 \rho_l \tau_0}{\mathrm{Re}_{l0}^2\, \mu_l^2} = \frac{8 R_l^{+2}}{\mathrm{Re}_{l0}^2}\,. \tag{5.155}$$

Consequently,

$$\left(-\frac{dp}{dz}\right)_f = \frac{2\tau_0}{r_0} = \frac{f_l G^2}{r_0 \rho_l} = \frac{f_l\, \mathrm{Re}_{l0}^2\, \mu_l^2}{4 r_0^3 \rho_l}\,. \tag{5.156}$$

Substituting (5.155) into (5.153) and solving the friction factor, we have

$$f_l = \frac{8}{\mathrm{Re}_{l0}^2 \exp\left[\dfrac{2a_2\alpha - 2a_1(1-\alpha)\hat{x}\hat{\rho}}{\alpha + (1-\alpha)\hat{x}\hat{\rho}}\right]}. \tag{5.157}$$

Substituting (5.155) into (5.154) yields

$$F(\alpha) = \frac{\sqrt{2}}{A\sqrt{f_l}} - \left(\frac{\alpha}{\hat{\rho}} + 1 - \alpha\right)\left(\ln \mathrm{Re}_{l0} + \frac{1}{2}\ln f_l - \frac{1}{2}\ln 8\right) - a_1(1-\alpha) - \frac{a_2\alpha}{\hat{\rho}} = 0. \tag{5.158}$$

For given x and Re_{l0}, the only unknown in (5.158) is void fraction, because friction factor can be eliminated by substituting (5.157).

Note that for both limits of single-phase liquid flow ($\alpha = 0$) and single-phase gas flow ($\alpha = 1$), (5.158) reduces to the classical Karman-Nikuradse relation (Bejan 2004), which is the turbulent friction factor formula embedded in the widely used Moody chart.

For given x and Re_{l0}, the void fraction in the tt domain can be solved from (5.158) by applying appropriate numerical algorithm, e.g., the secant method outlined below

$$\alpha^{n+1} = \alpha^n - \frac{\alpha^n - \alpha^{n-1}}{F(\alpha^n) - F(\alpha^{n-1})} F(\alpha^n), \tag{5.159}$$

where the superscripts $n-1$, n and $n+1$ denote void fraction values for three successive iteration steps. Once the void fraction is solved, the friction factor is readily obtained from (5.157).

5.6.1.2. *Heat transfer problem*

Similar to the velocity distributions, we adopt the universal turbulent temperature profile (Bejan 2004) to represent both the liquid and gas temperatures. For the liquid flow, we assume

$$T_l^+ = \mathrm{Pr}_l\, y_l^+ \quad \text{for } y_l^+ < y_{CSL}^+,\ T_l^+ = A_T \ln y_l^+ + B_T \quad \text{for } y_l^+ > y_{CSL}^+, \tag{5.159}$$

where

$$T_l^+ = \frac{(T_0 - T_l)\rho_l c_{pl} u_l^\tau}{q_0},\ A_T \cong 2.195,\ B_T \cong 13.2\,\mathrm{Pr}_l - 5.66,\ y_{CSL}^+ \cong 13.2, \tag{5.160}$$

and Pr_l is Prandtl number of the liquid.

For the gas flow, we assume

$$T_v^+ = A_T \ln y_T^+ + B_T', \tag{5.161}$$

where

$$T_v^+ = \frac{(T_0 - T_v)\rho_v c_{pv} u_v^\tau}{q_0},\ y_T^+ = \frac{(y_2 + r_1 - r)\rho_v u_v^\tau}{\mu_v}, \tag{5.162}$$

and y_2 and B_T' are two constants to be determined for matching the temperature and heat flux at the gas-liquid interface. Both the liquid and gas temperatures are scaled in terms of the wall heat flux, in consistence with Prandtl's assumption of constant apparent heat flux, which is the foundation of the universal temperature profile (Bejan 2004).

The continuity of the heat flux at the interface requires

$$k_l \frac{dT_l}{dr}\Big|_{r=r_1} = k_v \frac{dT_v}{dr}\Big|_{r=r_1}, \tag{5.163}$$

which yields

$$y_2 = (r_0 - r_1)\frac{\hat{c}_p\sqrt{\hat{\rho}}}{\hat{k}}. \tag{5.164}$$

The continuity of the temperature at the interface gives

$$B_T' = \frac{A_T}{\hat{c}_p\sqrt{\hat{\rho}}}\left\{\frac{B_T}{A_T} - \hat{c}_p\sqrt{\hat{\rho}}\ln\frac{\hat{c}_p\hat{\mu}}{\hat{k}} - \left(\hat{c}_p\sqrt{\hat{\rho}} - 1\right)\ln\left[\left(1 - \sqrt{\alpha}\right)R_l^+\right]\right\}, \tag{5.165}$$

where R_l^+ is defined in (5.142).

As a result, the velocity distributions can be written as

$$T_l = T_0 - \frac{q_0 r_0}{k_l}\left(1-\frac{r}{r_0}\right) \quad \text{for } r_0\left(1-\frac{y_{CSL}^+}{R_l^+}\right) \le r \le r_0, \tag{5.166}$$

$$T_l = T_0 - \frac{A_T q_0}{c_{pl}\sqrt{\tau_0 \rho_l}}\left\{\ln\left[\left(1-\frac{r}{r_0}\right)R_l^+\right] + \frac{B_T}{A_T}\right\} \quad \text{for } r_1 \le r \le r_0\left(1-\frac{y_{CSL}^+}{R_l^+}\right), \tag{5.167}$$

$$T_v = T_0 - \frac{A_T q_0}{c_{pl}\sqrt{\tau_0 \rho_l}}\left\{\hat{c}_p\sqrt{\hat{\rho}}\ln\left[1+\frac{\left(\sqrt{\alpha}-\frac{r}{r_0}\right)\hat{k}}{\left(1-\sqrt{\alpha}\right)\hat{c}_p\sqrt{\hat{\rho}}}\right] + \ln\left[\left(1-\sqrt{\alpha}\right)R_l^+\right] + \frac{B_T}{A_T}\right\} \quad \text{for } r \le r_1. \tag{5.168}$$

In terms of the velocity distribution (5.143)-(5.145) and the temperature distribution (5.166)-(5.68), the stream-wall temperature difference can be defined by

$$T_m - T_0 = \frac{\int_{r_1}^{r_0} \rho_l c_{pl} u_l (T_l - T_0) 2\pi r dr + \int_0^{r_1} \rho_v c_{pv} u_v (T_v - T_0) 2\pi r dr}{c_{pl}\dot{m}_l + c_{pv}\dot{m}_v}, \tag{5.169}$$

And the Nusselt number for annular flow of turbulent gas and liquid can be calculated by

$$\mathrm{Nu}_l \equiv \frac{2r_0 h_{npc}}{k_l} = \frac{2r_0 q_0}{k_l(T_0 - T_m)} = \frac{\mathrm{Pr}_l\,\mathrm{Re}_{l0}\left(1-x+x/\hat{c}_p\right)}{2AA_T I}, \tag{5.170}$$

where

$$I = \int_{\sqrt{\alpha}}^1 \left[\ln(1-\beta)+d_3\right]\left[\ln(1-\beta)+d_{3T}\right]\beta d\beta + \left[\ln(s-\beta)+\frac{d_4}{\sqrt{\hat{\rho}}}\right]\left[\ln(t-\beta)+\frac{d_{4T}}{\sqrt{\hat{\rho}}}\right]\beta d\beta, \tag{5.170a}$$

$$d_1 = 1-\sqrt{\alpha},\ t = \frac{d_1\hat{c}_p\sqrt{\hat{\rho}}}{\hat{k}} + \sqrt{\alpha}, \tag{5.170b}$$

$$d_2 = s - \sqrt{\alpha} = \frac{d_1\sqrt{\hat{\rho}}}{\hat{\mu}},\ d_{2T} = t - \sqrt{\alpha} = \frac{d_1\hat{c}_p\sqrt{\hat{\rho}}}{\hat{k}}, \tag{5.170c}$$

$$d_3 = \frac{B}{A} + \ln \mathrm{Re}_{l0} + \frac{1}{2}\ln f_l - \frac{1}{2}\ln 8\,,\ d_{3T} = \frac{B_T}{A_T} + \ln \mathrm{Re}_{l0} + \frac{1}{2}\ln f_l - \frac{1}{2}\ln 8 \quad (5.170\text{d})$$

$$d_4 = d_3 + \ln d_1 - \sqrt{\hat{\rho}}\ln d_2\,,\ d_{4T} = d_{3T} + \ln d_1 - \hat{c}_p\sqrt{\hat{\rho}}\ln d_{2T}\,. \quad (5.170\text{e})$$

The analytical result of integrating (5.170a) is not given here, because it is very involved and includes the nonelementary dilogarithm function (also called Spence's function), which needs to be evaluated numerically. Instead, direct numerical integration is recommended to evaluate (5.170a).

In the derivation of (5.170), the wall heat flux is not required to be constant, so (5.170) can be expected to be valid for various thermal boundary conditions, as long as the universal profiles for velocity and temperature are valid.

5.6.1.3. *Applicable domain*

The formulation presented in subsections 5.6.1.1 and 5.6.1.2 is only applicable to horizontal annular flow of turbulent gas and liquid, i.e., the tt domain, defined by

$$\mathrm{Re}_l \equiv (1-x)\mathrm{Re}_{l0} > \mathrm{Re}_{cr} \text{ and } \mathrm{Re}_v \equiv \sqrt{\alpha}\left[\frac{x}{\alpha} - \frac{2(1-x)}{\hat{\rho}(1-\alpha)}\right]\mathrm{Re}_{v0} > \mathrm{Re}_{cr}\,. \quad (5.171)$$

Since the annular flow in the tv domain is unlikely to occur in the engineering two-phase systems, as discussed in subsection 5.2.1.3, the real boundary of the tt domain should be the liquid transition line (LTL), $\mathrm{Re}_{l0} = \mathrm{Re}_{cr}/(1-x)$, together with a boundary that marks the unset of annular flow at low qualities.

5.6.2. Results and discussion

In this subsection, the results of the analytical model presented in subsections 5.6.1.1 and 5.6.1.2 are compared with prevailing correlations of void fraction, frictional

pressure drop, and heat transfer in the literature. All the comparisons are based on the air-water system at 20°C.

5.6.2.1. *Void fraction*

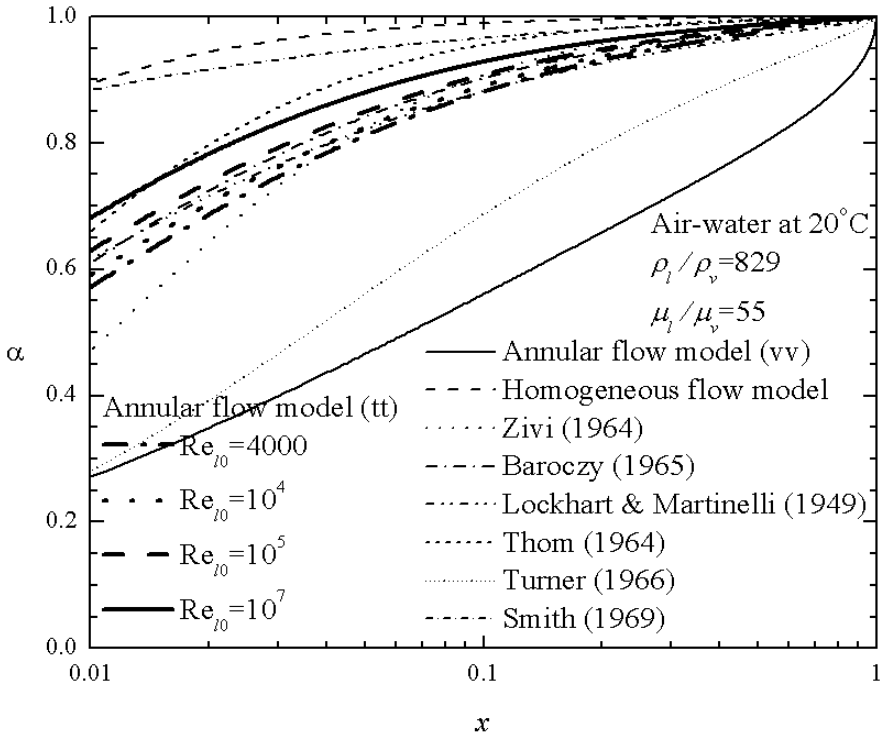

Figure 5.23 Comparison of prediction of (5.158) with empirical correlations of void fraction in the tt domain.

Figure 5.23 shows a comparison of the prediction of (5.158) with seven existing void fraction correlations (Table 5.2). Although (5.158) predicts that void fraction for annular flow in the tt domain is a function of Reynolds number, the empirical α - x correlations examined here are dependent upon density ratio and viscosity ratio only,

i.e., independent upon Reynolds number. It is clear from Figure 5.23 that the void fraction predictions by (5.158) for Reynolds number Re_{l0} between 10^4 and 10^5 are in excellent agreement with the Baroczy (1965) correlation.

5.6.2.2. *Frictional pressure drop*

Figure 5.24 shows a comparison of the prediction of (5.157) with two popular frictional pressure correlations (Table 5.7) for $\mathrm{Re}_{l0} = 4\times10^3$, 10^4 , 10^5 , and 10^7 , respectively, in the tt domain. It is clear from Figure 5.24 that except for very low qualities, the frictional factors predicted by the analytical model are significantly higher than the predictions of the empirical correlations. Although the trend of friction factor decreasing with increasing Reynolds number is correctly captured by all the model and correlations, the correlations predict much more profound effect of friction factor upon Reynolds number.

Table 5.7 Frictional factor correlations for the tt domain.

Correlation	$f_l \equiv r_0\rho_l\left(-dp/dz\right)_f / G^2$
Annular flow model	Equations (5.157) and (5.158)
Lockhart & Martinelli (1949)	$f_l = \dfrac{0.079\left(1-x\right)^{1.75}}{\mathrm{Re}_{l0}^{0.25}}\left(1+\dfrac{20}{X_{tt}}+\dfrac{1}{X_{tt}^2}\right),\ X_{tt}^2 = \dfrac{\hat{\mu}^{0.25}}{\hat{\rho}\hat{x}^{1.75}}$
Friedel (1979)	$\dfrac{0.079}{\mathrm{Re}_{l0}^{0.25}}\left[\left(1-x\right)^2+\dfrac{x^2\hat{\rho}}{\hat{\mu}^{0.25}}+3.23x^{0.78}\left(1-\mathrm{x}\right)^{0.224}\hat{\rho}^{0.91}\hat{\mu}^{-0.19}\left(1-\hat{\mu}^{-1}\right)^{0.7}\right]$

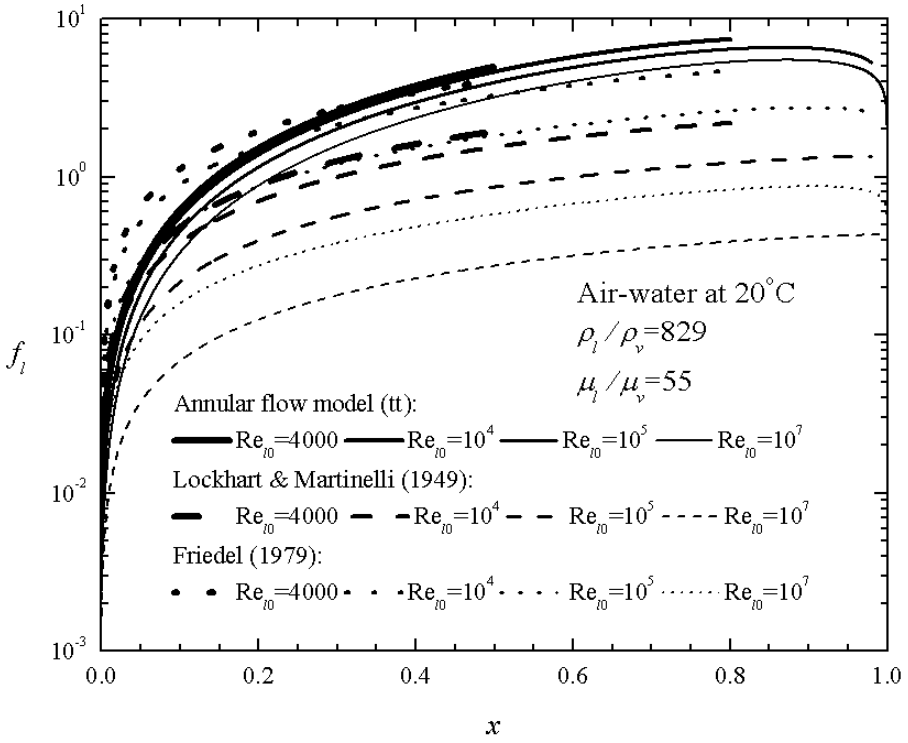

Figure 5.24 Comparison of prediction of (5.157) with empirical correlations of frictional pressure drop for two-phase flow in the tt domain.

5.6.2.3. *Heat transfer*

Since we cannot find any heat transfer correlation for gas-liquid two-phase flows without phase change, we compare in Figure 5.25 the prediction of (5.170) with two popular correlations that established through phase change two-phase flows, viz., the Shah (1979) and the Cavallini & Zecchin (1971) correlations (Table 5.4), for $\mathrm{Re}_{l0} = 4\times10^3$, 10^4, 10^5, and 10^7, respectively, in the tt domain. Both the correlations are in a form of a generalization of the classical heat transfer correlation of turbulent single-phase flow.

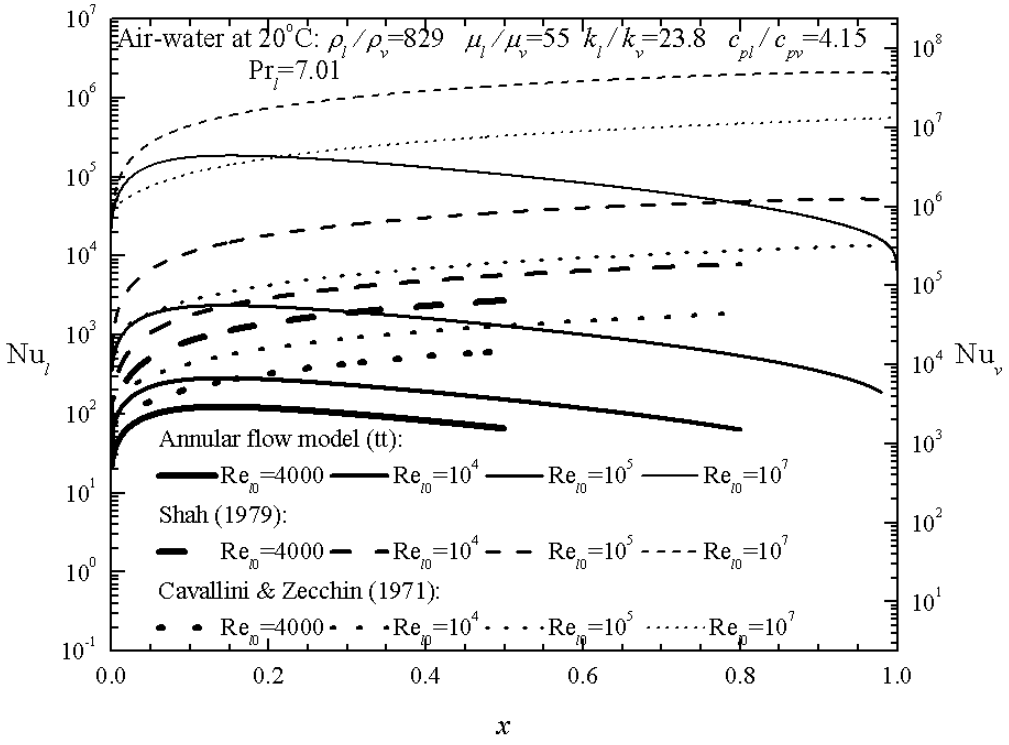

Figure 5.25 Comparison of prediction of (5.170) with empirical correlations of heat transfer in the tt domain.

It is clear from Figure 5.25 that the Nusselt numbers predicted by the analytical model are in significantly different trend, as compared with the predictions of the correlations. Figure 5.25 also shows that the correlations tend to overestimate the heat transfer at high qualities, which may be related to the fact that they are established based on experiments of phase change heat transfer, where heat transfer coefficient is defined in terms of wall-saturation temperature difference and assumes higher values at higher qualities due to the deceasing thickness of the liquid film.

5.6.3. Conclusions

An analytical model for convective annular flow of turbulent gas and liquid in a horizontal tube is presented. The model is based on the universal turbulent velocity and temperature profiles for the gas and liquid phases, and predicts void fraction, frictional pressure gradient, and heat transfer coefficient on a self-contained and self-consistent basis. In terms of the air-water system at room temperature as an example, modeling results are compared with the prevailing empirical correlations of void fraction, frictional pressure drop, and heat transfer for two-phase flow in detail. It has been shown that the modeling results of void fraction are generally different from the predictions of the empirical correlations, except that for Re_{l0} between 10^4 and 10^5, the predicted void fraction by the model is in excellent agreement with the Baroczy (1965) correlation. The two-phase friction factors predicted by the model are generally higher than the predictions of the Lockhart & Martinelli (1949) correlation and the Friedel (1979) correlation, especially for large Reynolds numbers and higher qualities. The model also predicts smaller Nusselt number at high qualities and significantly different quality dependency of the Nusselt number, as compared with the Shah (1979) and the Cavallini & Zecchin (1971) correlations.

5.7 Condensing/Evaporating Annular Flow of Turbulent Vapor and Liquid

5.7.1. Formulation of the problem

5.3.1.1 *Hydrodynamic problem*

When phase change (condensation or evaporation) occurs in the annular flow of turbulent vapor and liquid, the liquid velocity u_l and vapor velocity u_v depend upon both

r-coordinate and *z*-coordinate. In addition, since both the vapor and liquid flows are turbulent, the vapor velocity, liquid velocity and pressure are all unsteady. However, for most engineering applications, the main interest is in the time-average values of the pressure and velocities, which we consider as steady and still are denoted by p, u_v and u_l.

Following the classical boundary layer analysis (Schlichting 1968), if we assume that the *z*-direction characteristic length L is much greater than that of the *r*-direction, $r_0 << L$, the momentum balances, Navier-Stokes equations, for the liquid and vapor phases can be written respectively by (Bejan 2004)

$$\rho_l u_l \frac{\partial u_l}{\partial z} + \rho_l v_l \frac{\partial u_l}{\partial r} = -\frac{dp}{dz} + \frac{1}{r}\frac{\partial}{\partial r}\left[r\left(\mu_l + \rho_l \varepsilon_l\right)\frac{\partial u_l}{\partial r}\right], \tag{5.172}$$

$$\rho_v u_l \frac{\partial u_v}{\partial z} + \rho_v v_v \frac{\partial u_v}{\partial r} = -\frac{dp}{dz} + \frac{1}{r}\frac{\partial}{\partial r}\left[r\left(\mu_v + \rho_v \varepsilon_v\right)\frac{\partial u_v}{\partial r}\right], \tag{5.173}$$

where ε_l and ε_v are momentum eddy diffusivities for the liquid flow and the vapor flow, respectively, and the continuity equations for the two phases are

$$\frac{\partial u_l}{\partial z} + \frac{1}{r}\frac{\partial\left(r v_l\right)}{\partial r} = 0\,,\ \frac{\partial u_v}{\partial z} + \frac{1}{r}\frac{\partial\left(r v_v\right)}{\partial r} = 0\,. \tag{5.174}$$

Multiplying the continuity equations by the product of the corresponding density and velocity and adding it to the Navier-Stokes equations yields

$$\frac{\partial}{\partial z}\left(\rho_l {u_l}^2\right) + \frac{1}{r}\frac{\partial}{\partial r}\left(r\rho_l u_l v_l\right) = -\frac{dp}{dz} + \frac{1}{r}\frac{\partial}{\partial r}\left[r\left(\mu_l + \rho_l \varepsilon_l\right)\frac{\partial u_l}{\partial r}\right], \tag{5.175}$$

$$\frac{\partial}{\partial z}\left(\rho_v {u_v}^2\right) + \frac{1}{r}\frac{\partial}{\partial r}\left(r\rho_v u_v v_v\right) = -\frac{dp}{dz} + \frac{1}{r}\frac{\partial}{\partial r}\left[r\left(\mu_v + \rho_v \varepsilon_v\right)\frac{\partial u_v}{\partial r}\right]. \tag{5.176}$$

Integrating (5.175) and (5.176) over the cross sectional area and using Leibnitz's integral formula, we have

$$\frac{d}{dz}\left(\int_0^{r_1}\rho_v u_v{}^2 r dr+\int_{r_1}^{r_0}\rho_l u_l{}^2 r dr\right)+\left(r\rho_v u_v v_v\right)\Big|_0^{r_1}+\left(r\rho_l u_l v_l\right)\Big|_{r_1}^{r_0}=-\frac{r_0{}^2}{2}\frac{dp}{dz}$$
$$+\left[r\left(\mu_v+\rho_v\varepsilon_v\right)\frac{\partial u_v}{\partial r}\right]\Big|_0^{r_1}+\left[r\left(\mu_l+\rho_l\varepsilon_l\right)\frac{\partial u_l}{\partial r}\right]\Big|_{r_1}^{r_0}. \tag{5.177}$$

The boundary and connection conditions of the problem give

$$v_v\Big|_{r=0}=v_l\Big|_{r=r_0}=0,\ u_v\Big|_{r=r_1}=u_l\Big|_{r=r_1},\ \frac{\partial u_v}{\partial r}\Big|_{r=0}=0,\ \mu_v\frac{\partial u_v}{\partial r}\Big|_{r=r_1}=\mu_l\frac{\partial u_l}{\partial r}\Big|_{r=r_1},\ \mu_l\frac{\partial u_l}{\partial r}\Big|_{r=r_0}=-\tau_0. \tag{5.178}$$

The mass conservation at the phase change surface yields (Faghri and Zhang 2006)

$$\rho_v v_v\Big|_{r=r_1}=\rho_l v_l\Big|_{r=r_1}. \tag{5.179}$$

The existence of the laminar (vicious) sublayer of the turbulent liquid boundary layer near the wall gives

$$\varepsilon_l\Big|_{r=r_0}=0. \tag{5.180}$$

Substituting (5.178)-(5.180) into (5.177), we have

$$-\frac{dp}{dz}=\frac{2\tau_0}{r_0}+\frac{2}{r_0{}^2}\frac{d}{dz}\left(\int_0^{r_1}\rho_v u_v{}^2 r dr+\int_{r_1}^{r_0}\rho_l u_l{}^2 r dr\right)+\frac{2\sqrt{\alpha}}{r_0}\left(\rho_l\varepsilon_l\frac{\partial u_l}{\partial r}-\rho_v\varepsilon_v\frac{\partial u_v}{\partial r}\right)\Big|_{r=r_1}, \tag{5.181}$$

which shows the total pressure drop can be divided into a frictional component, an acceleration component, and an additional component related to the eddy shear stress jump across the vapor-liquid interface, i.e.

$$-\frac{dp}{dz}=\left(-\frac{dp}{dz}\right)_f+\left(-\frac{dp}{dz}\right)_a+\left(-\frac{dp}{dz}\right)_{eddy}, \tag{5.182}$$

where

$$\left(-\frac{dp}{dz}\right)_f=\frac{2\tau_0}{r_0}, \tag{5.183}$$

$$\left(-\frac{dp}{dz}\right)_a = \frac{2}{r_0^{\,2}}\frac{d}{dz}\left(\int_0^{r_1}\rho_v u_v^{\,2} r dr + \int_{r_1}^{r_0}\rho_l u_l^{\,2} r dr\right). \tag{5.184}$$

$$\left(-\frac{dp}{dz}\right)_{eddy} = \frac{2\sqrt{\alpha}}{r_0}\left(\rho_l \varepsilon_l \frac{\partial u_l}{\partial r} - \rho_v \varepsilon_v \frac{\partial u_v}{\partial r}\right)\Big|_{r=r_1}. \tag{5.185}$$

According to the mixing length assumption (Prandtl 1969) and the wall coordinate expressions shown in (5.136) and (5.138), we have

$$\varepsilon_l = \kappa^2 (r_0 - r)^2 \left|\frac{\partial u_l}{\partial r}\right|,\ \varepsilon_v = \kappa^2 (y_1 + r_1 - r)^2 \left|\frac{\partial u_v}{\partial r}\right|, \tag{5.186}$$

where κ is von Karman's constant. Taking the velocity distributions, (5.144) and (5.145), of annular flow of turbulent gas and liquid without phase change as approximate velocities for the phase change case, the velocity gradients at the vapor-liquid interface are given by

$$\frac{\partial u_l}{\partial r}\Big|_{r=r_1} = \frac{-A\sqrt{\tau_0}}{r_0\left(1-\sqrt{\alpha}\right)\sqrt{\rho_l}},\ \frac{\partial u_v}{\partial r}\Big|_{r=r_1} = \frac{-A\sqrt{\tau_0}\hat{\mu}}{r_0\left(1-\sqrt{\alpha}\right)\sqrt{\rho_l}}. \tag{5.187}$$

Substituting (5.186), (5.187) and (5.140) into (5.185) yields

$$\left(-\frac{dp}{dz}\right)_{eddy} = \frac{2\sqrt{\alpha}}{r_0}\left(\kappa^2 A^2 \tau_0 - \kappa^2 A^2 \tau_0\right) = 0, \tag{5.188}$$

which means the velocity distributions given by (5.144) and (5.145) provide not only continuous molecular shear stresses across the vapor-liquid interface, as is forced so by satisfying (5.139), but also continuous eddy shear stresses across the interface. This physically correct additional result serves as an evidence of the consistency and justification of the theory introduced here.

Taking the velocity distributions, (5.144) and (5.145), of no phase change case to approximate those of phase change case, and noting the time-average total mass flux G is a constant, the frictional pressure gradient in (5.183) can be expressed by

$$\left(-\frac{dp}{dz}\right)_f = \frac{f_l G^2}{r_0 \rho_l}, \tag{5.189}$$

where the friction factor should be evaluated based on (5.157) and (5.158). Similarly, the acceleration pressure gradient is determined to be

$$\left(-\frac{dp}{dz}\right)_a = \frac{A^2 G^2}{\rho_l}\frac{dx}{dz}\frac{d}{dx}\left[f_l\left(L_1 + L_1 + L_2 + L_3 + L_4 + L_5 + L_6 + L_7\right)\right], \tag{5.190}$$

where

$$L_1 = \frac{d_3^2(1-\alpha) + d_4^2\alpha}{2}, \tag{5.191}$$

$$L_2 = -d_3\left(d_1^2 \ln d_1 - \frac{1}{2}d_1^2 - 2d_1 \ln d_1 + 2d_1\right), \tag{5.192}$$

$$L_3 = d_4\sqrt{\hat{\rho}}\left(d_2^2 \ln d_2 - \frac{1}{2}d_2^2 - 2sd_2 \ln d_2 + 2sd_2\right), \tag{5.193}$$

$$L_4 = d_4\sqrt{\hat{\rho}}\left(s^2 \ln s - \frac{3}{2}s^2\right), \tag{5.194}$$

$$L_5 = -\left(\frac{1}{2}d_1^2 \ln^2 d_1 - \frac{1}{2}d_1^2 \ln d_1 + \frac{1}{4}d_1^2 - d_1 \ln^2 d_1 + 2d_1 \ln d_1 - 2d_1\right), \tag{5.195}$$

$$L_6 = \hat{\rho}\left(\frac{1}{2}d_2^2 \ln^2 d_2 - \frac{1}{2}d_2^2 \ln d_2 + \frac{1}{4}d_2^2 - sd_2 \ln^2 d_2 + 2sd_2 \ln d_2 - 2sd_2\right), \tag{5.196}$$

$$L_7 = \hat{\rho}\left(\frac{1}{2}s^2 \ln^2 s - \frac{3}{2}s^2 \ln s + \frac{7}{4}s^2\right), \tag{5.197}$$

$$d_1 = 1 - \sqrt{\alpha}, \tag{5.198}$$

$$d_2 = s - \sqrt{\alpha} = \frac{d_1\sqrt{\hat{\rho}}}{\hat{\mu}}, \tag{5.199}$$

$$d_3 = \frac{B}{A} + \ln \mathrm{Re}_{l0} + \frac{1}{2}\ln f_l - \frac{1}{2}\ln 8, \tag{5.200}$$

$$d_4 = d_3 + \ln d_1 - \sqrt{\hat{\rho}}\ln d_2. \tag{5.201}$$

In the above, f_l and α should be evaluated by (5.157) and (5.158). Equations (5.189) and (5.190) are the integral approximate solutions to the frictional and acceleration pressure gradients for condensing/evaporating annular flow of turbulent vapor and liquid.

5.5.1.2. *Heat transfer problem*

For phase change heat transfer of turbulent annular flow, if the phase change (condensation or evaporation) is assumed to take place at the liquid-vapor interface, we have

$$T\Big|_{r=r_1} = T_{sat}. \tag{5.202}$$

Substituting into the liquid temperature profile (5.160) yields

$$\frac{(T_0 - T_{sat})\rho_l c_{pl} u_l^{\tau}}{q_0} = A_T \ln\left(1-\sqrt{\alpha}\right) + A_T R_l^+ + B_T, \tag{5.203}$$

$$h_{pc} \equiv \frac{q_0}{T_0 - T_{sat}} = \frac{\rho_l c_{pl} u_l^{\tau}}{A_T \ln\left(1-\sqrt{\alpha}\right) + A_T R_l^+ + B_T}. \tag{5.204}$$

Therefore,

$$\mathrm{Nu}_l \equiv \frac{2r_0 h_{pc}}{k_l} = \frac{2\,\mathrm{Pr}_l R_l^+}{A_T \ln\left(1-\sqrt{\alpha}\right) + A_T R_l^+ + B_T}, \tag{5.205}$$

where

$$R_l^+ = \frac{\sqrt{f_l}\,\mathrm{Re}_{l0}}{\sqrt{8}}, \tag{5.206}$$

from (5.155).

As is clear in the above, (5.205) is derived solely based upon the liquid temperature distribution (5.160), without any additional restrictions, such as constant wall heat flux, or large latent-sensible heat ratio. Consequently, (5.205) can be expected to be valid over very wide applicable domains, as long as the turbulent temperature distribution (5.205) is valid.

For horizontal annular flow of turbulent gas and liquid without phase change, as a special case of vanished latent-sensible heat ratio, if we define heat transfer coefficient by

$$h_{npc} \equiv \frac{q_0}{T_0 - T_{\mathrm{int}}}, \tag{5.207}$$

where T_{int} is the temperature at the gas-liquid interface, the no phase change heat transfer can be measured by the following Nusselt number

$$\mathrm{Nu}_l \equiv \frac{2r_0 h_{npc}}{k_l} = \frac{2\,\mathrm{Pr}_l\,R_l^+}{A_T \ln\left(1-\sqrt{\alpha}\right) + A_T R_l^+ + B_T}, \tag{5.208}$$

which takes exactly the same form as (5.205).

5.7.1.3. *Applicable domain*

The formulation presented in subsections 5.7.1.1 and 5.7.1.2 is only applicable to horizontal annular flow of turbulent vapor and liquid, i.e., the tt domain, bounded by the the liquid transition line (LTL), $\mathrm{Re}_{l0} = \mathrm{Re}_{cr}/\left(1-x\right)$, together with a boundary that marks the unset of annular flow at low qualities.

5.7.2. Results and discussion

In this subsection, the results of the analytical model in section 5.7.1 are compared with prevailing correlations of void fraction, frictional pressure gradient, acceleration pressure gradient, and heat transfer in the literature. All the comparisons are based on the thermophysical properties of saturated water at 100^{o}C and saturated R-134a at 50^{o}C.

5.7.2.1. *Void fraction*

A comparison of the prediction of (5.158) with seven existing void fraction correlations (Table 5.2) is shown in Figure 5.26. It can be seen that among all the correlations examined here, the Baroczy (1965) correlation agrees best to the modeling predictions of the water case for Re_{l0} between 10^4 and 10^5. The same conclusion has been drawn for the air-water case based on Figure 5.23. However, Figure 5.26 also shows that the Baroczy (1965) correlation cannot consistently fit the modeling results for the R-134a case.

5.7.2.2. *Frictional pressure drop*

Figure 5.27 shows a comparison of the prediction of (5.157) with two popular frictional pressure correlations (Table 5.7) for $\mathrm{Re}_{l0} = 4\times10^3$, 10^4 , 10^5 , and 10^7 , respectively, in the tt domain. It is clear from Figure 5.27 that neither the Lockhart & Martinelli (1949) correlation nor the Friedel (1979) correlation agrees consistently with the model. Relatively speaking, the Friedel correlation (1979) is in a better agreement with the model, especially for the R-134a case at low Reynolds numbers.

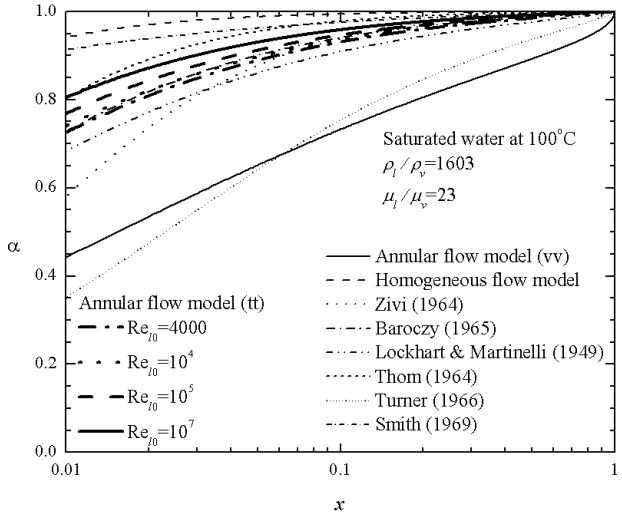

(a)

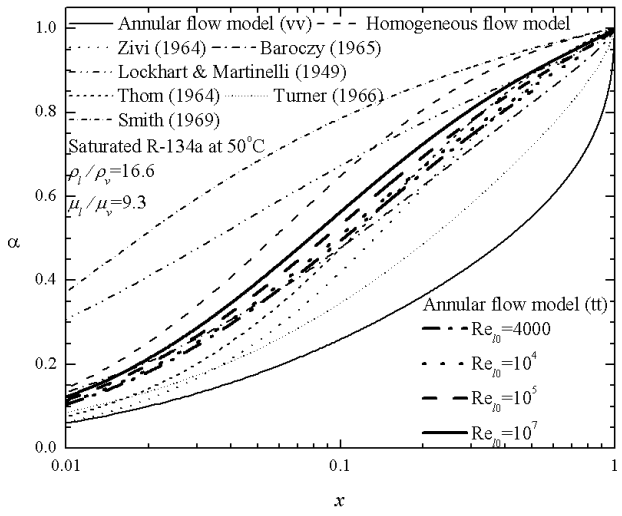

(b)

Figure 5.26 Comparison of prediction of (5.158) with empirical correlations of void fraction for saturated water and R-134a.

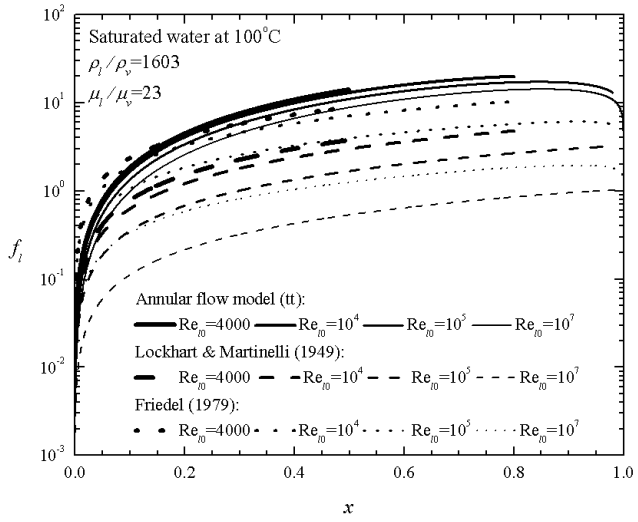

(a)

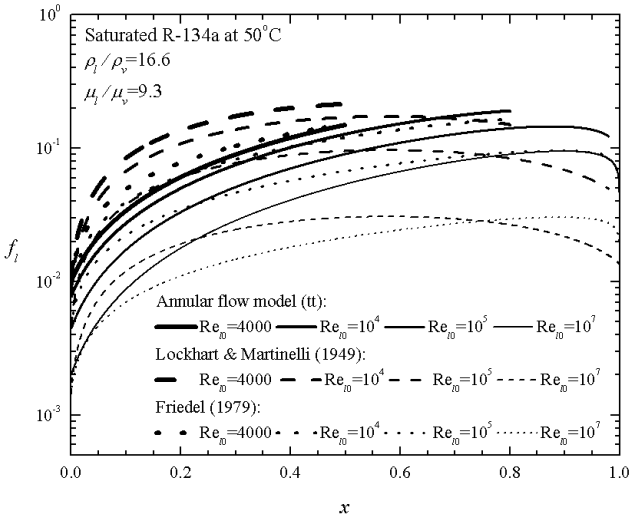

(b)

Figure 5.27 Comparison of prediction of (5.157) with empirical correlations of frictional pressure drop for saturated water and R-134a.

5.7.2.3. *Acceleration pressure drop*

Figure 5.28 shows a comparison of acceleration pressure gradients predicted by (5.190) and by the homogeneous and separated flow models (Table 5.5), for $\mathrm{Re}_{l0} = 4\times10^3$, 10^4, 10^5, and 10^7, respectively, in the tt domain. It is clear from Figure 5.28 that the homogeneous flow model cannot capture the quality dependence of the acceleration pressure gradient, while both the homogeneous flow model and the separated flow model systematically underestimate the acceleration pressure gradient by 3 orders of magnitude for the water case and 1 order of magnitude for the R-134a case. It is also shown in Figure 5.28 that the acceleration pressure gradient is very insensitive to the variation of the Reynolds number.

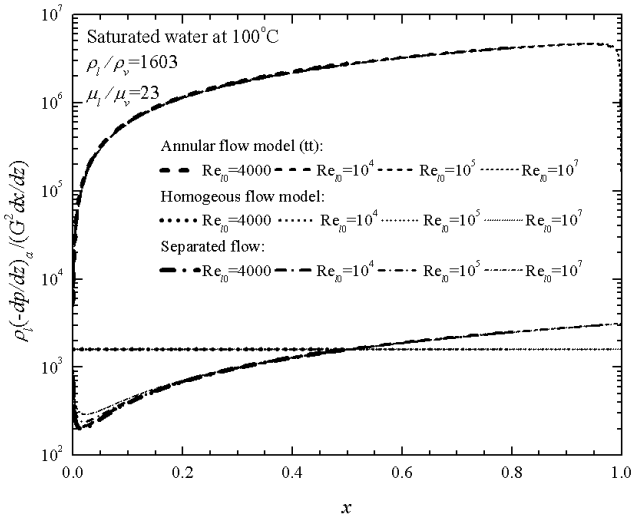

(a)

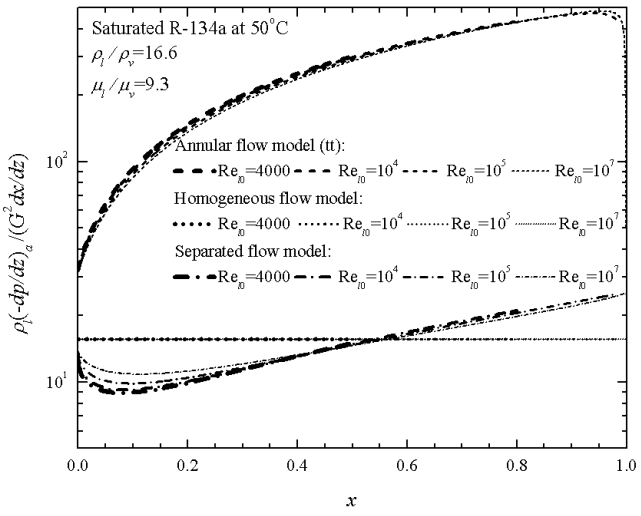

(b)

Figure 5.28 Comparison of acceleration pressure gradient in turbulent annular flow predicted by (5.190) and those by the homogeneous and separated flow models for saturated water and R-134a.

5.7.2.4. *Heat transfer*

In Figure 5.29 the prediction of (5.205) is compared with two popular correlations that established through phase change two-phase flows, viz., the Shah (1979) and the Cavallini & Zecchin (1971) correlations (Table 5.4), for $\mathrm{Re}_{l0} = 4 \times 10^3$, 10^4, 10^5, and 10^7, respectively, in the tt domain. Both the correlations are in a form of a generalization of the classical heat transfer correlation of turbulent single-phase flow. Note that the heat transfer coefficient of turbulent single-phase flow is defined based on wall-stream temperature difference, which is fundamentally different from the heat transfer coefficient defined bases on wall-interface (saturation) temperature difference and generally used for phase change two-phase flows, and the physical basis for the two empirical correlations is highly questionable.

It is interesting to see from Figure 5.28 that the modeling results agree better with the empirical correlations for water at higher Reynolds numbers and for R-134a at lower Reynolds numbers. There is no consistent agreement between the model and the correlations for the entire range of the Reynolds number examined.

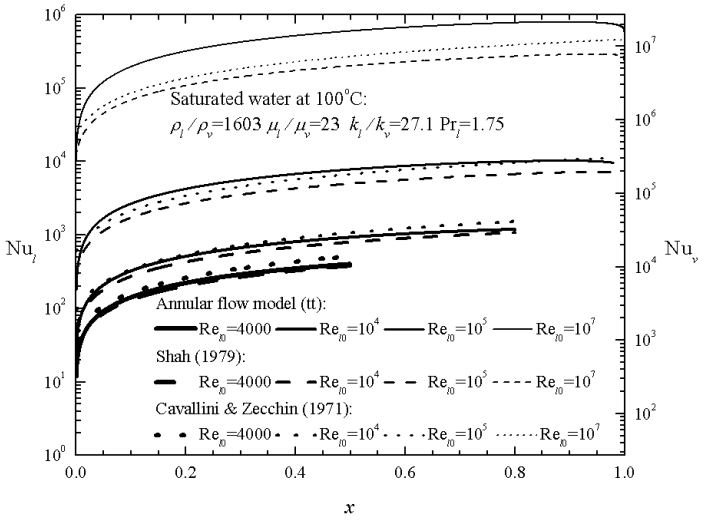

(a)

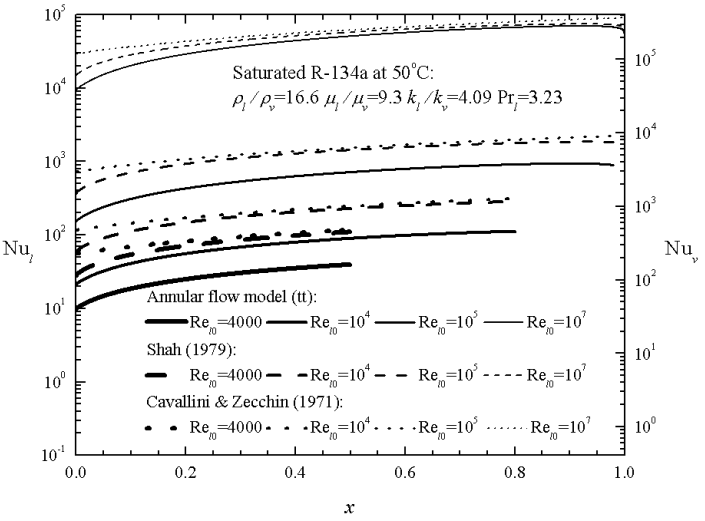

(b)

Figure 5.29 Comparison of Nusselt number predicted by (5.205) and those by empirical correlations of heat transfer for saturated water and R-134a.

5.7.3. Conclusions

An analytical model for condensing/evaporating annular flow of turbulent vapor and laminar liquid in a horizontal tube is presented. The model is based on approximation solutions of velocity and temperature distributions within the vapor and liquid phases, and predicts void fraction, frictional pressure gradient, acceleration pressure gradient, and heat transfer coefficient on a self-contained and self-consistent basis. In terms of saturated water at 100^{o}C and saturated R-134a at 50^{o}C as two examples, modeling results are compared with the predictions of the prevailing empirical correlations of void fraction, frictional pressure drop, acceleration pressure drop, and heat transfer for two-phase flow, and it is shown that the empirical correlations examined are generally inapplicable for horizontal annular flows of turbulent vapor and liquid.

Chapter 6

Concluding Remarks

This dissertation consists of two parts. The first part (chapters 2, 3 and 4) focuses on modeling tools development for loop heat pipes, with an emphasis on the prototype design of air-cooled loop heat pipes. The second part, analytical models of annular two-phase flow (chapter 5), is a fundamental research that may find its application in any two-phase flow system, definitely not limited to loop heat pipes or heat pipes.

In the first part, a set of modeling tools has been established, including a system level model for loop heat pipe operation, criteria of selecting working fluids for loop heat pipe, and individual component models for modularized loop heat pipe design.

The results of the system level model show that the condensation pressure drop always dominates the loop pressure drop in air-cooled loop heat pipes, suggesting the condenser component should be carefully designed, tested and modeled. Based on a detailed discussion of criteria for selecting working fluids, new figures of merit has been defined to measure capillary limit and heat leak effects. As for component models, a model for in-tube condensation, an air flow model for a fan-fin-tube system, and a model for loop heat pipe evaporator have been developed. The in-tube condensation model is based on the energy balance and entropy balance principles, and capable of incorporating correlations of void fraction, frictional pressure drop, acceleration, pressure drop, and heat transfer coefficient to calculate the variations of vapor quality, pressure, wall temperature, and wall heat flux in a condenser tube cooled by air flow.

A published loop heat pipe prototype for laptop computer cooling is simulated as a demonstration of the application of the modeling tools, and it has been revealed by the modeling results that the air flow consumes most of the allowed temperature difference and thus is the bottleneck of this prototype.

In the second part, analytical models for annular two-phase flow in a horizontal tube are presented. The treatment in this research is fundamentally different from the previous two-phase flow modeling methods in that both the velocity and temperature distributions for the liquid and gas/vapor phases are represented based on the governing equations for the laminar flows and based on the universal profiles for the turbulent flows, which is in clear contrast against the separated flow model, which assumes uniform velocity for each phase, and the homogeneous flow model, which treats the two-phase flow by a single phase flow that averages the actual two phase flow.

Based on physically reasonable definitions of Reynolds numbers for the gas/vapor and liquid phases, four possible domains of annular flow are identified, and the turbulent liquid and laminar gas/vapor domain (tv) is shown to be unlikely exist in the real two-phase systems. For the other three domains, viz., the laminar gas/vapor and liquid domain (vv), the turbulent gas/vapor and laminar liquid domain (vt), and the turbulent gas/vapor and liquid domain (tt), analytical formulation has been proposed for both phase change and no phase change cases. On a self-contained and self-consistent basis, the models provide the analytical relations of void fraction, frictional pressure gradient, acceleration pressure gradient, and heat transfer coefficient, and show that all these relations can

reduce to the corresponding classical single-phase limits when the two-phase annular flow approaches to single-phase gas/vapor or liquid flows.

The modeling results are compared in detail with the prevailing empirical correlations in engineering practice of void fraction, frictional pressure drop, acceleration pressure drop, and heat transfer (Nusselt number). It has been shown that the empirical correlations examined generally fail to provide reliable and accurate predictions for annular two-phase flows for all the vv, vt, and tt domains. Only under occasional situations, some empirical correlations agree well with the analytical model at certain flow conditions, for example, the Turner (1966) correlation for void fraction in the vt domain, the Baroczy (1965) correlation for void fraction in the tt domain.

The basic reason for the failure of the empirical correlations is that they are all established based on very limited experimental data and lack physically sound theoretical foundation. As an example, a comment by Hewitt and Hall-Taylor (1970) on the Lockhart-Martinelli (1949) correlation of frictional pressure drop is cited here: “The most commonly used method of calculating two-phase pressure drops is that of Martinelli and co-workers. Although the model was based on an attempt to consider frictional pressure gradient in two-phase flow in the absence of interaction between the phases, the theoretical justification is, at best, obscure and the reader is advised to ignore this and to treat this model as a purely empirical one.”

Another example is the generalization of the single phase turbulent Nusselt number correlation to the phase change two-phase heat transfer systems, as in the Shah (1979) and the Cavallini & Zecchin (1971) correlations. We know that the heat transfer coefficient of the single-phase flow is defined based on wall-mean stream temperature

difference, while that of the phase change two-phase system is commonly measured in the laboratories based on the wall-saturation temperature difference, which is close to the wall-interface temperature difference for annular flow. Since the heat transfer coefficients are defined in fundamentally different ways, how can we expect the generalized relation to be applicable to a wide domain?

Finally, as the last example, I'd like to point out the importance of the definition of Reynolds number for two-phase flow. In this research, the liquid phase Reynolds number is defined based on hydraulic diameter and average liquid velocity, resulting in a same definition as that widely adopted in the literature. However, the definition of gas/vapor Reynolds number in this work is fundamentally different from that widely adopted in the literature, which is popular but lacks of physical basis. In this research, the gas/vapor Reynolds number is defined based on the average gas/vapor velocity minus the liquid velocity at the gas/vapor-liquid interface, i.e., viewing the liquid film as a imaginary wall for the core gas/vapor flow, because the liquid is much more viscous than the gaseous phase. Such defined gas/vapor Reynolds number has clear physical basis and provides a solid foundation for determining the vv, tv, vt and tt domains of annular flow. Indeed, the above four domains have been proposed for ages, but the criteria to identify them can never be established without a physically correct definition of gas/vapor Reynolds number.

REFERENCES

Baroczy, C. J., 1965, Correlations of liquid fraction in two-phase flow with applications to liquid metals, Chemical Engineering Process Symposium Series, 61, 179-191.

Bejan, A., 2004, Convection Heat Transfer, 3rd edition, John Wiley & Sons, New York.

Bejan, A., and Sciubba, E., 1992, The optimal spacing of parallel plates cooled by forced convection, International Journal of Heat and Mass Transfer, 35 (12), 3259-3264.

Bergman, T. L., Faghri, A. and Viskanta, R., 2008, Frontiers in transport phenomena research and education: Energy systems, biological systems, security, information technology and nanotechnology, International Journal of Heat and Mass Transfer, 51, 4599-4613.

Breber, G., Palen J. W., and Taborek, J., 1980, Prediction of horizontal tubeside condensation of pure components using flow regime criteria., Journal of Heat Transfer, 102, 471-476.

Cao, Y., and Faghri, A., 1994a, Analytical solutions of flow and heat transfer in a porous structure with partial heating and evaporation on the upper surface, International Journal of Heat and Mass Transfer, 37 (10), 1525-1533.

Cao, Y., and Faghri, A., 1994b, Conjugate analysis of a flat-plate type evaporator for capillary pumped loops with three-dimensional vapor flow in the groove, International Journal of Heat and Mass Transfer, 37 (3), 401-409.

Cavallini, A., 2006, In-tube condensation performance of refrigerants, 11th Int. Refrig. Air Conditioning Conf. at Purdue, p. 1-11.

Cavallini, A., and Zecchin, R., 1971, High velocity condensation of organic refrigerants inside tubes, 8th Int. Congr. of Refrig., vol 2, Washington DC, p. 193-200.

Cavallini, A., and Zecchin, R., 1974, A dimensionless correlation for heat transfer in forced convection condensation, 6th Int. Heat Transfer Conf Tokyo, P. 309-313.

Chato, J. C., 1962, Laminar condensation inside horizontal and inclined tubes, ASHRAE Journal, 4, 52-60.

Chernysheva, M. A., et al., 2007, Operating temperature and distribution of a working fluid in LHP, International Journal of Heat and Mass Transfer, 50, 2704-2713.

Chi, S. W., 1976, Heat Pipe Theory and Practice, McGraw-Hill, New York.

Chisholm, D., 1983, Two-phase flow in pipelines and heat exchangers, Longman Inc., New York.

Cicchitti, A., Lombardi, C., Silvestri, M., Soldaini, G., and Zavattarelli, R., 1960, Two-phase cooling experiments – pressure drop, heat transfer and burnout measurements, Energia Nucleare, 7 (6), 407-425.

Demidov, A. S., and Yatsenko, E. S., 1994, Investigation of heat and mass transfer in the evaporation zone of heat pipe operating by the 'inverted meniscus' principle, International Journal of Heat and Mass Transfer, 37 (14), 2155-2163.

Dukler, A. E., Wics III, M., and Cleveland, R. G., 1964, Frictional pressure drop in two-phase flow, AIChE J. , 10 (1), 38-51.

Dunbar, N., and Cadell, P., 1998, Working fluids and figures of merit for CPL/LHP applications, CPL-98 Workshop Proc., Aerospace Corporation, El Segundo, CA, Mar. 2–3.

Dunn P. D., and Reay, D. A., 1994, Heat Pipes, Pergamon Press, New York.

Faghri, A., 1995, Heat Pipe Science and Technology, Taylor & Francis.

Faghri, A., and Zhang, Y., 2006, Transport Phenomena in Multiphase Systems, Elsevier Academic Press.

Figus, C., Le Bray, Y., Bories, S., and Prat, M., 1999, Heat and mass transfer with phase change in a porous structure partially heated: continuum model and pore network simulations, International Journal of Heat and Mass Transfer, 42, 2257-2569.

Friedel, L., 1979, Improved friction pressure drop correlations for horizontal and vertical two-phase pipe flow, Paper no. E2, European Two-Phase Flow Group Meeting, Ispra, Italy.

Friedel, L., 1980, Pressure drop during gas/vapor-liquid flow in pipes, International Chemical Engineering, 20 (3), 352-367.

Furukawa, M., 2006, Model-based method of theoretical design analysis of a loop heat pipe, Journal of Thermophysics and Heat Transfer, 20, 111-121.

Hewitt, G. F., 1983, Gas-liquid flow, in Schlunder, E. U. (ed.), Heat Exchanger Design Handbook, Hemisphere Publishing Corp.

Hewitt, G. F., and Hall-Taylor, N. S., 1970, Annular Two-Phase Flow, Pergamon Press, Oxford.

Hoang, T., and Kaya, T.,, 1999, Mathematical modeling of loop heat pipes with two-phase pressure drop, AIAA paper 1999-3448.

Hoang, T., and Ku, J.,, 2003, Transient modeling of loop heat pipes, AIAA paper 2003-6082.

Kaya, T., and Goldak, J., 2006, Numerical analysis of heat and mass transfer in the capillary structure of a loop heat pipe, International Journal of Heat and Mass Transfer, 49, 3211-3220.

Kaya, T., and Hoang, T., 1999, Mathematical modeling of loop heat pipes and experimental validation, Journal of Thermophysics and Heat Transfer, 13, 314-320.

Khrustalev, D., and Faghri, A., 1995, Heat transfer in the inverted meniscus type evaporator at high heat fluxes, International Journal of Heat and Mass Transfer, 38 (16), 3091-3101.

Ku J., 1999, Operating characteristics of loop heat pipes, SAE paper 1999-01-2007.

Launay, S., et al., 2007a, Transient modeling of loop heat pipes for the oscillating behavior study, Journal of Thermophysics and Heat Transfer, 21, 487-495.

Launay, S., et al., 2007b, Parametric analysis of loop heat pipe operation: a literature review, International Journal of Thermal Sciences, 46, 621-636.

Lockhart, R. W., and Martinelli, R. C., 1949, Proposed correlations of data for isothermal two-phase, two-component flow in pipes, Chemical Engineering Process Symposium Series, 45, 39-48.

Marto, P. J., 1998, Chapter 14: Condensation, in Rohsenow, W. M., Hartnett, J. P., and Cho, Y. I. (eds), Handbook of Heat Transfer, 3rd ed., McGraw-Hill.

Maydanik, Yu. F., 2005, loop heat pipes, Applied Thermal Engineering, 25, 635-657.

McAdams, W. H., Woods, W. K., and Heroman, L. C., 1942, Vaporization inside horizontal tubes II – Benzene-oil mixtures, Trans. ASME, 64 (3), 193-200.

Miyara, A., et al., 2000, Condensation heat transfer and flow pattern inside a herringbone-type micro-fin tube, Int. J. Refrigeration, 23, 141-152.

Muraoka, I., Ramos, F. M., and Vlassov, V. V., 2001, Analysis of the operational characteristics and limits of a loop heat pipe with porous element in the condenser, International Journal of Heat and Mass Transfer, 44, 2287-2297.

Prandtl, L., 1969, Essentials of Fluid Dynamics, Black & Son, London.

Ochterbeck, J. M., 2003, Heat Pipes, in: Bejan, A., and Kraus, A. D. (eds.), Heat Transfer Handbook, John Wiley & Sons.

Owens W. L., 1962, Two-phase pressure gradient. In: International Development in Heat Transfer, 1961, Part II, 363-368, New York, ASME.

Ren, C., and Wu, Q.-S., 2007, Heat transfer in loop heat pipes capillary wick: effect of effective thermal conductivity, Journal of Thermophysics and Heat Transfer, 21, 134-140.

Ren, C., Wu, Q.-S., and Hu, M.-B., 2007, Heat transfer in loop heat pipes capillary wick: effect of porous structure parameters, Journal of Thermophysics and Heat Transfer, 21, 702-711.

Ren, C., Wu, Q.-S., and Hu, M.-B., 2007, Heat transfer with flow and evaporation in loop heat pipe's wick at low or moderate heat fluxes, International Journal of Heat and Mass Transfer, 50, 2296-2308.

Schlichting, H., 1968, Boundary-Layer Theory, McGraw-Hill.

Shah, M. M., 1979, A general correlation for heat transfer during film condensation inside pipes, International Journal of Heat and Mass Transfer**,** 22, 547-556.

Shah, R. K., and London, A. L., 1978, Laminar Flow Forced Convection in Ducts, Academic Press, New York, Advances in Heat Transfer, Supplement 1.

Singh, R., Akbarzadeh, A., Dixon, C., Mochizuki, M., and Riehl, R. R., 2007, Miniature loop heat pipe with flat evaporator for cooling computer CPU, IEEE Transactions on Components and Packaging Technologies, 30, 42-49.

Smith, S. L., 1969, Void fraction in two-phase flow: a correlation based upon an equal velocity head model, Proceedings of the Institution of Mechanical Engineers, Thermodynamics and Fluid Mechanics Group, 647-657.

Thom, J. R. S., 1964, Prediction of pressure drop during forced circulation boiling of water, International Journal of Heat and Mass Transfer, 7, 709-724.

Turner, J. M., 1966, Annular two-phase flow, Ph. D. dissertation, Dartmouth College, Hanover, NH.

Wallis, G. B., 1969, One-dimensional two-phase flow, McGraw-Hill Inc., New York.

Webb, R. L., and Kim, N.-H., 2005, Principles of Enhanced Heat Transfer, 2nd edition, Taylor & Francis, New York.

Yu, J., and S. Koyama, 1998, Condensation heat transfer of pure refrigerants in microfin tubes, Proc 1998 Int. Refrig. Conf. at Purdue, p. 325-330.

Zhao, T. S., and Liao, Q., 2000, On capillary-driven flow and phase-change heat transfer in a porous structure heated by a finned surface: measurements and modeling, International Journal of Heat and Mass Transfer, 43, 1141-1155.

Zivi, S. M., 1964, Estimation of steady-state steam void-fraction by means of the principle of minimum entropy production, Journal of Heat Transfer, 86, 247-252.

VITA

Mr. Shimin Wang was born in Chicheng, a mountain county neighboring to Beijing, China. He received his BS degree in Geology, MS degree in Geodynamics, and Ph.D. degree in Solid Mechanics, all from Peking University, where he also served as an Assistant Professor and Associate Professor in the Department of Geophysics between 1998 and 2005. As a geoscientist, Mr. Wang's research on plate tectonics and geodynamics won national awards from *the Chinese Geophysical Society* and *the Chinese Society of Theoretical and Applied Mechanics* and a number of grants from *the National Natural Science Foundation of China*. His papers published in leading international journals were cited by peers from all over the world, and his findings were introduced to the general public by the prestigious *Natural History* magazine.

Mr. Wang started his second Ph.D. program in January 2006 at University of Missouri-Columbia. His current research area is thermal-fluid engineering, with an emphasis on theoretical study of the fundamentals of two-phase flow and modeling-based design of energy systems, HVAC components, and electronics cooling devices. After successfully accomplishing several industry-oriented projects, Mr. Wang's dissertation work on *Modeling tools and prototype design of Loop Heat Pipe for electronics cooling* obtained support from Dell Inc. Mr. Wang also taught at University of Missouri-Columbia. He has been a Teaching Assistant of *Thermal and Fluid Science Lab* for one semester, and the Instructor of *Engineering Thermodynamics* for three semesters.

Mr. Wang has a solid background and well-rounded training in theoretical, experimental, and especially numerical analysis of solid structure, fluid flow and heat transfer problems. His professional interests are in the areas of multi-phase fluid flow and heat transfer, electrohydrodynamic force control in microfluidics, and thermodynamic optimization of sustainable energy systems.